The Roles of eIF2α Kinases PKR and GCN2 During Mouse Adenovirus Type 1 Infection

by

Danielle E. Goodman

A dissertation submitted in partial fulfillment
of the requirements for the degree of
Doctor of Philosophy
(Cellular and Molecular Biology)
in The University of Michigan
2019

Doctoral Committee:

Professor Katherine R. Spindler, Chair
Professor Michael J. Imperiale
Professor Billy Tsai
Professor Christiane Wobus

Danielle E. Goodman

danigood@umich.edu

ORCID iD: 0000-0003-3033-9147

DEDICATION

I dedicate this work to my parents, Christine and Neil Goodman, as it has been their unconditional love and support throughout my educational career that has made this possible.

ACKNOWLEDGMENTS

I would like to start by thanking my mentor, Kathy Spindler. Kathy was always there with an open door and a listening ear to help me solve problems, give me suggestions, and help me interpret results. She always advocated for me when I needed it, and she helped me to improve my confidence, presentation and writing skills, and research instincts. Thank you for welcoming me into your lab back in 2013 and for helping me grow immensely as a scientist. Your mentorship has been invaluable, and I could not have completed my PhD without you.

I also thank my committee members Christiane Wobus, Michael Imperiale, and Billy Tsai for all of the advice, suggestions, and data analysis they gave me during my committee meetings. These meetings really helped me to keep my projects on track and made future directions much clearer.

Next, I thank my current and past lab members, including Carla Pretto-Kernahan, Jennifer Medlin, Tomas Krepostman, Asa Smith, Joshua Squires, and Luiza Castro-Jorge. Thank you all for being there with me day in and day out (special shout out to Carla, who has been with me my entire tenure in the Spindler lab), ready to lend a hand, listen to me vent, teach me something new, or just chat about what was going on. You all made the lab a happy and fun place to be.

I am also grateful for my undergraduate research mentors, Dr. Joseph Stukey and Dr. Virginia McDonough, for taking a chance on a green college sophomore and teaching me how to

do research. The projects, encouragement, and time you spent teaching me absolutely allowed me to get into my top choice graduate program, and I can't thank you enough for getting me started in my research career.

I also thank all of my PIBS, CMB, and Micro friends, especially Sara Wong, Travis Kochan, Jim Ropa, Corey Cunningham, Ray Joe, Megan Ludwig, Angela Griggs, and Zach Mendel. Thanks to you all for making suggestions when I was having problems, listening to me complain, lending me reagents or equipment, escaping to lunch, having a beer, playing intramurals, getting up at obscene hours to run obscene distances, celebrating the high holidays of Halloween and St. Paddy's Day, and just generally making my life here in Ann Arbor that much more awesome. In addition to my graduate student friends, I have been so lucky to have also been blessed with many more friends, both near and far, that have significantly ($P < 0.0001$) increased my happiness during my time in graduate school. This includes my three best friends from high school, Michelle Vanhala, Megan Kuk, and Brittany Buckingham, my three best friends from college, Cassie Cramer, Elizabeth Billquist, and Jo Forst, and my wonderful boyfriend Phil Rzeczycki. Thanks to all of you for being there when I needed you, talking, going on trips, exercising, having a beer, binging Netflix, eating all the food, playing trivia, and just having a great time together.

Finally, I am grateful for my family. I am very lucky to have had extended family that I absolutely adore living near Ann Arbor who could spend time with me and feed me all the food, including Melissa and Bryan Elkus and the Roneys, in addition to the rest of my extended family who always supported me from afar. I thank my sister and brother, Drew and Ethan Goodman, for our weekly exchanges of memes and amusing texts that always brightened my day. Many

thanks to my furry brother and sister, Indiana and Maggie, for always cheering me up with a snuggle or humorous antic.

Finally, I am grateful to my mom and dad, Christine and Neil Goodman, for always supporting me throughout my entire academic career. Starting all the way back with taking me to Math and Science nights during elementary school, they continuously encouraged me to pursue my passions. Whenever I was having a bad day, I knew I could always count on them to be by the phone when I called to cheer me up. They frequently made time to visit me regularly in college and in graduate school, and also bought me all the food and gas I could need when they were here. I certainly could not have done this without them, and I am so thankful for their unconditional love and support.

TABLE OF CONTENTS

DEDICATION ii

ACKNOWLEDGMENTS iii

LIST OF FIGURES x

ABSTRACT xii

CHAPTER

I. Introduction 1

Adenoviruses 1

Translation control by eIF2α kinases 5

Protein degradation within the cell 7

Immune response to adenovirus infection 10

Virus interactions with host protein PKR 12

Virus interactions with host protein GCN2 16

Conclusion 22

Bibliography 22

II. Enhanced replication of mouse adenovirus type 1 following virus-induced degradation of protein kinase R (PKR) 32

Abstract 32

Importance 33

Introduction 33

Results 36

Viral yield is increased in PKR-/- mouse embryonic fibroblasts 36

There is no difference in survival between N-PKR$^{-/-}$ and wild type mice 38

Mouse PKR is depleted during MAV-1 infection 38

huPKR is not degraded by MAV-1 43

MAV-1 does not cause PKR depletion by reducing steady-state levels of PKR mRNA 45

MAV-1 infection effects on PKR translation 45

PKR is depleted by proteasomal degradation during MAV-1 infection 50

PKR is not detectably ubiquitinated during MAV-1 infection 56

PKR is actively depleted early in infection 56

An early viral function is required for PKR depletion by MAV-1 58

E1A and E3 are not required for PKR degradation during MAV-1 infection 63

Discussion 65

Materials and Methods 71

Cells, mice, virus, and infections 71

Plasmids 73

Immunoblots 73

Ubiquitination immunoprecipitations 74

Viral yield analysis by qPCR 75

mRNA analysis by qPCR 76

Proteasome inhibition 76

Lysosome inhibition and DQ BSA assay 77

Ribosome pelleting 78

Polyribosome gradients 78

Nanoluciferase assays 79

Statistical analyses 80

Acknowledgments 80

Bibliography 81

III. Changes in immune response in GCN2$^{-/-}$ mice and macrophages during mouse adenovirus type 1 infection 89

Abstract 89

Introduction 90

Results 94

Atc mice are more susceptible to infection by MAV-1 than wild type mice 94

Viral yield is increased in *atc* peritoneal macrophages 94

Atchoum mice only have significantly higher viral titers in the cecum during infection 97

MAV-1-infected *atc* mice have a different inflammatory cytokine response than wild type mice in the brain 99

Discussion 104

Materials and Methods 106

Virus, mice, and cells 106

Genotyping for GCN2 mutation 108

Immunoblots (Information for Fig. 4.2) 108

Mouse infections 109

Quantitating viral yield by qPCR from cells and tissue 110

Mouse brain and liver plaque assays 110

Histology 111

Analysis of cytokine and chemokine levels 111

Statistical analyses 112

Acknowledgments 112

Bibliography 112

IV. Conclusions and Future Directions 117

Protein kinase R (PKR) Chapter Overview 117

Determining which early protein is responsible for PKR degradation during MAV-1 infection 117

Effects of PKR phosphorylation on PKR degradation rate during MAV-1 infection 121

In vivo degradation of mPKR during MAV-1 infection 122

MAV-1 replication kinetics in $PKR^{-/-}$ N-MEFs versus C-MEFs 123

Human PKR and MAV-1 124

Ubiquitination of PKR during MAV-1 infection 126

General control derepressible 2 (GCN2) Chapter Overview 126

GCN2 activation by general control of amino-acid synthesis 1 (GCN1) 127

GCN2 activation by 25-hydroxycholesterol (25OHC) 128

GCN2 activation through amino acid deprivation 129

Phosphorylation of eukaryotic translation initiation factor 2α 130

Effects of GCN2 deficiency on T-cell proliferation during MAV-1 infection 130

Cell-type specific effects of GCN2 132

Conclusions 133

Bibliography 134

LIST OF FIGURES

Figure 1.1 Adenovirus life cycle 3

Figure 1.2 MAV-1 genome structure 4

Figure 1.3 Translation control by eIF2α 6

Figure 1.4 Lysosomal degradation 8

Figure 1.5 Ubiquitination of protein substrates 9

Figure 1.6 Translation arrest by PKR 11

Figure 1.7 PKR degradation by Rift Valley Fever Virus (RVFV), adapted from Figure 5E from Mudhasani et al. 13

Figure 1.8 PKR degradation by enterovirus A71, adapted from Figure 8 from Chang et al 15

Figure 1.9 Translation arrest by GCN2 17

Figure 1.10 HIV-1 interactions with GCN2, adapted from Figure 7F from Jiang et al 21

Figure 2.1 Fragments of PKR protein expressed in $PKR^{-/-}$ MEFs, adapted from Figure 1A and 5B from Baltzis et al 37

Figure 2.2 Viral yield is increased in $PKR^{-/-}$ mouse embryonic fibroblasts and peritoneal macrophages 39

Figure 2.3 Survival rate during MAV-1 infection is increased or unchanged in $PKR^{-/-}$ mice compared to wild-type mice 40

Figure 2.4 Mouse PKR is depleted during MAV-1 infection 42

Figure 2.5 Human PKR is not depleted during MAV-1 infection 44

Figure 2.6 MAV-1 does not cause PKR depletion by reducing steady state levels of PKR mRNA at times when the protein levels are already reduced 46

Figure 2.7 MAV-1 infection does not affect PKR translation 47

Figure 2.8 PKR mRNA 5' UTR does not result in altered reporter protein levels upon MAV-1 infection 51

Figure 2.9 PKR is not depleted by lysosomal degradation during MAV-1 infection..... 52

Figure 2.10 PKR is depleted by proteasomal degradation during MAV-1 infection 54

Figure 2.11 Delayed proteasome inhibition does not prevent PKR depletion during MAV-1 infection 55

Figure 2.12 PKR is not detectably ubiquitinated during MAV-1 infection..... 57

Figure 2.13 PKR is actively depleted early in infection 59

Figure 2.14 Viral replication can be detected at 24 hpi by qPCR..... 60

Figure 2.15 Early gene expression is required for PKR depletion by MAV-1 61

Figure 2.16 E1A and E3 are not required for PKR degradation during MAV-1 infection..... 64

Figure 3.1 GCN2 (*Eif2ak4*) domains, adapted from Figure 1B from Jaspart et al 91

Figure 3.2 *Atc* mutation reduces survival of MAV-1-infected mice..... 95

Figure 3.3 Viral yield in wild type and GCN2$^{-/-}$ primary macrophages and MEFs 96

Figure 3.4 Viral load is increased in the cecum of GCN2$^{-/-}$ (*atc*) mice 98

Figure 3.5 Comparison of infectious virus and viral DNA yields in brains and livers of MAV-1-infected wild type and GCN2$^{-/-}$ mice 99

Figure 3.6 Changes in cytokine levels between MAV-1-infected *atchoum* and wild type mouse brains..... 102

Figure 4.1 PKR degradation during MAV-1 infection 118

Figure 4.2 *Atc* peritoneal macrophages have a higher increase in phosphorylated eIF2α during MAV-1 infection..... 131

ABSTRACT

During viral infection, a major innate host defense mechanism is to reduce global protein synthesis by phosphorylation of eukaryotic translation inhibition factor 2α (eIF2α). eIF2α is phosphorylated by four different cellular kinases, protein kinase R (PKR), general control nonderepressible 2 (GCN2), PKR-like endoplasmic reticulum kinase, and heme-regulated inhibitor, each responding to a different cellular stress. GCN2, which phosphorylates eIF2α in response to amino acid starvation, UV irradiation, and oxidative stress, can also phosphorylate eIF2α in response to viral infection. PKR senses double-stranded RNA produced by virus infection. Many viruses have methods of inhibiting PKR activation or its downstream effects, thus circumventing protein synthesis shutdown. These methods include sequestering double-stranded RNA or producing proteins that bind to and inhibit PKR activation.

Here we describe our finding that PKR was antiviral in mouse adenovirus type 1 (MAV-1) infection. We also showed that in multiple cell types, PKR was depleted during MAV-1 infection. Inhibiting the proteasome reduced the PKR depletion seen in MAV-1-infected cells, indicating that proteasomal degradation is responsible for PKR degradation during MAV-1 infection. Time course experiments showed that the degradation occurred early after infection. Infecting cells with UV-inactivated virus prevented PKR degradation, whereas inhibiting viral DNA replication did not. Together these results suggest that an early viral gene is responsible for the degradation. Degradation of PKR is a rare mechanism to oppose PKR activity, and it has

only been described in six RNA viruses. To our knowledge, this is the first example of a DNA virus counteracting PKR by degrading it.

In addition to PKR being degraded by MAV-1 during infection, we tested whether GCN2 plays an antiviral role, as seen for several other viruses. Here we describe that $GCN2^{-/-}$ deficient (*atc*) mice and peritoneal macrophages were significantly more susceptible to infection by MAV-1. However, *atc* mouse embryonic fibroblasts had similar viral yields compared to wild type mouse embryonic fibroblasts, suggesting that there is a cell-type specific antiviral effect of GCN2. There were no differences in viral yields in infected organs of *atc* mice at 8 days post infection compared to wild type organs, except for the cecum, indicating that the difference in survival between *atc* and wild type mice is not likely a result of increased viremia in *atc* mice. There was also no significant difference in histology of organs from MAV-1-infected *atc* and wild type mice. However, cytokine analysis showed that MAV-1-infected *atc* mice had significantly higher levels of interleukin 1α, interleukin 1β, and interferon γ in the brain compared to infected wild type mouse brains at 7 days post infection, suggesting that a difference in inflammatory response could be responsible for the decreased survival of *atc* mice in response to MAV-1 infection. Determining how GCN2 affects the immune response to MAV-1 infection could provide insight into how GCN2 is playing an antiviral role in DNA virus infection.

Chapter I

Introduction

Adenoviruses

Adenoviruses are non-enveloped double-stranded (ds) DNA viruses that have an icosahedral shape and replicate in the nucleus. Within the *Adenoviridae* family, there are five genera, encompassing hundreds of different adenoviruses that infect almost every vertebrate species (1). Depending on the serotype, human adenoviruses (hAds) can cause upper respiratory, ocular, or gastrointestinal tract infections (1, 2). In immunocompromised patients, hAd infections can also result in viral encephalitis, hepatitis, myocarditis, and pneumonia (2). Adenoviruses are generally species-specific, with productive infections limited to the natural host (1). Thus, little is known about how hAds cause such severe complications, because there is a lack of a good small animal models of hAd infection. Mouse adenovirus type 1 (MAV-1) provides a good model to study adenovirus pathogenesis. It has some features in common with hAd pathogenesis, for example, it causes similar disseminated infection and encephalitis in immunocompromised mice (3-5) as well as maintaining a similar persistence after acute infection (6-8). MAV-1 infects brain endothelial cells, astrocytes, microglia, monocytes, and macrophages (9) and causes a breakdown of the blood-brain barrier by reducing the number of tight junction proteins expressed on brain endothelial cells (10). This breakdown in the blood-brain barrier allows leukocytes to infiltrate, and it leads to viral encephalitis. Viral encephalitis is associated with increased levels

of cytokines and chemokines, including MCP-1, IL-6, IL-1α, IL-1β, and IL-10 (11). During MAV-1 infection, IL-1 plays an important role and without it, IFN-β signaling can lead to increased neuroinflammation (12). MAV-1 infection also triggers an adaptive immune response in T-cells and B-cells (13, 14). Mice deficient in T- and/or B-cells are highly susceptible to MAV-1 infection (13-16); B-cells are important to prevent dissemination of the virus within mice due to the production of early T-cell-independent neutralizing antibody and antiviral immunoglobulin M (13). T-cells contribute to acute immunopathology and to long term control of MAV-1 infection (14).

Adenovirus infection can be classified into six stages (Fig. 1.1) (17). First, the adenovirus binds to receptors on the outside of the cell using the fiber knobs (18). The virus is then endocytosed by the cell and the virion sheds the fiber proteins and escapes the endosome (19). Once the adenovirus has escaped the endosome and reached the nucleus, the viral DNA is injected into the nucleus, and transcription of early genes by the host polymerase II begins (19, 20). After the synthesis of early proteins, viral DNA replication begins in the nucleus. Next, transcription of late viral genes begins and late viral proteins are translated. Once late viral proteins have been produced, the virions can be assembled (21). After the virion is matured, it escapes the cell.

The adenovirus genome is transcribed from both DNA strands (Fig. 1.2). The early genes are expressed prior to viral DNA replication, and the late genes are produced once the viral DNA has been replicated (22). The early genes, E1, E2, E3, and E4 are categorized into four groups based on the locations of the promoters (23). The late genes largely consist of structural proteins and are divided into five groups, L1-L5, and include proteins encoding hexon, penton base, fiber,

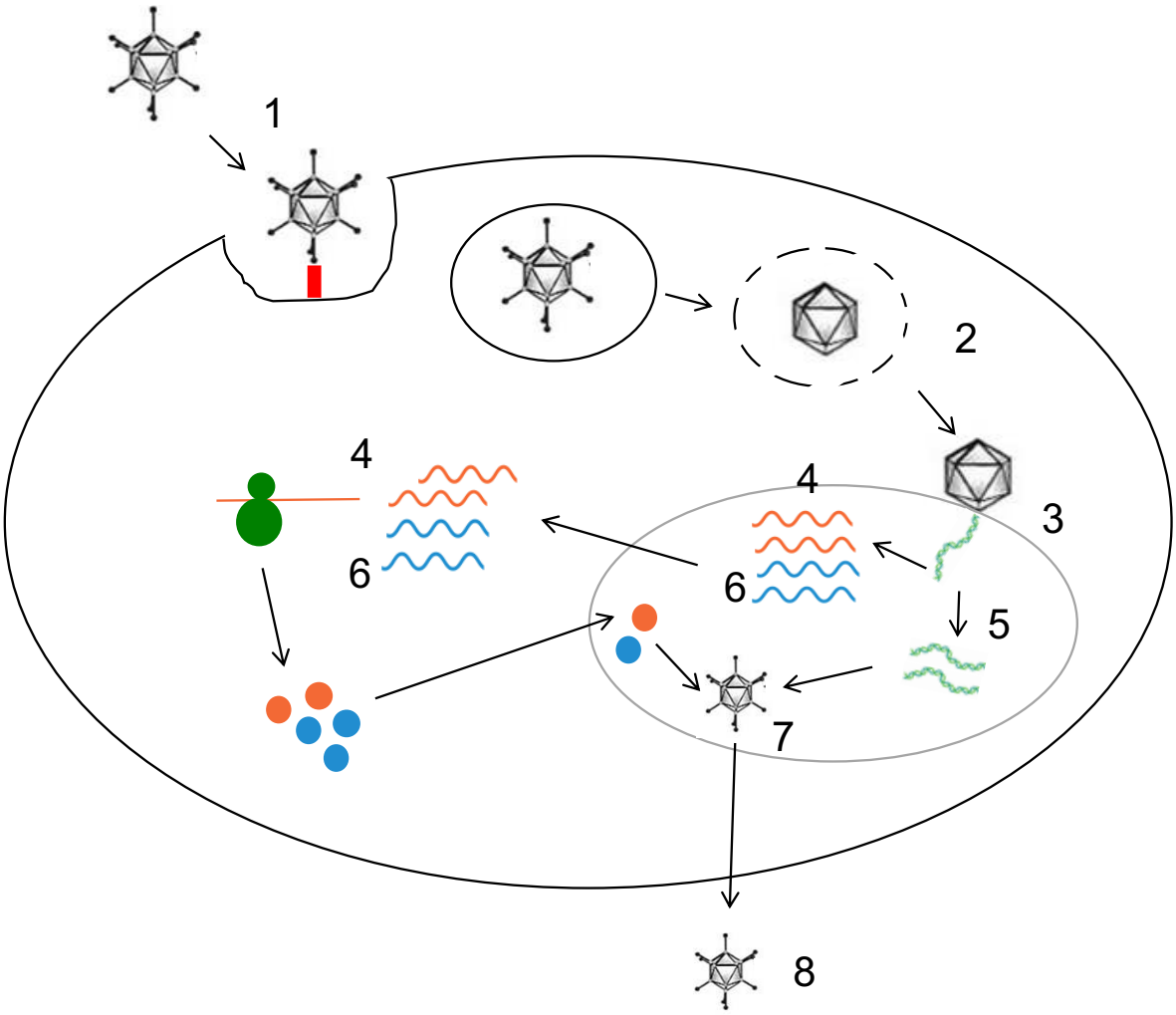

Figure 1.1 Adenovirus life cycle. (1) The adenovirus virion binds to receptors on the outside of the cell and is endocytosed into the cell. (2) The virion sheds fiber proteins and escapes the endosome. (3) Viral DNA is injected into the nucleus (green). (4) Early viral genes are transcribed (orange) and early viral proteins are translated. (5) Viral DNA is replicated in the nucleus. (6) Late viral genes are transcribed (blue) and late viral proteins are translated. (7) New virions are assembled. (8) New virions escape the cell.

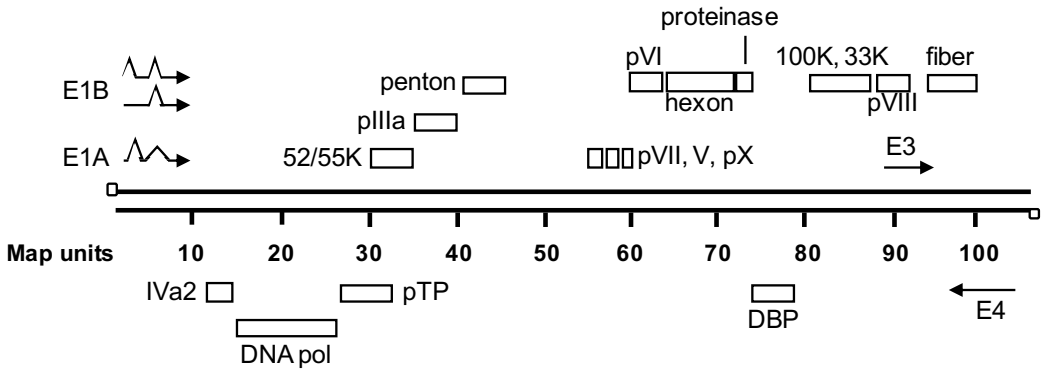

Figure 1.2 MAV-1 genome structure. The adenovirus genome is divided into early genes and late genes. Early genes (E1, E3, E4, and E2 genes encoding DNA polymerase [DNA pol], the precursor of the terminal protein [pTP], and the DNA binding protein [DBP]) are produced before viral DNA replication, and late genes (52/55K, pIIIa, penton, pVII, V, pX, pVI, hexon, proteinase, 100K, 33K, pVIII, fiber, and IVa2) are produced after viral DNA replication.

and core proteins (24-26). Transcription of these late genes is driven by the major late promoter, which is about 16.8 map units from the left end of the genome in hAd (27, 28) and each late mRNA contains the same 5' untranslated region called the tripartite leader, which enhances translation of these genes during infection (29, 30).

Translation control by eIF2α kinases

Translation control in the cell involves eukaryotic translation initiation factor 2α (eIF2α) (Fig. 1.3). eIF2α functions as part of the initiation complex during translation by forming a ternary complex with Met-tRNA and GTP in a reaction catalyzed by eIF2B (31). This complex then binds to the 40S ribosome subunit to form a pre-initiation complex. When eIF2α is phosphorylated on serine residue 51 (specific residue for human eIF2α) by an eIF2α kinase (purple oval, Fig. 1.3), eIF2α forms a stable complex with eIF2B instead of Met-tRNA, leading to a reduction in protein synthesis (7, 32-34).

The cell is able to respond to specific stresses and inhibit translation through four eIF2α kinases that phosphorylate eIF2α in response to different stimuli. These kinases, protein kinase R (PKR), heme-regulated eIF2α kinase, general control nonderepressible 2 (GCN2), and PKR-like endoplasmic reticulum kinase, all share homology in their kinase domains, but have unique activation domains (35-40). PKR functions as part of the innate immune system, becoming activated when it binds to dsRNA produced by viruses (41-43); heme-regulated eIF2α kinase is primarily expressed in erythrocytes and is activated by low levels of heme within the cell (44); PKR-like endoplasmic reticulum kinase is a transmembrane kinase that is activated by endoplasmic reticulum stress (35); and GCN2 senses uncharged tRNA and becomes activated under amino acid starvation conditions, UV irradiation, and oxidative stress (45, 46). PKR also

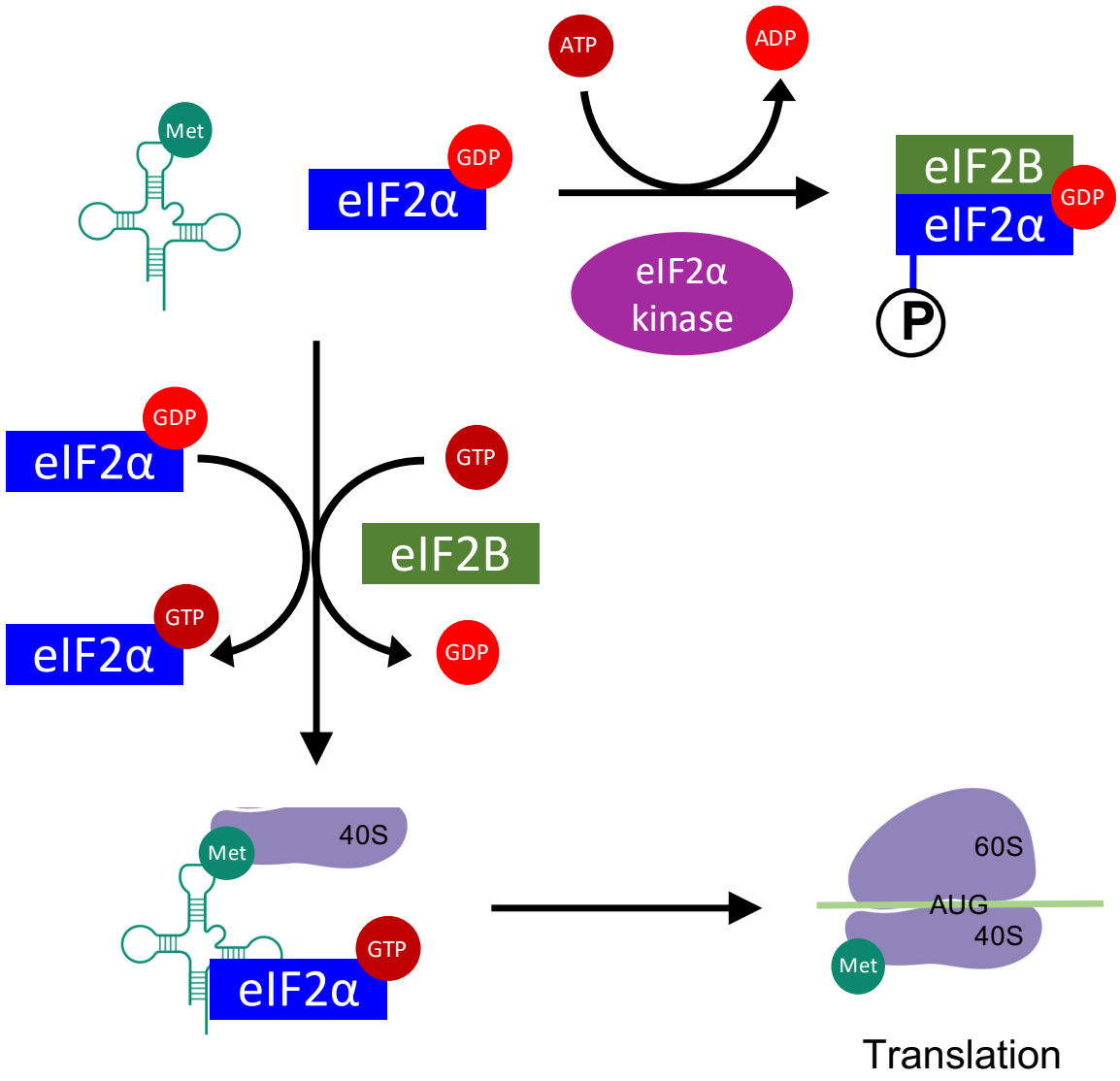

Figure 1.3 Translation control by eIF2α. Translation factor eIF2α forms a ternary complex with GTP and a Met-tRNA in a reaction catalyzed by eIF2B. This complex binds to the 40S ribosomal subunit to form a pre-initiation complex that scans to the initiator AUG, and with GDP hydrolysis, binds the 60S subunit, leading to translation. When eIF2α is phosphorylated by an eIF2α kinase, it forms a stable complex with eIF2B and no longer forms a pre-initiation complex, leading to a reduction in translation.

can contribute to the establishment of the antiviral state in some viral infections by indirectly stabilizing type I interferon mRNAs (47).

Protein degradation within the cell

While the eIF2α kinases affect protein production through translational control, the lysosomal and proteasomal degradation pathways modulate protein degradation. Lysosomes are membrane-bound organelles that contain various digestive enzymes (48). Proteins can enter the lysosome through chaperone-mediated autophagy, the fusion of an autophagosome with the lysosome (macroautophagy), or by invagination of the lysosomal membrane to specifically uptake cytosolic proteins (microautophagy) (Fig. 1.4) (49). Most proteins, however, are degraded by the ubiquitin-proteasome pathway (50).

Proteasomal degradation generally involves modification of the protein to be degraded by ubiquitin. Ubiquitin is a highly conserved, 76-residue protein that is conjugated to proteins using three distinct enzymes (Fig. 1.5) (51). First, a ubiquitin activating enzyme, E1, activates ubiquitin. Next, the ubiquitin is transferred from the ubiquitin-E1 complex to a ubiquitin-conjugating enzyme, E2. Finally, E2 conjugates the ubiquitin to the targeted protein that is bound to an E3 ubiquitin ligase. The E3 ligases, along with other adaptor proteins, serve as the scaffolding to bring together the ubiquitin-E2 complex and the protein to be targeted for proteasomal degradation and allow for much of the specificity of the ubiquitin-proteasome pathway (52). Though most proteins are targeted to the proteasome through ubiquitin conjugation, there are a few ubiquitin-independent mechanisms (53). These include proteins that have ubiquitin-independent degron sequences, or chaperone proteins that cause proteasomal localization.

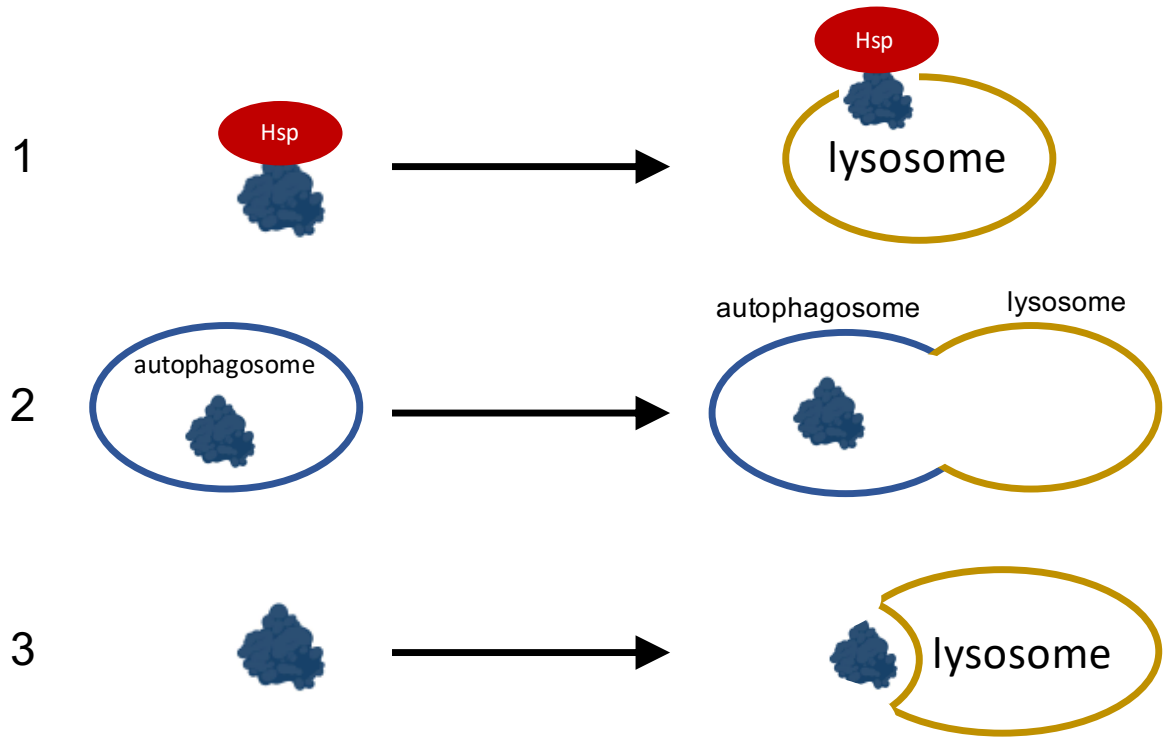

Figure 1.4 Lysosomal degradation. Proteins (blue) can be degraded by the lysosome through three methods: (1) Chaperone-mediated autophagy, where a chaperone protein (red, here Hsp as an example) guides another protein directly into the lysosome; (2) macroautophagy, where proteins are enclosed in an autophagosome that fuses to a lysosome, leading to protein degradation; or (3) microautophagy, where the lysosome itself invaginates to take in specific cytosolic proteins.

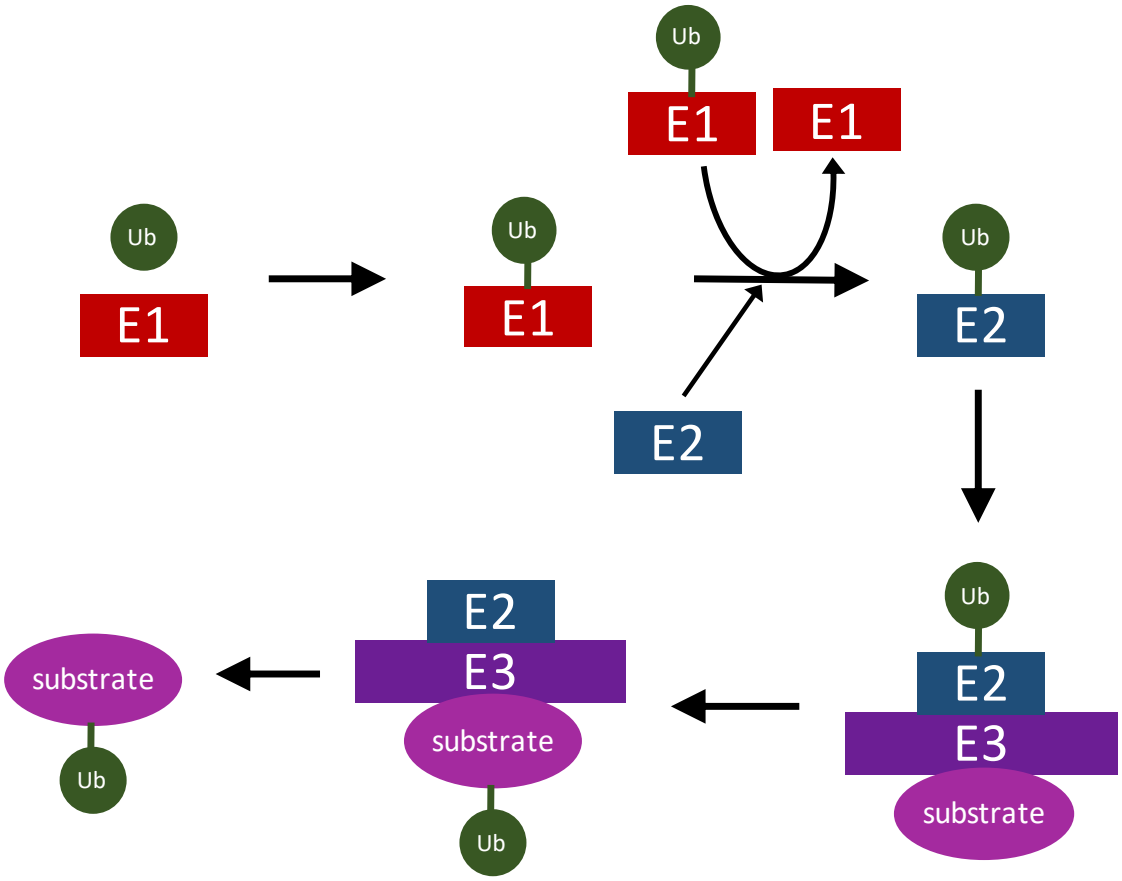

Figure 1.5 Ubiquitination of protein substrates. Proteins are conjugated to a ubiquitin (green) using three enzymes. First, E1 binds to ubiquitin. Next, ubiquitin is transferred to E2. Finally, the E2/ubiquitin complex binds to E3, which serves as the adaptor protein for the substrate to be degraded. The ubiquitin is then transferred to the substrate protein.

Once a protein has been ubiquitinated (or localized to the proteasome by ubiquitin-independent means), it is then degraded by the 26S proteasome (51, 52, 54). The proteasome is comprised of a 20S barrel-shaped core, with two 19S subunits on either end. Ubiquitinated proteins enter the proteasome through one of the 19S subunits, where the ubiquitin chain is cleaved off, broken down, and released into the cytoplasm. The protein then travels through the 20S barrel, is degraded, and then small amino acid products exit through the other 19S subunit. This activity of the proteasome helps to mediate protein turnover and remove any improperly folded or damaged proteins within the cell. Additionally, the proteasome plays a role in immunity by generating antigenic peptides that can be presented on the outside of the cell so that the host can identify foreign peptides more readily (52, 55).

Immune response to adenovirus infection

During viral infection, one trigger of the innate immune response is dsRNA fragments produced by the virus during replication (56, 57). The presence of dsRNA has been confirmed in cells infected with hAds, herpes simplex virus, and vaccinia virus using a dsRNA-specific antibody or other methods (58, 59). In DNA viruses, it has been proposed that dsRNA results from overlapping convergent transcription during infection.

Activation of PKR is a major innate immune response to viral infection (Fig. 1.6). PKR is an interferon-induced protein that is comprised of two major domains, an N-terminal dsRNA binding domain and a C-terminal serine/threonine kinase domain (39, 60). When PKR binds to dsRNA (41-43), it becomes activated by dimerizing and transautophosphorylating on multiple resides, including residues S242, T255, T258, and T446 (61-66). When activated, PKR phosphorylates eIF2α, causing inhibition of protein synthesis and reduced viral replication

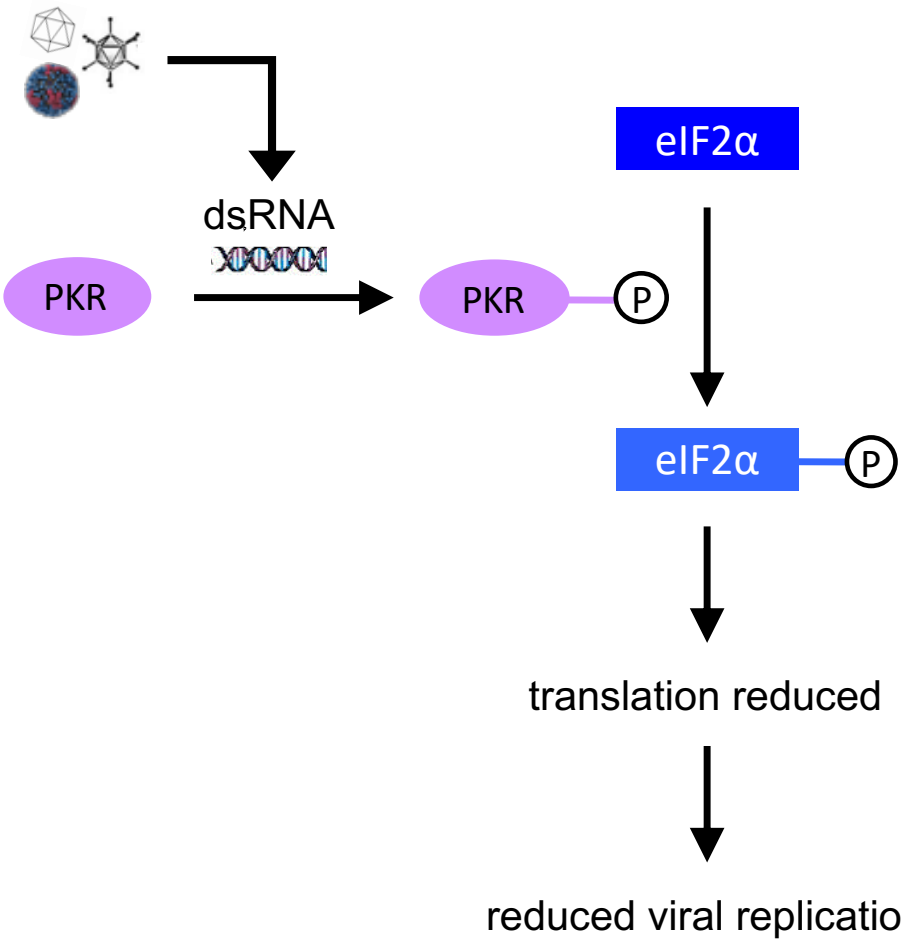

Figure 1.6 Translation arrest by PKR. PKR is activated by dsRNA, which is produced by viruses when they replicate. When PKR is activated, it phosphorylates translation factor eIF2α, which reduces translation and leads to reduced viral replication.

(7, 32-34). This inhibition is not specific to viral mRNA, and leads to an overall global reduction in translation. However, there is an upregulation in transcription of specific stress response genes such as ATF-3, which can lead to apoptosis (67).

Virus interactions with host protein PKR

Many viruses encode gene products that block PKR activation or inhibit its ability to phosphorylate eIF2α (68). A common mechanism is to produce a viral protein that binds and sequesters dsRNA, blocking its interaction with PKR. Examples of this are vaccinia virus E3L (69-71), influenza virus NS1 (72, 73), and Ebola virus protein VP35 (74). Other viruses produce proteins or RNA that bind directly to PKR to inhibit its activation, such as herpes simplex virus US11 (75, 76), HIV-1 Tat protein (77, 78) or TAR RNA (79), and hAd virus-associated (VA) RNAs (7, 80-82).

Degradation of PKR by viruses is a less documented method of regulating PKR. To date PKR degradation has been reported in six RNA viruses: Toscana virus (TOSV) (83), Rift Valley fever virus (RVFV) (84-86), poliovirus (87, 88), foot-and-mouth disease virus (FMDV) (89, 90), encephalomyocarditis virus (EMCV, strain mengovirus) (91, 92), and enterovirus A71 (93).

RVFV and TOSV both degrade PKR via proteasomal mechanisms involving a viral nonstructural protein (NSs) (86, 94, 95). RVFV NSs recruits a SCF (SKP1-CUL1-F-box)^{FBXW11} E3 ubiquitin ligase to ubiquitinate PKR and target it to the proteasome (Fig. 1.7) (86, 95). This degradation occurs in nuclear and cytoplasmic compartments, even though PKR mRNA levels are increased during infection, and degradation does not require PKR phosphorylation (85). However, even though an E3 ubiquitin ligase is recruited to PKR and PKR is degraded by the proteasome, ubiquitination could not be demonstrated (86). This is also true for another host

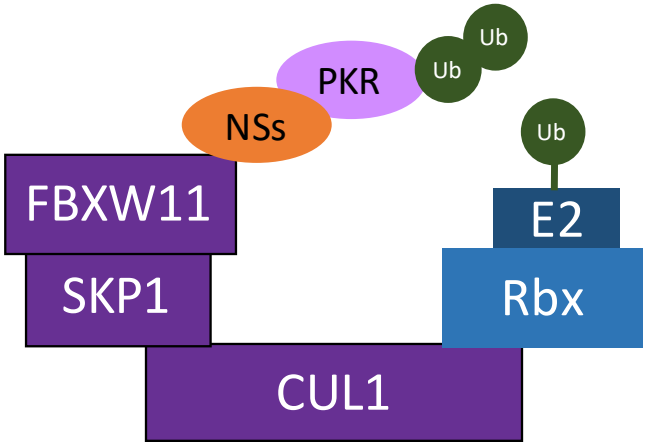

Figure 1.7 PKR degradation by Rift Valley fever virus (RVFV), adapted from Figure 5E from Mudhasani et al. As described in Mudhasani et al., 2016 and Kainulainen et al., 2016, NSs from RVFV binds to PKR and recruits the E3 ligase complex consisting of CUL1, SKP1, and FBXW11. This complex, in addition to an E2 enzyme and the E2 adaptor Rbx, conjugates ubiquitin (green) to PKR, leading to its degradation.

protein, p62, which is involved in transcriptional regulation, and which is degraded by a similar E3 ligase complex recruited by RVFV NSs (96). p62 degradation is a result of proteasome activity mediated by NSs, yet ubiquitination could not be demonstrated. The mechanism for PKR proteasomal degradation by NSs has not been described for TOSV (94). However, similar to RVFV, TOSV NSs interacts with PKR, and PKR phosphorylation is not required for degradation by TOSV NSs.

In FMDV infection, although PKR mRNA levels are increased, phospho-PKR and PKR protein levels begin decreasing as soon as 12 hours post infection (hpi) in PK-15 cells (89, 90). Additionally, if the interferon stimulation pathway is interrupted, PKR protein levels start to decrease as soon as 6 hpi. FMDV uses the other major cellular protein degradation pathway, the lysosome, to degrade PKR during infection (90). Though the mechanism is unclear, expression of the major FMDV protease $3C^{pro}$ is required for PKR degradation by the lysosome. However, $3C^{pro}$ does not interact with PKR, nor is its protease activity required for PKR degradation.

The enterovirus A71 protease $3C^{pro}$ causes PKR degradation by direct interaction, cleaving PKR at a site distinct from where PKR is cleaved during apoptosis (93). Interestingly, the kinase activity of PKR reduces enterovirus A71 replication, but a kinase-dead PKR increases viral protein accumulation. Viral $3C^{pro}$ cleaves PKR between the dsRNA-binding domain and the kinase domain, so the free dsRNA-binding domain then binds free dsRNA and prevents further activation of functional PKR molecules (Fig. 1.8).

The mechanism of PKR depletion by poliovirus is unclear, though gene expression is required, and the major poliovirus proteases (2A and 3C) are not directly involved (87, 88). Overexpression of the 2A, 3C, or 3CD proteases in HeLa cells does not reduce PKR protein levels; however, the addition of EDTA, a protease inhibitor, or trypsin to poliovirus-infected

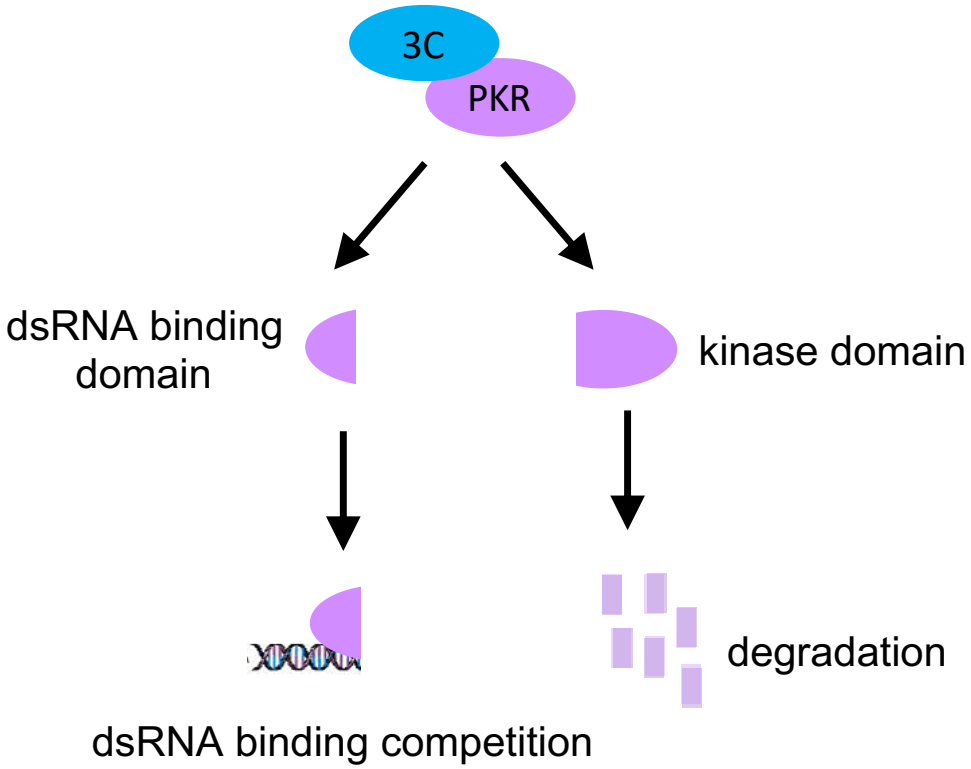

Figure 1.8 PKR degradation by enterovirus A71, adapted from Figure 8 from Chang et al. As described in Chang et al., 2017, $3C^{pro}$ (3C, blue) from enterovirus A71 binds to PKR and cleaves it at Q188-S189, between the dsRNA binding domain and the kinase domain. Once cleaved, the fragment with the kinase domain is degraded, and the fragment with the dsRNA binding domain binds to and sequesters dsRNA produced by the virus. Sequestering dsRNA reduces the activation of uncleaved PKR proteins, thus increasing viral replication.

extracts prevents PKR depletion, suggesting a protease with a cation requirement is responsible for PKR degradation (87). Additionally, treatment of infected extracts with RNase A or RNase III also prevents PKR degradation, indicating that there is also an RNA component required for PKR depletion by poliovirus. Much like RVFV and TOSV, PKR phosphorylation is not required for PKR depletion.

During EMCV infection in HeLa cells, PKR is depleted as early 2 hpi, and phospho-PKR is depleted by 4 hpi. When the HeLa cells were treated with interferon prior to infection, both phospho-PKR and PKR protein levels were elevated at 2 and 4 hpi. This is not surprising, because PKR is an interferon-stimulated gene (39, 60). However, even with the initial increase in PKR protein, both phospho-PKR and PKR protein levels begin to decrease by 6 hpi, indicating that the virus depletes PKR. It is likely that the depletion takes longer than in non-interferon-stimulated cells because there is more PKR present in the cell to begin with. The mechanism by which EMCV depletes PKR during infection is unknown (91, 92).

Virus interactions with host protein GCN2

There is much research implicating PKR in the innate immune response to a wide range of viruses, and there are a variety of virus counter-responses. In contrast, GCN2, which becomes activated and phosphorylates eIF2α in response to amino acid deprivation, UV irradiation, and oxidative stress, is less well studied as a player in the innate immune response to viruses (Fig. 1.9). Virus infections may be indirectly activating GCN2 by triggering changes in amino acid metabolism.

For example, mouse cytomegalovirus (MCMV) infection leads to the production of 25-hydroxycholesterol, reducing the levels of intracellular cysteine and/or generating oxidative

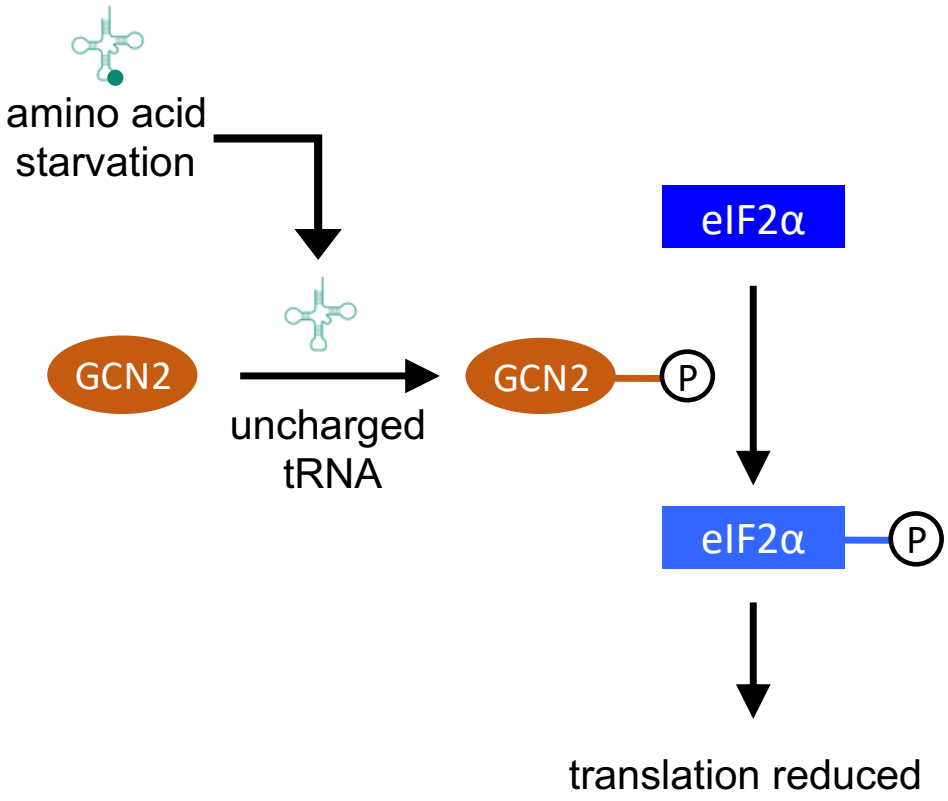

Figure 1.9 Translation arrest by GCN2. GCN2 is activated by amino acid deprivation, which causes an increase in uncharged tRNA binding to GCN2. When GCN2 is activated by phosphorylation, it phosphorylates translation factor eIF2α, which reduces translation.

stress, thus activating GCN2 (97). 25-hydroxycholesterol triggers antiviral eIF2α phosphorylation, but only when GCN2 is present in the cells (97). Additionally, when $GCN2^{-/-}$ peritoneal macrophages and mice are infected with MCMV, they have significantly increased susceptibility compared to wild type macrophages and mice (98). Taken together, these results show that GCN2 is activated during MCMV during infection and plays an important antiviral role.

Another virus that triggers GCN2 activation by depleting amino acids is the yellow fever virus vaccine (YF-17D) (99). After incubation with YF-17D, dendritic cells have significantly lower levels of free arginine and a subsequent increase in phosphorylated GCN2 and eIF2α. In $GCN2^{-/-}$ dendritic cells incubated with YF-17D, autophagy is reduced compared to wild type dendritic cells and there is reduction in the proliferation of $CD8^{+}$ and $CD4^{+}$ YF-17D-specific T-cells, suggesting that GCN2 plays a role in promoting antigen cross presentation and priming secondary immunity during YF-17D immunization.

Another possible explanation for GCN2 playing an antiviral role during infection is when viruses directly activate GCN2. For example, Sindbis virus (SV) RNA binds and activates GCN2 directly (100). Two specific regions in the SV RNA, GCN2-activating regions, bind directly to the HisRS-like domain of GCN2 as long as they are not denatured, suggesting that the secondary structures of these regions may mimic uncharged tRNAs. In the presence of SV RNA, GCN2 and eIF2α phosphorylation are increased, leading to a reduction in SV RNA replication. Additionally, overexpression of GCN2 in SV-infected cells reduces virus yield, assayed by plaque assays. These data show that GCN2 plays an antiviral role during SV infection by inhibiting SV RNA replication through eIF2α phosphorylation after being activated by SV RNA.

The prunnus necrotic ringspot virus (PNRSV), a plant virus, produces a movement protein, MP, that enlarges the plasmodesmata pores to allow for cell-to-cell movement of the virus. MP increases eIF2α phosphorylation when it is expressed in yeast (101). Since GCN2 is the only eIF2α kinase in yeast, this suggests that MP may activate GCN2 during PNRSV infection of plants. However, the mechanism for this activation is unknown.

Data suggest that GCN2 plays an antiviral role during vesicular stomatitis virus (VSV) infection, but the mechanism is unknown. VSV has increased viral replication and viral protein accumulation in $GCN2^{-/-}$ mouse embryonic fibroblasts (MEFs) compared to wild type MEFs (102, 103). Additionally, when a mutant of GCN2 containing only the eIF2α kinase domain is transfected into VSV-infected cells and becomes activated, viral protein accumulation is reduced compared to cells in which this mutant protein is present but inactive (103). When MEFs expressing a non-phosphorylatable form of eIF2α are infected with VSV, there is no difference in viral protein accumulation compared to wild type MEFs (103). This suggests that GCN2 activation combats VSV infection in an eIF2α-independent manner, implying that there are antiviral downstream targets for activated GCN2 other than eIF2α during infection.

While MCMV, YF-17D, SV, and PNRSV activate GCN2 directly or indirectly, some viruses have also evolved methods for inactivating or inhibiting GCN2 activity, either by direct interaction with GCN2 or by affecting an upstream or downstream effector of GCN2. Herpes simplex virus 1 (HSV-1) indirectly inhibits GCN2 by targeting GCN1, an upstream activator of GCN2 (104, 105). HSV-1 glycoprotein H (gH) directly interacts with GCN1, changing its localization from the cytoplasm to the nuclear rim, and overexpression of gH reduces eIF2α phosphorylation compared to cells with no gH (104). Taken together, these results suggest that HSV-1 reduces eIF2α phosphorylation by sequestering GCN1 and keeping it from activating

GCN2 during infection. Severe acute respiratory syndrome-related coronavirus also indirectly inhibits GCN2 by causing a depletion of GCN2 protein from the cell late in infection, likely causing this reduction by decreasing host gene transcription overall (106).

The K3L protein from vaccinia virus also inactivates GCN2 (107). K3L binds to the kinase domain of GCN2, and this binding does not require the GCN2 kinase activity. When K3L is expressed in yeast, it reduces GCN2 and eIF2α phosphorylation, even under starvation conditions, when GCN2 would normally be activated and eIF2α should have increased phosphorylation.

Like SV RNA, HIV-1 RNA also triggers GCN2 activation directly by binding to the HisRS-like domain of GCN2, causing an increase in eIF2α phosphorylation (Fig. 1.10) (108). However, HIV-1 encodes two different proteins that interact with GCN2. The first is HIV-1^{pro}, a protease that cleaves human and mouse GCN2 after amino acid 560/559 (108). Once GCN2 is cleaved by HIV-1^{pro}, it loses nearly all of its capability to phosphorylate eIF2α. The second viral protein employed by HIV-1 to inhibit GCN2 activity is integrase (IN) (109, 110). HIV-1 IN is involved in HIV-1 genome integration into the host DNA during infection (110). While IN does not activate GCN2, it binds directly to the kinase domain of GCN2 in the same region that eIF2α and K3L bind. This suggests that IN may act as a substrate for GCN2 and reduce its activity, because translation is higher in the presence of IN (109, 110). However, GCN2 phosphorylates HIV-1 IN, leading to reduced IN enzymatic activity and fewer integration events during infection (110).

Interestingly, HIV-1 also has mechanisms that use GCN2 activation to its advantage. When the GCN2/eIF2α phosphorylation pathway is activated and global translation is decreased, expression of some host genes involved in amino acid biosynthesis is upregulated, including

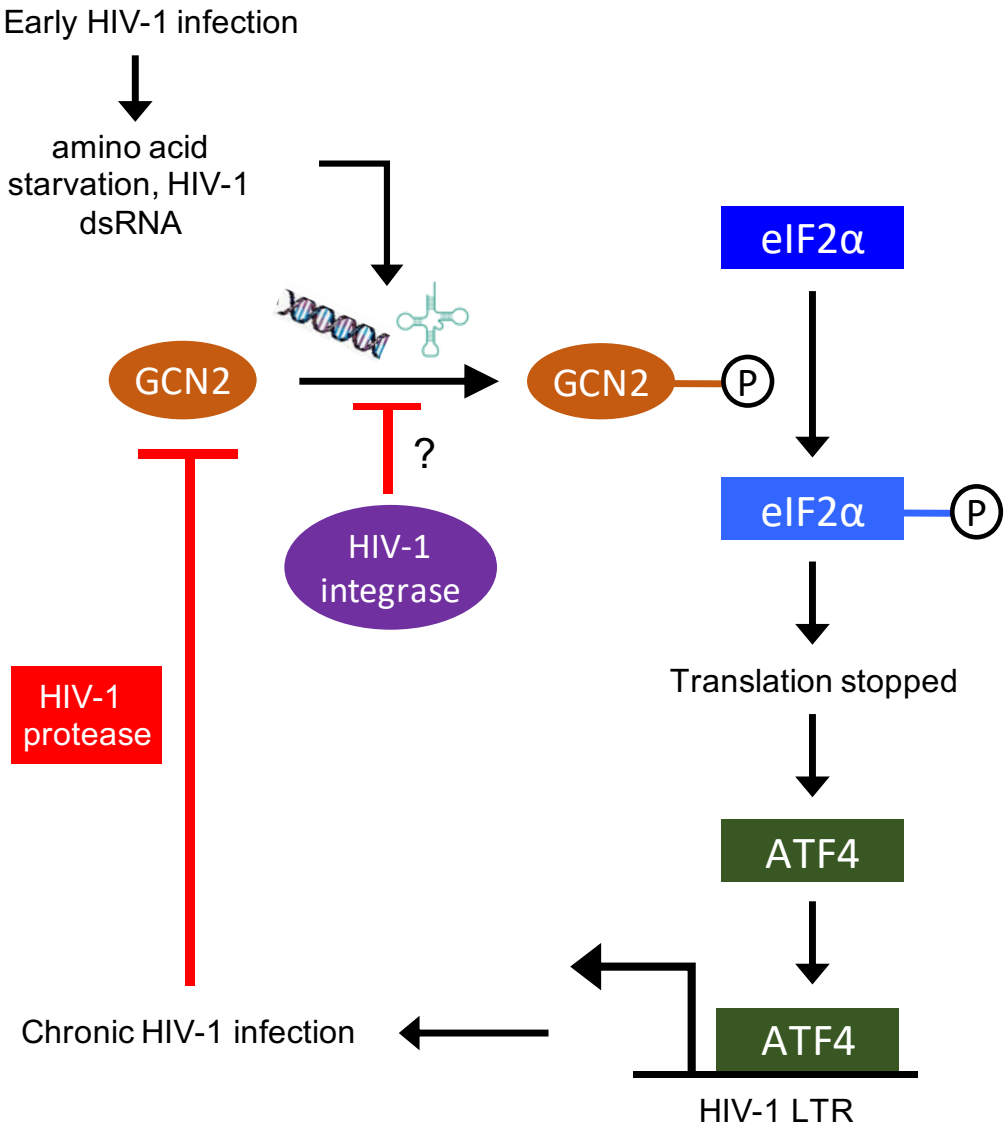

Figure 1.10 HIV-1 interactions with GCN2, adapted from Figure 7F from Jiang et al. As described in Jiang et al., 2017 and del Pino et al., 2012, HIV-1 activates GCN2 by producing RNA that binds to the HisRS domain of GCN2 and by reducing free amino acid levels. GCN2 activation leads to eIF2α phosphorylation, which reduces translation but stimulates the transcription of ATF4. ATF4 binds to the LTR of HIV-1 and causes reactivation of latent HIV-1, leading to increased viral replication. HIV-1 produces a protease that cleaves GCN2, and thus viral protein translation can occur. HIV-1 integrase also binds to GCN2 and acts as a psuedosubstrate for GCN2, though it is unclear if that reduces eIF2α phosphorylation.

ATF4 (111). ATF4 mRNA binds to the HIV-1 LTR and enhances HIV-1 transcription and replication (112). Taken together, these data suggest that not only can HIV-1 use GCN2 activation to its advantage, but it can also impair GCN2 activity to maintain protein translation in HIV-1-infected cells.

Conclusion

In the next two chapters, I will discuss the role of PKR and GCN2 during MAV-1 infection. $PKR^{-/-}$ mice, macrophages, and MEFs were more susceptible to MAV-1 infection compared to wild type mice and cells. PKR mRNA transcription was significantly increased by 72 hpi in infected macrophages compared mock infected macrophages, but PKR protein levels at that time point were significantly reduced in infected macrophages. PKR protein was also almost completely depleted by 24 hpi in C57BL/6 MEFs and CMT93 cells. Treating cells with proteasome inhibitors prevented PKR depletion, indicating that MAV-1 infection causes PKR to be degraded by the proteasome. PKR was only degraded when early viral genes were expressed during infection, indicating that an early viral gene is responsible for mediating PKR degradation. Degradation of PKR has not previously been reported for a DNA virus. $GCN2^{-/-}$ (*atchoum*) mice and macrophages were more susceptible to MAV-1 infection compared with wild type animals, though there was no difference in viral yield between organs from wild type and *atchoum* mice.

Bibliography

1. Harrach B, Benko M, Both GW, Brown M, Davison AJ, Echavarria M, Hess M, Jones MS, Kajon A, Lehmkuhl HD, Mautner V, Mittal SK, Wadell G. 2011. Virus Taxonomy: Ninth report of the international committee on taxonomy of viruses, p 128. *In* King AMQ, Adams MJ, Carstens EB, Lefkowitz EJ (ed). Elsevier.

2. Ghebremedhin B. 2014. Human adenovirus: Viral pathogen with increasing importance. Eur J Micro Immunol 4:26-33.

3. Guida JD, Fejer G, Pirofski LA, Brosnan CF, Horwitz MS. 1995. Mouse adenovirus type 1 causes a fatal hemorrhagic encephalomyelitis in adult C57BL/6 but not BALB/c mice. J Virol 69:7674-81.

4. Spindler KR, Fang L, Moore ML, Hirsch GN, Brown CC, Kajon A. 2001. SJL/J mice are highly susceptible to infection by mouse adenovirus type 1. J Virol 75:12039-46.

5. Kring SC, King CS, Spindler KR. 1995. Susceptibility and signs associated with mouse adenovirus type 1 infection of adult outbred Swiss mice. J Virol 69:8084-8.

6. Smith K, Brown CC, Spindler KR. 1998. The role of mouse adenovirus type 1 early region 1A in acute and persistent infections in mice. J Virol 72:5699-706.

7. Berk AJ. 2013. Adenoviridae: The viruses and their replication. *In* Knipe DM, Howley P (ed), Fields Virology, 6th ed, vol 2. Lippincott Williams & Wilkins, Philadelphia.

8. Zhang Y, Huang W, Ornelles DA, Gooding LR. 2010. Modeling adenovirus latency in human lymphocyte cell lines. J Virol 84:8799-810.

9. Ashley SL, Pretto CD, Stier MT, Kadiyala P, Castro-Jorge L, Hsu TH, Doherty R, Carnahan KE, Castro MG, Lowenstein PR, Spindler KR. 2017. Matrix Metalloproteinase Activity in Infections by an Encephalitic Virus, Mouse Adenovirus Type 1. J Virol 91.

10. Gralinski LE, Ashley SL, Dixon SD, Spindler KR. 2009. Mouse adenovirus type 1-induced breakdown of the blood-brain barrier. J Virol 83:9398-410.

11. Michael BD, Griffiths MJ, Granerod J, Brown D, Davies NW, Borrow R, Solomon T. 2016. Characteristic Cytokine and Chemokine Profiles in Encephalitis of Infectious, Immune-Mediated, and Unknown Aetiology. PLoS One 11:e0146288.

12. Castro-Jorge LA, Pretto CD, Smith AB, Foreman O, Carnahan KE, Spindler KR. 2017. A Protective Role for Interleukin-1 Signaling during Mouse Adenovirus Type 1-Induced Encephalitis. J Virol 91.

13. Moore ML, McKissic EL, Brown CC, Wilkinson JE, Spindler KR. 2004. Fatal disseminated mouse adenovirus type 1 infection in mice lacking B cells or Bruton's tyrosine kinase. J Virol 78:5584-90.

14. Moore ML, Brown CC, Spindler KR. 2003. T cells cause acute immunopathology and are required for long-term survival in mouse adenovirus type 1-induced encephalomyelitis. J Virol 77:10060-70.

15. Charles PC, Guida JD, Brosnan CF, Horwitz MS. 1998. Mouse adenovirus type-1 replication is restricted to vascular endothelium in the CNS of susceptible strains of mice. Virology 245:216-28.

16. Pirofski L, Horwitz MS, Scharff MD, Factor SM. 1991. Murine adenovirus infection of SCID mice induces hepatic lesions that resemble human Reye syndrome. Proc Natl Acad Sci U S A 88:4358-62.

17. Ginsberg HS. 1999. The life and times of adenoviruses. Adv Virus Res 54:1-13.

18. Philipson L, Lonberg-Holm K, Pettersson U. 1968. Virus-receptor interaction in an adenovirus system. J Virol 2:1064-75.

19. Greber UF, Willetts M, Webster P, Helenius A. 1993. Stepwise dismantling of adenovirus 2 during entry into cells. Cell 75:477-86.

20. Ginsberg HS. 1958. Characteristics on the adenoviruses. III. Reproductive cycle of types 1 to 4. J Exp Med 107:133-52.

21. Velicer LF, Ginsberg HS. 1970. Synthesis, transport, and morphogenesis of type adenovirus capsid proteins. J Virol 5:338-52.

22. Thomas GP, Mathews MB. 1980. DNA replication and the early to late transition in adenovirus infection. Cell 22:523-33.

23. Berk AJ, Sharp PA. 1977. Sizing and mapping of early adenovirus mRNAs by gel electrophoresis of S1 endonuclease-digested hybrids. Cell 12:721-32.

24. Berget SM, Sharp PA. 1979. Structure of late adenovirus 2 heterogeneous nuclear RNA. J Mol Biol 129:547-65.

25. Larsson S, Svensson C, Akusjarvi G. 1992. Control of adenovirus major late gene expression at multiple levels. J Mol Biol 225:287-98.

26. Meissner JD, Hirsch GN, LaRue EA, Fulcher RA, Spindler KR. 1997. Completion of the DNA sequence of mouse adenovirus type 1: sequence of E2B, L1, and L2 (18-51 map units). Virus Res 51:53-64.

27. Young CS. 2003. The structure and function of the adenovirus major late promoter. Curr Top Microbiol Immunol 272:213-49.

28. Song B, Hu SL, Darai G, Spindler KR, Young CS. 1996. Conservation of DNA sequence in the predicted major late promoter regions of selected mastadenoviruses. Virology 220:390-401.

29. Logan J, Shenk T. 1984. Adenovirus tripartite leader sequence enhances translation of mRNAs late after infection. Proc Natl Acad Sci U S A 81:3655-9.

30. Berkner KL, Sharp PA. 1985. Effect of the tripartite leader on synthesis of a non-viral protein in an adenovirus 5 recombinant. Nucleic Acids Res 13:841-57.

31. Pakos-Zebrucka K, Koryga I, Mnich K, Ljujic M, Samali A, Gorman AM. 2016. The integrated stress response. EMBO Rep 17:1374-1395.

32. Wek RC. 2018. Role of eIF2alpha kinases in translational control and adaptation to cellular stress. Cold Spring Harb Perspect Biol 10.

33. Farrell PJ, Balkow K, Hunt T, Jackson RJ, Trachsel H. 1977. Phosphorylation of initiation factor elF-2 and the control of reticulocyte protein synthesis. Cell 11:187-200.

34. Tahara SM, Traugh JA, Sharp SB, Lundak TS, Safer B, Merrick WC. 1978. Effect of hemin on site-specific phosphorylation of eukaryotic initiation factor 2. Proc Natl Acad Sci USA 75:789-93.

35. Harding HP, Zhang Y, Ron D. 1999. Protein translation and folding are coupled by an endoplasmic-reticulum-resident kinase. Nature 397:271-4.

36. Berlanga JJ, Herrero S, de Haro C. 1998. Characterization of the hemin-sensitive eukaryotic initiation factor 2alpha kinase from mouse nonerythroid cells. J Biol Chem 273:32340-6.

37. Chen JJ, Throop MS, Gehrke L, Kuo I, Pal JK, Brodsky M, London IM. 1991. Cloning of the cDNA of the heme-regulated eukaryotic initiation factor 2 alpha (eIF-2 alpha) kinase of rabbit reticulocytes: homology to yeast GCN2 protein kinase and human double-stranded-RNA-dependent eIF-2 alpha kinase. Proc Natl Acad Sci U S A 88:7729-33.

38. Shi Y, Vattem KM, Sood R, An J, Liang J, Stramm L, Wek RC. 1998. Identification and characterization of pancreatic eukaryotic initiation factor 2 alpha-subunit kinase, PEK, involved in translational control. Mol Cell Biol 18:7499-509.

39. Meurs E, Chong K, Galabru J, Thomas NS, Kerr IM, Williams BR, Hovanessian AG. 1990. Molecular cloning and characterization of the human double-stranded RNA-activated protein kinase induced by interferon. Cell 62:379-90.

40. Ramirez M, Wek RC, Hinnebusch AG. 1991. Ribosome association of GCN2 protein kinase, a translational activator of the GCN4 gene of Saccharomyces cerevisiae. Mol Cell Biol 11:3027-36.

41. Feng GS, Chong K, Kumar A, Williams BR. 1992. Identification of double-stranded RNA-binding domains in the interferon-induced double-stranded RNA-activated p68 kinase. Proc Natl Acad Sci USA 89:5447-51.

42. Kuhen KL, Samuel CE. 1997. Isolation of the interferon-inducible RNA-dependent protein kinase Pkr promoter and identification of a novel DNA element within the 5'-flanking region of human and mouse Pkr genes. Virology 227:119-30.

43. Patel RC, Sen GC. 1992. Identification of the double-stranded RNA-binding domain of the human interferon-inducible protein kinase. J Biol Chem 267:7671-6.

44. Ranu RS. 1979. Regulation of protein synthesis in rabbit reticulocyte lysates: the hemeregulated protein kinase (HRI) and double stranded RNA induced protein kinase (dRI) phosphorylate the same site(s) on initiation factor eIF-2. Biochem Biophys Res Commun 91:1437-44.

45. Wek RC, Ramirez M, Jackson BM, Hinnebusch AG. 1990. Identification of positive-acting domains in GCN2 protein kinase required for translational activation of GCN4 expression. Mol Cell Biol 10:2820-31.

46. Grallert B, Boye E. 2013. GCN2, an old dog with new tricks. Biochem Soc Trans 41:1687-91.

47. Schulz O, Pichlmair A, Rehwinkel J, Rogers NC, Scheuner D, Kato H, Takeuchi O, Akira S, Kaufman RJ, Reis e Sousa C. 2010. Protein kinase R contributes to immunity against specific viruses by regulating interferon mRNA integrity. Cell Host Microbe 7:354-61.

48. Cooper GM. 2000. Protein Degradation, The Cell: A Molecular Approach, 2nd ed. Sinauer Associates, Sunderland, MA.

49. Klionsky DJ. 2005. The molecular machinery of autophagy: unanswered questions. J Cell Sci 118:7-18.

50. Rock KL, Gramm C, Rothstein L, Clark K, Stein R, Dick L, Hwang D, Goldberg AL. 1994. Inhibitors of the proteasome block the degradation of most cell proteins and the generation of peptides presented on MHC class I molecules. Cell 78:761-71.

51. Glickman MH, Ciechanover A. 2002. The ubiquitin-proteasome proteolytic pathway: destruction for the sake of construction. Physiol Rev 82:373-428.

52. Lecker SH, Goldberg AL, Mitch WE. 2006. Protein degradation by the ubiquitin-proteasome pathway in normal and disease states. J Am Soc Nephrol 17:1807-19.

53. Erales J, Coffino P. 2014. Ubiquitin-independent proteasomal degradation. Biochim Biophys Acta 1843:216-21.

54. Voges D, Zwickl P, Baumeister W. 1999. The 26S proteasome: a molecular machine designed for controlled proteolysis. Annu Rev Biochem 68:1015-68.

55. Shastri N, Schwab S, Serwold T. 2002. Producing nature's gene-chips: the generation of peptides for display by MHC class I molecules. Annu Rev Immunol 20:463-93.

56. Marcus PI, Sekellick MJ. 1977. Defective interfering particles with covalently linked [+/-]RNA induce interferon. Nature 266:815-9.

57. Jacobs BL, Langland JO. 1996. When two strands are better than one: the mediators and modulators of the cellular responses to double-stranded RNA. Virology 219:339-49.

58. Weber F, Wagner V, Rasmussen SB, Hartmann R, Paludan SR. 2006. Double-stranded RNA is produced by positive-strand RNA viruses and DNA viruses but not in detectable amounts by negative-strand RNA viruses. J Virol 80:5059-64.

59. Duesberg PH, Colby C. 1969. On the biosynthesis and structure of double-stranded RNA in vaccinia virus-infected cells. Proc Natl Acad Sci U S A 64:396-403.

60. McCormack SJ, Thomis DC, Samuel CE. 1992. Mechanism of interferon action: identification of a RNA binding domain within the N-terminal region of the human RNA-dependent P1/eIF-2 alpha protein kinase. Virology 188:47-56.

61. Dey M, Mann BR, Anshu A, Mannan MA. 2014. Activation of protein kinase PKR requires dimerization-induced cis-phosphorylation within the activation loop. J Biol Chem 289:5747-57.

62. Taylor DR, Lee SB, Romano PR, Marshak DR, Hinnebusch AG, Esteban M, Mathews MB. 1996. Autophosphorylation sites participate in the activation of the double-stranded-RNA-activated protein kinase PKR. Mol Cell Biol 16:6295-302.

63. Dabo S, Meurs EF. 2012. dsRNA-dependent protein kinase PKR and its role in stress, signaling and HCV infection. Viruses 4:2598-635.

64. Mundschau LJ, Faller DV. 1994. Endogenous inhibitors of the dsRNA-dependent eIF-2 alpha protein kinase PKR in normal and ras-transformed cells. Biochimie 76:792-800.

65. Hovanessian AG, Galabru J. 1987. The double-stranded RNA-dependent protein kinase is also activated by heparin. Eur J Biochem 167:467-73.

66. Galabru J, Hovanessian A. 1987. Autophosphorylation of the protein kinase dependent on double-stranded RNA. J Biol Chem 262:15538-44.

67. Guerra S, Lopez-Fernandez LA, Garcia MA, Zaballos A, Esteban M. 2006. Human gene profiling in response to the active protein kinase, interferon-induced serine/threonine protein kinase (PKR), in infected cells. Involvement of the transcription factor ATF-3 IN PKR-induced apoptosis. J Biol Chem 281:18734-45.

68. Dzananovic E, McKenna SA, Patel TR. 2018. Viral proteins targeting host protein kinase R to evade an innate immune response: A mini review. Biotechnol Genet Eng Rev 34:33-59.

69. Chang HW, Jacobs BL. 1993. Identification of a conserved motif that is necessary for binding of the vaccinia virus E3L gene products to double-stranded RNA. Virology 194:537-47.

70. Rice AD, Turner PC, Embury JE, Moldawer LL, Baker HV, Moyer RW. 2011. Roles of vaccinia virus genes E3L and K3L and host genes PKR and RNase L during intratracheal infection of C57BL/6 mice. J Virol 85:550-67.

71. Carroll K, Elroy-Stein O, Moss B, Jagus R. 1993. Recombinant vaccinia virus K3L gene product prevents activation of double-stranded RNA-dependent, initiation factor 2 alpha-specific protein kinase. J Biol Chem 268:12837-42.

72. Lu Y, Wambach M, Katze MG, Krug RM. 1995. Binding of the influenza virus NS1 protein to double-stranded RNA inhibits the activation of the protein kinase that phosphorylates the elF-2 translation initiation factor. Virology 214:222-8.

73. Tan SL, Katze MG. 1998. Biochemical and genetic evidence for complex formation between the influenza A virus NS1 protein and the interferon-induced PKR protein kinase. J Interferon Cytokine Res 18:757-66.

74. Cardenas WB, Loo YM, Gale M, Jr., Hartman AL, Kimberlin CR, Martinez-Sobrido L, Saphire EO, Basler CF. 2006. Ebola virus VP35 protein binds double-stranded RNA and inhibits alpha/beta interferon production induced by RIG-I signaling. J Virol 80:5168-78.

75. Poppers J, Mulvey M, Khoo D, Mohr I. 2000. Inhibition of PKR activation by the proline-rich RNA binding domain of the herpes simplex virus type 1 Us11 protein. J Virol 74:11215-21.

76. Cassady KA, Gross M, Roizman B. 1998. The herpes simplex virus US11 protein effectively compensates for the gamma1(34.5) gene if present before activation of protein kinase R by precluding its phosphorylation and that of the alpha subunit of eukaryotic translation initiation factor 2. J Virol 72:8620-6.

77. Cai R, Carpick B, Chun RF, Jeang KT, Williams BR. 2000. HIV-I TAT inhibits PKR activity by both RNA-dependent and RNA-independent mechanisms. Arch Biochem Biophys 373:361-7.

78. McMillan NA, Chun RF, Siderovski DP, Galabru J, Toone WM, Samuel CE, Mak TW, Hovanessian AG, Jeang KT, Williams BR. 1995. HIV-1 Tat directly interacts with the interferon-induced, double-stranded RNA-dependent kinase, PKR. Virology 213:413-24.

79. Park H, Davies MV, Langland JO, Chang HW, Nam YS, Tartaglia J, Paoletti E, Jacobs BL, Kaufman RJ, Venkatesan S. 1994. TAR RNA-binding protein is an inhibitor of the interferon-induced protein kinase PKR. Proc Natl Acad Sci USA 91:4713-7.

80. Thimmappaya B, Weinberger C, Schneider RJ, Shenk T. 1982. Adenovirus VAI RNA is required for efficient translation of viral mRNAs at late times after infection. Cell 31:543-51.

81. Mathews MB, Grodzicker T. 1981. Virus-associated RNAs of naturally occurring strains and variants of group C adenoviruses. J Virol 38:849-62.

82. Reich PR, Forget BG, Weissman SM. 1966. RNA of low molecular weight in KB cells infected with adenovirus type 2. J Mol Biol 17:428-39.

83. Kalveram B, Ikegami T. 2013. Toscana virus NSs protein promotes degradation of double-stranded RNA-dependent protein kinase. J Virol 87:3710-8.

84. Habjan M, Pichlmair A, Elliott RM, Overby AK, Glatter T, Gstaiger M, Superti-Furga G, Unger H, Weber F. 2009. NSs protein of Rift Valley fever virus induces the specific degradation of the double-stranded RNA-dependent protein kinase. J Virol 83:4365-75.

85. Ikegami T, Narayanan K, Won S, Kamitani W, Peters CJ, Makino S. 2009. Rift Valley fever virus NSs protein promotes post-transcriptional downregulation of protein kinase PKR and inhibits eIF2alpha phosphorylation. PLoS Pathog 5:e1000287.

86. Mudhasani R, Tran JP, Retterer C, Kota KP, Whitehouse CA, Bavari S. 2016. Protein kinase R degradation Is essential for Rift Valley fever virus infection and is regulated by SKP1-CUL1-F-box (SCF)FBXW11-NSs E3 ligase. PLoS Pathog 12:e1005437.

87. Black TL, Barber GN, Katze MG. 1993. Degradation of the interferon-induced 68,000-M(r) protein kinase by poliovirus requires RNA. J Virol 67:791-800.

88. Black TL, Safer B, Hovanessian A, Katze MG. 1989. The cellular 68,000-Mr protein kinase is highly autophosphorylated and activated yet significantly degraded during poliovirus infection: Implications for translational regulation. J Virol 63:2244-51.

89. Li W, Zhu Z, Cao W, Yang F, Zhang X, Li D, Zhang K, Li P, Mao R, Liu X, Zheng H. 2016. Esterase D enhances type I interferon signal transduction to suppress foot-and-mouth disease virus replication. Mol Immunol 75:112-21.

90. Li C, Zhu Z, Du X, Cao W, Yang F, Zhang X, Feng H, Li D, Zhang K, Liu X, Zheng H. 2017. Foot-and-mouth disease virus induces lysosomal degradation of host protein kinase PKR by 3C proteinase to facilitate virus replication. Virology 509:222-231.

91. Rabouw HH, Langereis MA, Knaap RC, Dalebout TJ, Canton J, Sola I, Enjuanes L, Bredenbeek PJ, Kikkert M, de Groot RJ, van Kuppeveld FJ. 2016. Middle East respiratory coronavirus accessory protein 4a inhibits PKR-mediated antiviral stress responses. PLoS Pathog 12:e1005982.

92. Hovanessian AG, Galabru J, Meurs E, Buffet-Janvresse C, Svab J, Robert N. 1987. Rapid decrease in the levels of the double-stranded RNA-dependent protein kinase during virus infections. Virology 159:126-36.

93. Chang YH, Lau KS, Kuo RL, Horng JT. 2017. dsRNA binding domain of PKR is proteolytically released by enterovirus A71 to facilitate viral replication. Front Cell Infect Microbiol 7:284.

94. Kalveram B, Ikegami T. 2013. Toscana virus NSs protein promotes degradation of double-stranded RNA-dependent protein kinase. J Virol 87:3710-8.

95. Kainulainen M, Lau S, Samuel CE, Hornung V, Weber F. 2016. NSs virulence factor of Rift Valley fever virus engages the F-box proteins FBXW11 and beta-TRCP1 to degrade the antiviral protein kinase PKR. J Virol 90:6140-7.

96. Ly HJ, Ikegami T. 2016. Rift Valley fever virus NSs protein functions and the similarity to other bunyavirus NSs proteins. Virol J 13:118.

97. Shibata N, Carlin AF, Spann NJ, Saijo K, Morello CS, McDonald JG, Romanoski CE, Maurya MR, Kaikkonen MU, Lam MT, Crotti A, Reichart D, Fox JN, Quehenberger O, Raetz CR, Sullards MC, Murphy RC, Merrill AH, Jr., Brown HA, Dennis EA, Fahy E, Subramaniam S, Cavener DR, Spector DH, Russell DW, Glass CK. 2013. 25-Hydroxycholesterol activates the integrated stress response to reprogram transcription and translation in macrophages. J Biol Chem 288:35812-23.

98. Won S, Eidenschenk C, Arnold CN, Siggs OM, Sun L, Brandl K, Mullen TM, Nemerow GR, Moresco EM, Beutler B. 2012. Increased susceptibility to DNA virus infection in mice with a GCN2 mutation. J Virol 86:1802-8.

99. Ravindran R, Khan N, Nakaya HI, Li S, Loebbermann J, Maddur MS, Park Y, Jones DP, Chappert P, Davoust J, Weiss DS, Virgin HW, Ron D, Pulendran B. 2014. Vaccine activation of the nutrient sensor GCN2 in dendritic cells enhances antigen presentation. Science 343:313-317.

100. Berlanga JJ, Ventoso I, Harding HP, Deng J, Ron D, Sonenberg N, Carrasco L, de Haro C. 2006. Antiviral effect of the mammalian translation initiation factor 2alpha kinase GCN2 against RNA viruses. EMBO J 25:1730-1740.

101. Aparicio F, Aparicio-Sanchis R, Gadea J, Sanchez-Navarro JA, Pallas V, Murguia JR. 2011. A plant virus movement protein regulates the Gcn2p kinase in budding yeast. PLoS One 6:e27409.

102. Berlanga JJ, Ventoso I, Harding HP, Deng J, Ron D, Sonenberg N, Carrasco L, de Haro C. 2006. Antiviral effect of the mammalian translation initiation factor 2alpha kinase GCN2 against RNA viruses. EMBO J 25:1730-40.

103. Krishnamoorthy J, Mounir Z, Raven JF, Koromilas AE. 2008. The eIF2alpha kinases inhibit vesicular stomatitis virus replication independently of eIF2alpha phosphorylation. Cell Cycle 7:2346-51.

104. Hirohata Y, Kato A, Oyama M, Kozuka-Hata H, Koyanagi N, Arii J, Kawaguchi Y. 2015. Interactome analysis of herpes simplex virus 1 envelope glycoprotein H. Microbiol Immunol 59:331-7.

105. Vazquez de Aldana CR, Marton MJ, Hinnebusch AG. 1995. GCN20, a novel ATP binding cassette protein, and GCN1 reside in a complex that mediates activation of the eIF-2 alpha kinase GCN2 in amino acid-starved cells. EMBO J 14:3184-99.

106. Krahling V, Stein DA, Spiegel M, Weber F, Muhlberger E. 2009. Severe acute respiratory syndrome coronavirus triggers apoptosis via protein kinase R but is resistant to its antiviral activity. J Virol 83:2298-309.

107. Qian W, Zhu S, Sobolev AY, Wek RC. 1996. Expression of vaccinia virus K3L protein in yeast inhibits eukaryotic initiation factor-2 kinase GCN2 and the general amino acid control pathway. J Biol Chem 271:13202-7.

108. del Pino J, Jimenez JL, Ventoso I, Castello A, Munoz-Fernandez MA, de Haro C, Berlanga JJ. 2012. GCN2 has inhibitory effect on human immunodeficiency virus-1 protein synthesis and is cleaved upon viral infection. PLoS One 7:e47272.

109. Cosnefroy O, Jaspart A, Calmels C, Parissi V, Fleury H, Ventura M, Reigadas S, Andreola ML. 2013. Activation of GCN2 upon HIV-1 infection and inhibition of translation. Cell Mol Life Sci 70:2411-21.

110. Jaspart A, Calmels C, Cosnefroy O, Bellecave P, Pinson P, Claverol S, Guyonnet-Duperat V, Dartigues B, Benleulmi MS, Mauro E, Gretteau PA, Parissi V, Metifiot M, Andreola ML. 2017. GCN2 phosphorylates HIV-1 integrase and decreases HIV-1 replication by limiting viral integration. Sci Rep 7:2283.

111. Harding HP, Novoa I, Zhang Y, Zeng H, Wek R, Schapira M, Ron D. 2000. Regulated translation initiation controls stress-induced gene expression in mammalian cells. Mol Cell 6:1099-108.

112. Jiang G, Santos Rocha C, Hirao LA, Mendes EA, Tang Y, Thompson GR, 3rd, Wong JK, Dandekar S. 2017. HIV Exploits antiviral host innate GCN2-ATF4 signaling for establishing viral replication early in infection. MBio 8.

Chapter II

Enhanced replication of mouse adenovirus type 1 following virus-induced degradation of protein kinase R (PKR)

Modified from:

Goodman DE, Pretto CD, Krepostman TA, Carnahan KE, and Spindler KR. "Enhanced replication of mouse adenovirus type 1 following virus-induced degradation of protein kinase R (PKR)." In press, *mBio*, March 2019.

Abstract

Protein kinase R (PKR) plays a major role in activating host immunity during infection by sensing double-stranded (ds) RNA produced by viruses. Once activated by dsRNA, PKR phosphorylates the translation factor eIF2α, halting cellular translation. Many viruses have methods of inhibiting PKR activation or its downstream effects, circumventing protein synthesis shutdown. These include sequestering dsRNA or producing proteins that bind to and inhibit PKR activation. Here we describe our finding that in multiple cell types, PKR was depleted during mouse adenovirus type 1 (MAV-1) infection. MAV-1 did not appear to be targeting PKR at a transcriptional or translational level because total PKR mRNA levels and levels of PKR mRNA bound to polysomes were unchanged or increased during MAV-1 infection. However, inhibiting the proteasome reduced the PKR depletion seen in MAV-1-infected cells, whereas inhibiting the

lysosome had no effect. This suggests that proteasomal degradation alone is responsible for PKR degradation during MAV-1 infection. Time course experiments indicate that the degradation occurs early after infection. Infecting cells with UV-inactivated virus prevented PKR degradation, whereas inhibiting viral DNA replication did not. Together these results suggest that an early viral gene is responsible. Degradation of PKR is a rare mechanism to oppose PKR activity, and it has only been described in only six RNA viruses. To our knowledge, this is the first example of a DNA virus counteracting PKR by degrading it.

Importance

The first line of defense in cells during viral infection is the innate immune system, which is activated by different viral products. PKR is a part of this innate immune system and is induced by interferon (IFN) and activated by dsRNA produced by DNA and RNA viruses. PKR is such an important part of the antiviral response that many viral families have gene products to counteract its activation or the resulting effects of its activity. Although a few RNA viruses degrade PKR, this method of counteracting PKR has not been reported for any DNA viruses. MAV-1 does not encode virus-associated (VA) RNAs, a human adenoviral defense against PKR activation. Instead, MAV-1 degrades PKR, and it is the first DNA virus reported to do so. The innate immune evasion by PKR degradation is a previously unidentified way for a DNA virus to circumvent the host antiviral response.

Introduction

Activation of PKR is a major innate immune response to viral infection. PKR is an IFN-induced protein that is comprised of two major domains, an N-terminal dsRNA binding domain

and a C-terminal serine/threonine kinase domain (1, 2). PKR binds to dsRNA (3-5) and once bound, it becomes activated by dimerizing and autophosphorylating (6-9). When activated, PKR phosphorylates eukaryotic translation initiation factor 2α (eIF2α), causing inhibition of protein synthesis and reduced viral replication (10-13). Many viruses encode gene products that block PKR activation or inhibit its ability to phosphorylate eIF2α (14). A common mechanism is to produce a viral protein that binds and sequesters dsRNA, blocking its interaction with PKR. Examples of this are vaccinia virus E3L (15-17), influenza virus NS1 (18, 19), and Ebola virus protein VP35 (20). Other viruses produce proteins or RNA that bind directly to PKR to inhibit its activation, such as herpes simplex virus US11 (21, 22), HIV-1 Tat protein (23, 24) or TAR RNA (25), and human adenovirus (hAd) VA RNAs (10, 26-28).

Degradation of PKR by viruses is a less documented method of regulating PKR. To date PKR degradation has been reported in six RNA viruses: Toscana virus (TOSV) (29), Rift Valley fever virus (RVFV) (30-32), poliovirus (33, 34), foot-and-mouth disease virus (FMDV) (35, 36), encephalomyocarditis virus (EMCV, strain mengovirus) (37, 38), and enterovirus 71 (39). RVFV and TOSV both degrade PKR via proteasomal mechanisms involving a viral nonstructural protein (NSs) (32, 40, 41). RVFV NSs recruits a SCF (SKP1-CUL1-F-box)^{FBXW11} E3 ubiquitin ligase to ubiquitinate PKR and target it to the proteasome, though PKR ubiquitination could not be demonstrated (32, 41). The mechanism for PKR proteasomal degradation by NSs has not been described for TOSV (40). FMDV uses the other major cellular protein degradation pathway, the lysosome, to degrade PKR during infection (36). Though the mechanism is unclear, expression of the major FMDV protease $3C^{pro}$ is required for PKR degradation by the lysosome. However, $3C^{pro}$ does not interact with PKR, nor is its protease activity required for PKR degradation. The enterovirus A71 $3C^{pro}$ causes PKR degradation by direct interaction (39). The mechanism of

PKR depletion by poliovirus is unclear, though gene expression is required, and the major poliovirus proteases (2A and 3C) are not directly involved (33). The mechanism by which mengovirus depletes PKR during infection is unknown (37, 38).

Adenoviruses are species-specific, making the study of hAd pathogenesis difficult in an animal model. MAV-1 is a useful alternative to study adenovirus pathogenesis (42-46). MAV-1 has molecular, genetic, and pathogenic similarities and differences to hAd. Their genomic structures are similar at a gross level, and both contain early genes involved in pathogenesis and immune evasion. Pathogenically, their tropisms vary, with hAd infecting epithelial cells, leading to upper respiratory and GI tract infections, and conjunctivitis, while MAV-1 infects endothelial cells and monocytes, causing encephalitis and myocarditis. We and others have been investigating the adaptive and innate immune responses to MAV-1.

HAd VA RNAs bind PKR as a monomer, preventing its transautophosphorylation (47). However, MAV-1 does not produce VA RNAs (48), and it is not known whether MAV-1 induces PKR activation. In our studies of MAV-1 pathogenesis and the innate response, we discovered that during MAV-1 infection, PKR was depleted from cells as early as 12 hours post infection (hpi). Total PKR mRNA levels and PKR mRNA bound to polysomes were unchanged or increased during MAV-1 infection, suggesting that MAV-1 did not appear to be targeting PKR at a transcriptional or translational level. However, inhibiting the proteasome blocked the PKR depletion seen in MAV-1-infected cells, indicating that proteasomal degradation is responsible for PKR depletion during MAV-1 infection. We report results indicating that an early viral gene is likely responsible for mediating PKR degradation. To our knowledge, this is the first example of a DNA virus counteracting PKR by degrading it.

Results

Viral yield is increased in PKR$^{-/-}$ mouse embryonic fibroblasts

While PKR is an important part of the innate immune response, PKR$^{-/-}$ cells in culture are not always more susceptible to viral infection than wild type cells (49-51). PKR$^{-/-}$ mouse embryonic fibroblasts (MEFs) show increased viral yields compared to wild type MEFs when infected with vesicular stomatitis virus and influenza A (49, 50), but there is no change in viral yield during vaccinia virus infection compared to wild type cells (51). However, it was later discovered that the PKR$^{-/-}$ MEF lines used are not complete PKR knockouts (52). There are two categories of PKR$^{-/-}$ MEFs derived from knockout mice: N-PKR$^{-/-}$ MEFs and C-PKR$^{-/-}$ MEFs (pronounced N minus or C minus MEFs) (Fig. 2.1) (52). The PKR$^{-/-}$ MEFs derived from mice created in the Weissmann lab (53) are designated N-PKR$^{-/-}$ MEFs, because the C-terminal fragment of PKR is still expressed and can be detected by immunoblot when there is IFN induction (52). The fragment has the kinase catalytic activity of PKR, but it does not bind dsRNA (52). The PKR$^{-/-}$ MEFs derived from mice created in the Bell lab (54) are designated as C-PKR$^{-/-}$ MEFs, because the N-terminal fragment of PKR is still expressed and can be detected by immunoblot with specific PKR antibodies (52). The fragment is catalytically inactive, but it can still bind dsRNA (52). Susceptibility of these PKR$^{-/-}$ MEFs to specific viruses may be dependent on the PKR mutation and the mechanism used by each virus to circumvent PKR.

To determine whether PKR plays an important role during MAV-1 infection, we tested the susceptibility of both PKR$^{-/-}$ MEF lines and primary peritoneal macrophages from N-PKR$^{-/-}$ mice to MAV-1 infection. We infected wild type MEFs, N-PKR$^{-/-}$ MEFs, C-PKR$^{-/-}$ MEFs, C57BL/6 (wild type) macrophages, and N-PKR$^{-/-}$ macrophages with MAV-1 at an MOI of 1 and collected cell pellets at 24, 48, and 72 hpi. DNA was purified from the cell pellets and analyzed

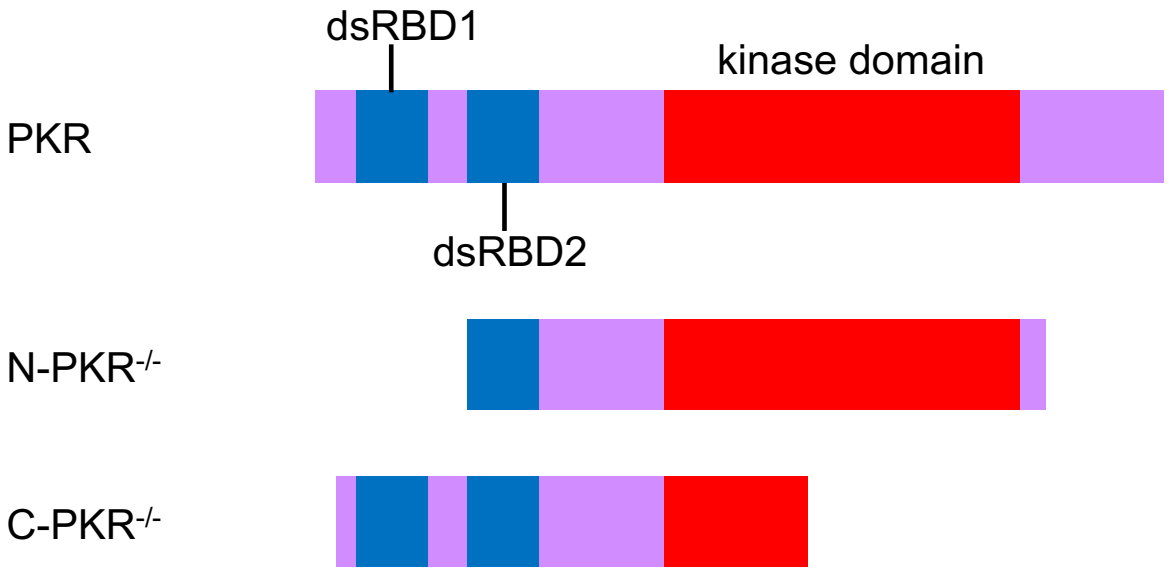

	dsRNA Binding Activity	Kinase Activity
PKR	+	+
N-PKR$^{-/-}$	-	+
C-PKR$^{-/-}$	+	-

Figure 2.1 Fragments of PKR protein expressed in PKR$^{-/-}$ MEFs, adapted from Figure 1A and 5B from Baltzis et al. As described in Baltzis et al., 2002, the two PKR$^{-/-}$ MEF lines each expresses a fragment of PKR. The N-PKR$^{-/-}$ MEFs express a C-terminal fragment that has kinase activity, but no dsRNA binding activity. The C-PKR$^{-/-}$ MEFs express a N-terminal fragment that has dsRNA binding activity, but no kinase activity.

for MAV-1 genome copies by qPCR. N-PKR$^{-/-}$ MEFs produced a significantly higher viral yield than wild type MEFs at 48 hpi, and both PKR mutant MEF lines had a significantly higher viral yield than wild type MEFs at 72 hpi (Fig. 2.2A). In the peritoneal macrophages, virus yield was almost doubled in the N-PKR$^{-/-}$ macrophages compared to the wild type macrophages by 72 hpi (Fig. 2.2B). Although we have not confirmed the production of truncated PKR proteins in the cells in our laboratory, the results of Fig. 2.2 indicate that PKR activation is an important antiviral response during MAV-1 infection *in vitro*.

There is little difference in survival between N-PKR$^{-/-}$ and wild type mice

Using the N-PKR$^{-/-}$ mice (53), we assayed whether PKR has an antiviral function during MAV-1 infection *in vivo*. We infected N-PKR$^{-/-}$ and C57BL/6 (wild type) mice intraperitoneally with $5x10^1$, 10^1, 10^2, or 10^3 PFU MAV-1, and survival was recorded for 21 days post infection. At $5x10^1$, 10^1, and 10^3 PFU, there was no significant difference in survival rates between N-PKR$^{-/-}$ and wild type mice, and at 10^2 PFU, the N-PKR$^{-/-}$ mice had a significantly higher survival rate than the wild type mice (Fig. 2.3). These results suggest that *in vivo*, there are few effects of the N-PKR mutation. This could be due to residual PKR protein being made, or there may be redundancies between PKR and the other three eIF2α kinases.

Mouse PKR is depleted during MAV-1 infection

To determine whether MAV-1 affects PKR during infection, we infected several cell types and analyzed PKR protein expression. We infected immortalized C57BL/6 MEFs, C57BL/6 primary peritoneal macrophages, and CMT93 cells (mouse rectal carcinoma cells) with MAV-1 at an MOI of 10 and collected cell lysates 24, 48, and 72 hpi. We analyzed cell lysates

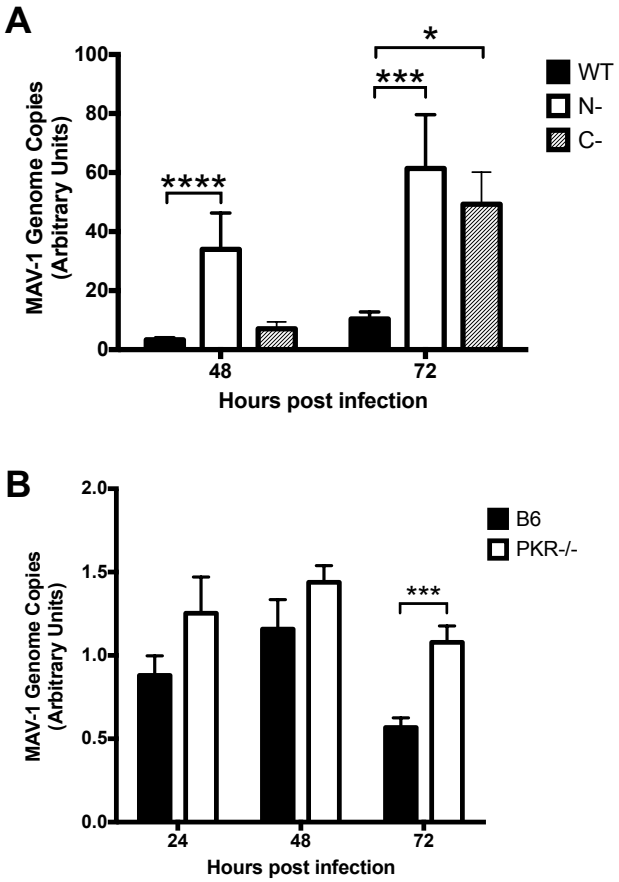

Figure 2.2 Viral yield is increased in PKR$^{-/-}$ mouse embryonic fibroblasts and peritoneal macrophages. (A) PKR WT MEFs (WT), N-PKR$^{-/-}$ MEFs (N-), and C-PKR$^{-/-}$ MEFs (C-) or (B) primary peritoneal macrophages from C57BL/6 (B6) or PKR$^{-/-}$ mice were infected with MAV-1 at MOI 1 and collected at 48 and 72 hpi. DNA was purified from cell pellets and analyzed for MAV-1 genome copies by qPCR. Both graphs are representative of three experiments, (A) 14 or (B) 18 biological replicates per cell line per time point. Error bars are standard error of the mean (SEM). *$P \leq 0.05$, ***$P \leq 0.0002$, ****$P \leq 0.0001$.

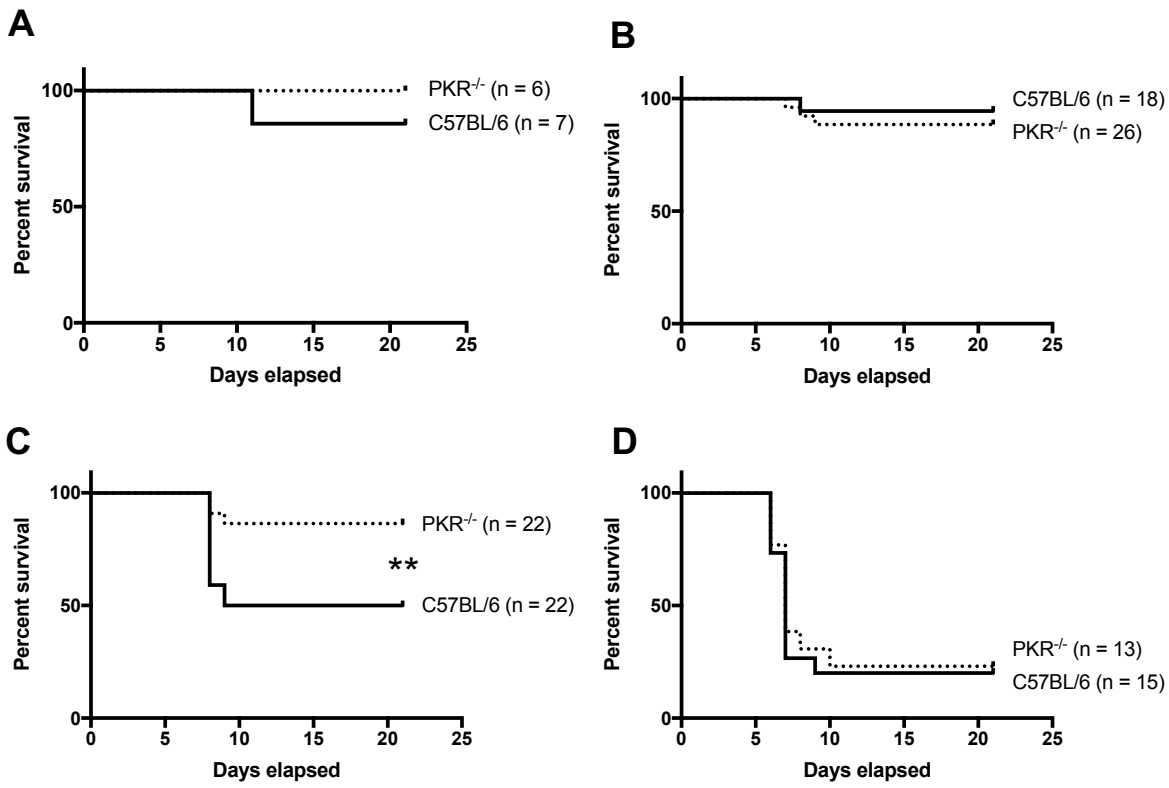

Figure 2.3 Survival during MAV-1 infection is increased or unchanged in $PKR^{-/-}$ mice compared to wild-type mice. Wild-type mice (C57BL/6) and $PKR^{-/-}$ mice were infected intraperitoneally with (A) 10^1 pfu MAV-1, (B) $5x10^1$ pfu MAV-1, (C) 10^2 pfu MAV-1, or (D) 10^3 pfu MAV-1 and survival was recorded for 21 days. $^{**}P \leq 0.01$. The data shown are pooled from independent experiments. The number of mice in each group is listed next to the line label.

for the presence of PKR by immunoblot using a polyclonal antibody that detects mouse PKR. We probed blots with antibodies to actin as a loading control. To our surprise, in C57BL/6 MEFs, PKR was almost completely depleted from lysates 24 hpi and remained depleted through 72 hpi (Fig. 2.4A and B). We also observed depletion of PKR in other cell types. In CMT93 (mouse rectal carcinoma) cells, PKR was nearly undetectable at 24 hpi (Fig. 2.4A). In C57BL/6 primary peritoneal macrophages, PKR was decreased at 48 hpi compared to mock lysates, and absent in infected lysates at 72 hpi (Fig. 2.4A). This indicates that MAV-1 causes PKR depletion during infection.

To determine whether kinase activity of PKR is important for the depletion, we assayed infection of MEFs expressing a mutant form of mouse PKR with a point mutation in the kinase domain (K271R) (55). These cells, designated K271R SV40-MEFs, showed an even more rapid depletion of PKR than in WT SV40-MEFs (Fig. 2.4C). At 24 hpi, in K271R SV40-MEFs, 28% of PKR remained, compared to 60% in the WT SV40-MEFs. The fraction remaining at 72 hpi in K271R SV40-MEFs was 10%, compared to 30% in WT SV40-MEFs (Fig. 2.4C). This indicates that the PKR kinase does not have to be functional to be depleted during MAV-1 infection. Also, comparing the PKR immunoblot bands in the mock-infected WT SV40 MEFs and mutant K271R SV40-MEFs suggests that the upper band of the PKR doublet usually seen in wild type cells is a phospho-PKR band, because only the lower band of the PKR doublet is seen in kinase-dead mutant K271R SV40-MEFs. The data in Fig. 2.4A and C thus indicate that both PKR and phospho-PKR are depleted during MAV-1 infection.

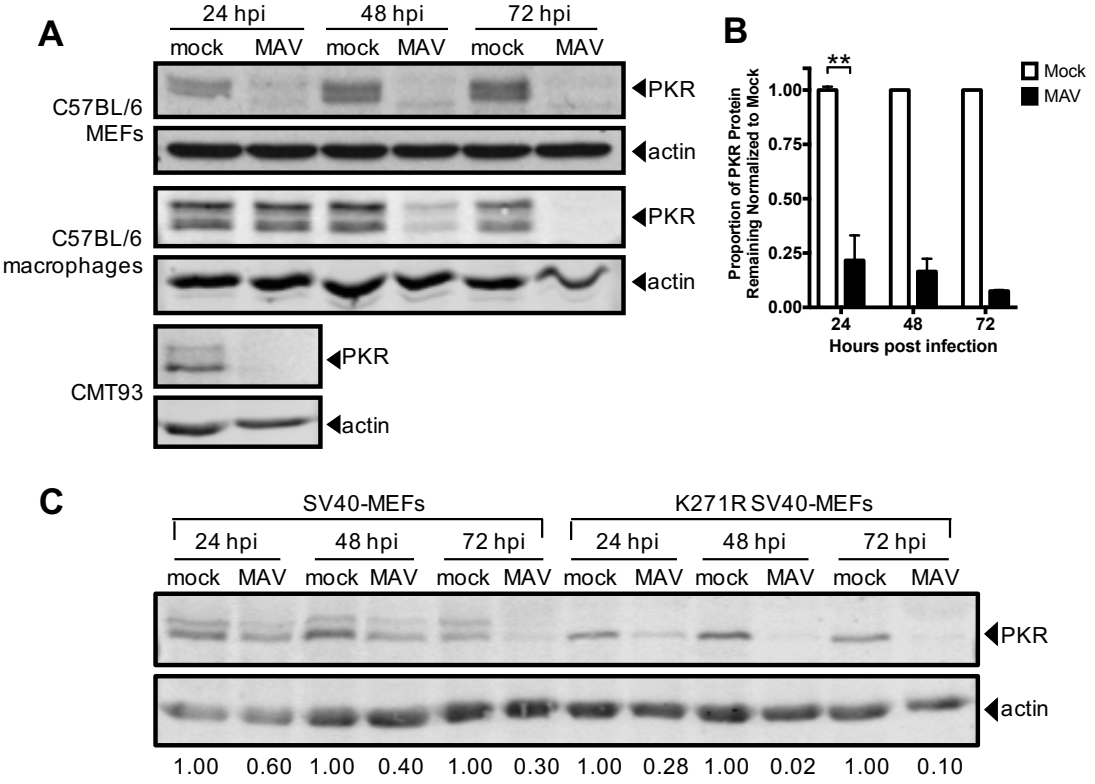

Figure 2.4 Mouse PKR is depleted during MAV-1 infection. (A) Cells (indicated at left) were infected with MAV-1 (MAV) at an MOI of 10 or mock infected (mock). Cell lysates were collected at the indicated times and analyzed by immunoblot with antibodies for PKR (B-10 for C57BL/6 MEFs and D-20 for C57BL/6 primary peritoneal macrophages and CMT93 cells) and actin. Blots are representative of a minimum of three independent experiments per cell line. (B) Densitometry quantitation of five C57BL/6 MEFs immunoblots from A. Error bars are SEM. N=5 for 24 hpi, n=4 for 48 hpi, and n=2 for 72 hpi. $^{**}P \leq 0.01$. (C) SV40-MEFs or kinase-dead (K271R) SV40-MEFs were infected with MAV-1 at an MOI of 10. Cell lysates were immunoblotted as in A with PKR D-20. Numbers below are the proportion of PKR protein for each time point, normalized to actin and the mock PKR protein levels from the corresponding time point.

huPKR is not degraded by MAV-1

Mouse PKR and human PKR share 58% amino acid identity and are 71% similar. To determine whether MAV-1 depletes human PKR in a manner similar to mouse PKR, we used $PKR^{-/-}$ MEFs transfected to constitutively express FLAG-tagged full length, kinase-dead, or RNA binding-deficient human (hu) PKR (56). We infected each of these cell lines with MAV-1 at an MOI of 10, collected lysates at 72 hpi, and analyzed huPKR protein levels by immunoblot with antibodies to FLAG. Human PKR was not depleted at any time point during infection, and in fact levels of all three huPKR types were increased in infected lysates compared to mock lysates at 72 hpi (Fig. 2.5A). This suggests that the depletion of mouse PKR is species-specific and that a region of mouse PKR sequence not found in human PKR may be a determinant.

To confirm MAV-1 was replicating successfully in all three of these cell lines, we infected the vector, full length, kinase-dead, or RNA binding-deficient human PKR lines with MAV-1 at an MOI of 10 and collected cell pellets at 48 and 72 hpi. DNA was purified from the cell pellets and analyzed for MAV-1 genome copies by qPCR. The virus replicated efficiently in the vector, full length, and RNA binding-deficient huPKR lines, demonstrating that the lack of huPKR degradation was not due to a lack of MAV-1 replication in the cell lines (Fig. 2.5B). However, MAV-1 replicated poorly in the kinase-dead huPKR line and thus a conclusion cannot be drawn about the lack of degradation of the human kinase-dead PKR. The presence of the full length huPKR doubled the amount of MAV-1 replication compared to the vector cell line, which contained no PKR at all. This could mean that the kinase domain of huPKR increases MAV-1 infection. We have not investigated this further.

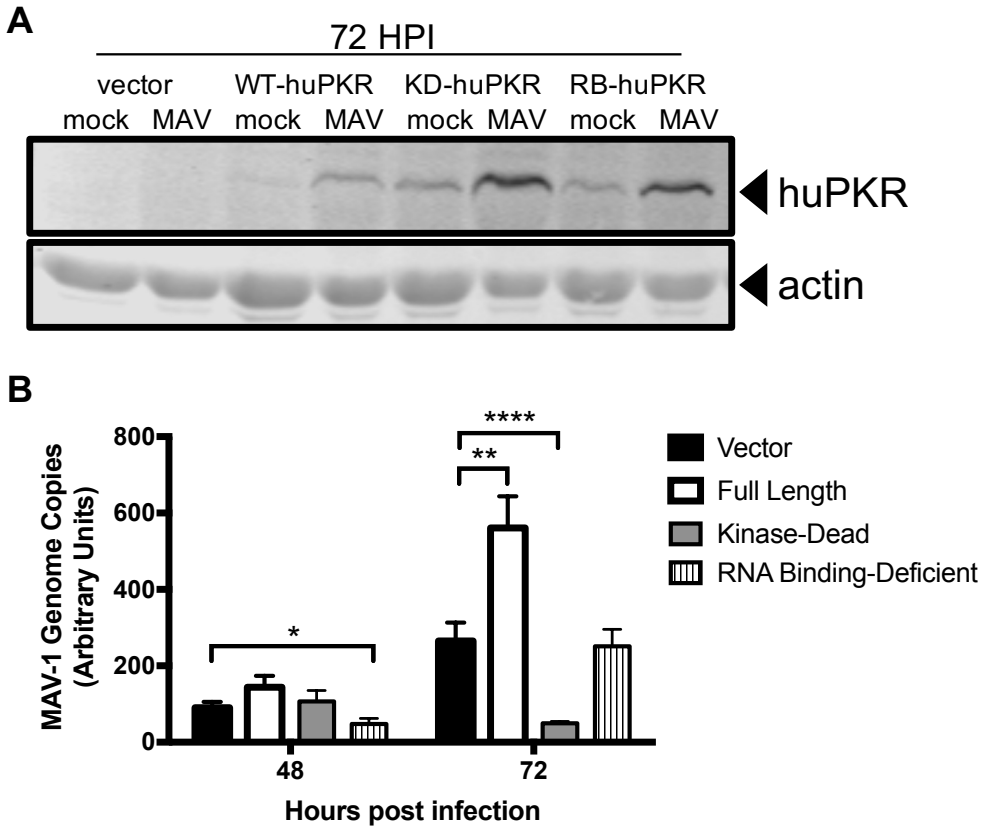

Figure 2.5 Human PKR is not depleted during MAV-1 infection. (A) PKR$^{-/-}$ MEFs reconstituted with FLAG-tagged full length (WT-huPKR), kinase dead (KD-huPKR), or RNA-binding mutant human PKR (RB-huPKR) (indicated above) were infected with MAV-1 (MAV) at an MOI of 10 or mock infected (mock). Cell lysates were collected at the indicated times and analyzed by immunoblot with antibodies for FLAG and actin. Blots are representative of a minimum of three independent experiments per cell line. (B) PKR$^{-/-}$ MEFs reconstituted with FLAG-tagged full length, kinase dead, or RNA-binding mutant human PKR were infected with MAV-1 at MOI 10 and collected at 48 and 72 hpi. DNA was purified from cell pellets and analyzed for MAV-1 genome copies by qPCR. Both graphs are representative of three experiments, 17-19 biological replicates per cell line per time point. Error bars are SEM. *$P \leq 0.05$, ***$P \leq 0.0002$, ****$P \leq 0.0001$.

MAV-1 does not cause PKR depletion by reducing steady-state levels of PKR mRNA

To determine the mechanism of PKR depletion, we first assayed whether reduction in PKR protein during MAV-1 infection was due to reduced PKR mRNA steady-state levels. We mock-infected or infected C57BL/6 MEFs and primary peritoneal macrophages at an MOI of 10 and collected cell lysates at 24, 48, and 72 hpi. We synthesized cDNA from RNA purified from these cell lysates and assayed for PKR mRNA by qPCR. In C57BL/6 MEFs, PKR mRNA levels were similar between mock and infected lysates at 24 hpi (Fig. 2.6A), a time point in which PKR protein levels were already greatly depleted in the infected lysates compared to mock lysates (Fig. 2.4A). Although PKR mRNA levels were depleted 33% at 48 hpi and 40% 72 hpi in MAV-1-infected lysates compared to mock lysates, this does not correlate to the 84% and 94% reduction, respectively, in PKR protein levels at those time points. In C57BL/6 primary peritoneal macrophages, PKR mRNA levels in the infected lysates were 2-3 times higher than levels in mock lysates at all three time points assayed (Fig. 2.6B), even though PKR protein levels were almost completely depleted in infected lysates at 72 hpi (Fig. 2.4A). This is evidence that MAV-1 is not causing PKR protein depletion by reducing PKR steady-state mRNA levels during infection.

MAV-1 infection effects on PKR translation

Because MAV-1 did not reduce PKR mRNA steady-state levels, we determined whether MAV-1 causes PKR depletion by reducing translation of its mRNA. We first assayed total PKR mRNA bound to ribosomes during infection. C57BL/6 MEFs were mock infected or infected at an MOI of 5, and lysates were collected at 48 hpi in the presence of cycloheximide to keep the mRNA bound to the ribosomes (57). Lysates were centrifuged through 25% sucrose to pellet

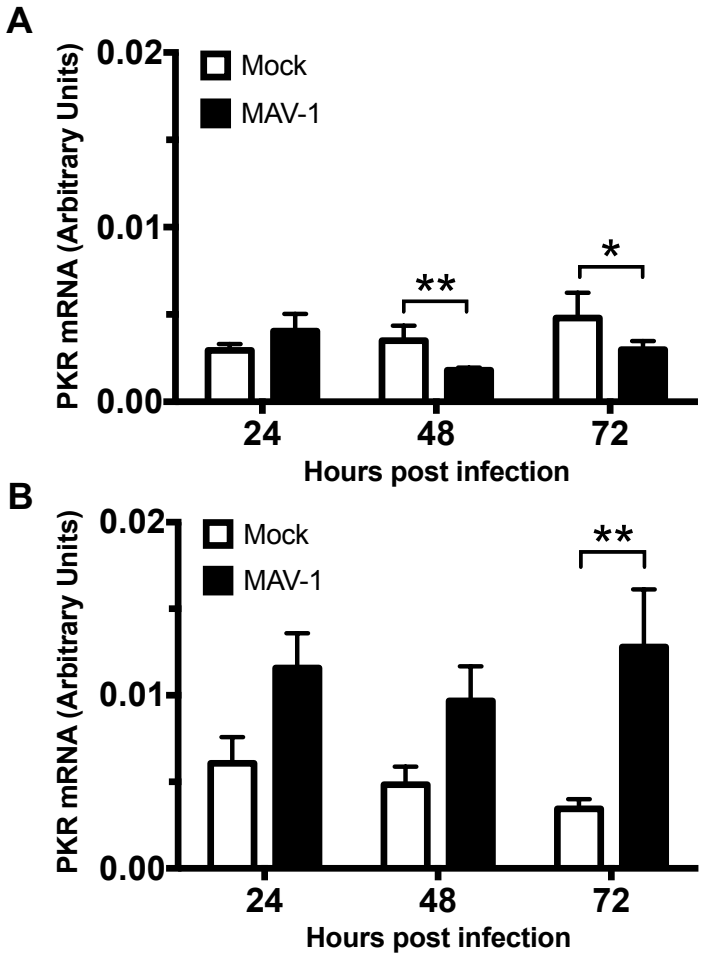

Figure 2.6 MAV-1 does not cause PKR depletion by reducing steady state levels of PKR mRNA at times when the protein levels are already reduced. MEFs (A) or isolated primary peritoneal macrophages (B) were harvested and infected with MAV-1 at an MOI of 10 or mock infected. The cell pellets were collected and RNA was isolated. cDNA was generated from the RNA, and qPCR was used to quantitate PKR mRNA levels. Each graph contains 5-7 replicates for each time point from three pooled experiments. Error bars are SEM. *$P \leq 0.05$ and **$P \leq 0.01$.

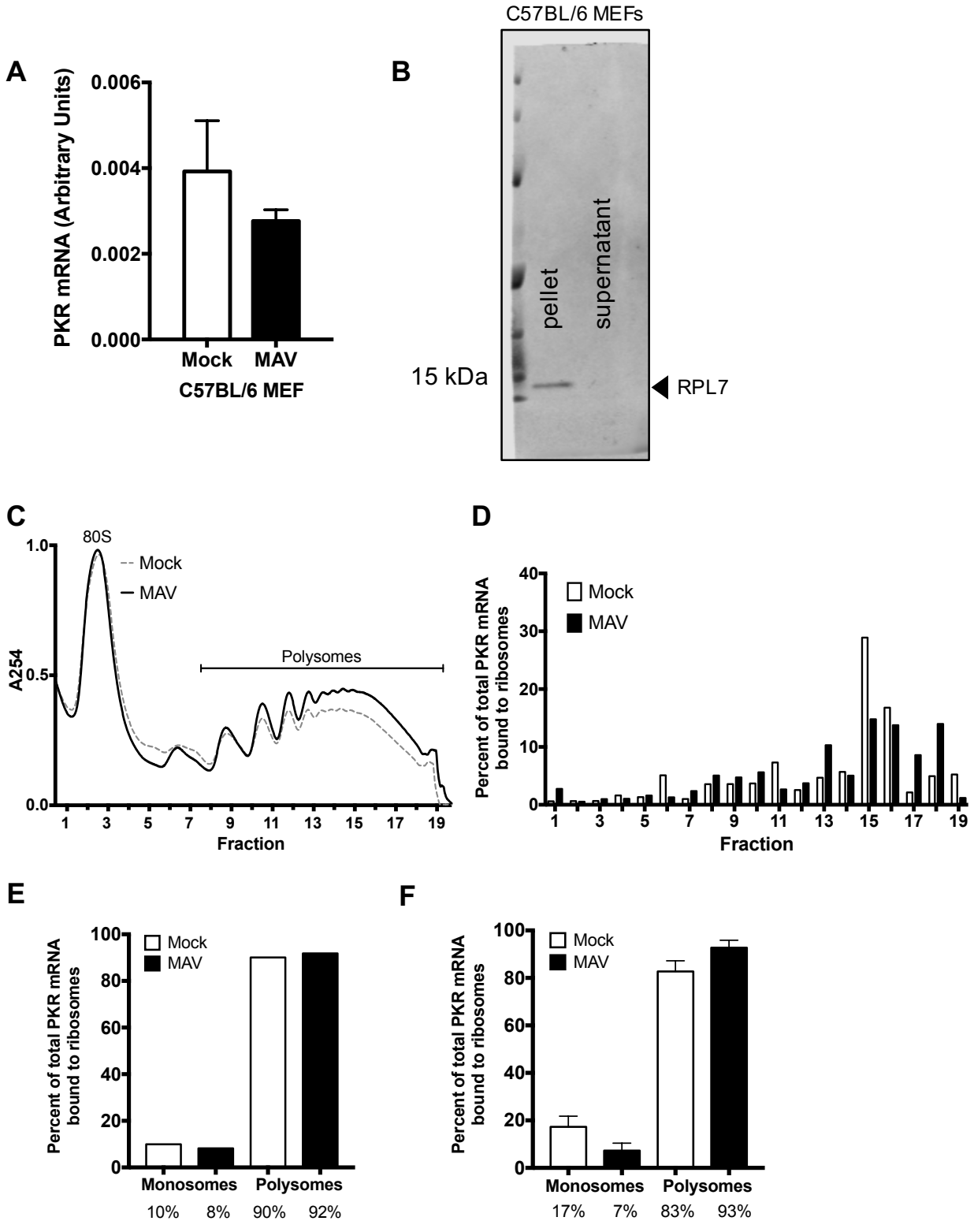
A
PKR mRNA (Arbitrary Units)
0.006
0.004
0.002
0.000
Mock
MAV
C57BL/6 MEF
B
C57BL/6 MEFs
pellet
supernatant
15 kDa
RPL7
C
80S
Mock
MAV
Polysomes
A254
1.0
0.5
0.0
1 3 5 7 9 11 13 15 17 19
Fraction
D
Mock
MAV
Percent of total PKR mRNA bound to ribosomes
40
30
20
10
0
1 3 5 7 9 11 13 15 17 19
Fraction
E
Mock
MAV
Percent of total PKR mRNA bound to ribosomes
100
80
60
40
20
0
Monosomes
Polysomes
10% 8% 90% 92%
F
Mock
MAV
Percent of total PKR mRNA bound to ribosomes
100
80
60
40
20
0
Monosomes
Polysomes
17% 7% 83% 93%

Figure 2.7 MAV-1 infection does not affect PKR translation. (A) C57BL/6 MEFs were infected with MAV-1 (MAV) at an MOI of 5 or mock infected (mock) and collected at 48 hpi. Cells were lysed, and cleared lysates from three 10 cm plates were layered onto 25% sucrose and centrifuged to pellet ribosomes. RNA was purified from the pellets, cDNA was generated from the RNA, and qPCR was used to quantitate the PKR mRNA levels. The graph contains 9 replicates for each time point, pooled from 3 independent experiments. Error bars show the SEM. (B) To confirm that most ribosomes ended up in the pellet after centrifugation through sucrose, a sample of the pellet and the corresponding supernatant were analyzed by immunoblot with antibodies for RPL7 (ribosomal protein L7, Abcam, 1:2000, ab72550). (C) C57BL/6 MEFs were infected with MAV-1 (MAV) at an MOI of 2 or mock infected (mock). Cells were collected at 25 hpi and lysed; cleared lysates were layered onto 10-50% sucrose gradients and centrifuged. Gradients were collected from the top and pumped through a UV spectrophotometer, and 34 fractions were collected. The gradients are displayed with the bottom fractions to the right. The UV trace of the first 10 fractions (including 40S and 60S ribosomal subunits) is not shown. (D) RNA was purified from each fraction of the gradients in B; fractions are renumbered here with the first fraction corresponding to fraction 11 of the original gradient. cDNA was generated from the RNA, and qPCR was used to quantitate PKR mRNA in each fraction and displayed as the percent of total PKR mRNA associated with ribosomes. C and D are results from one representative experiment of 3 independent experiments. (E) Percentage of total PKR mRNA associated with monosomes (fractions 1-6) and polysomes (fractions 7-19) from the trial displayed in C and D were pooled for mock and infected samples. The percentages represented by each bar are displayed below each bar. (F) Pooled monosome and polysome data as described in E from three independent experiments. Error bars are SEM. The percentages represented by each bar are displayed below each bar. There were no significant differences between mock and infected samples (A, F).

ribosomes, and RNA was purified from the pellets. The purified RNAs were used to generate cDNA, which we assayed for PKR mRNA by qPCR (Fig. 2.7A). As a control for pelleting of ribosomes, we assayed the pellets and sucrose cushion supernatants by immunoblot with antibodies to ribosomal protein RPL7. We confirmed that RPL7 was only present in the pellets and not the supernatants (Fig. 2.7B). There was no significant difference between the amount of PKR mRNA in the ribosome pellet of mock infected lysates compared to MAV-1-infected lysates (Fig. 2.7A).

To confirm the results seen in total mRNA bound to ribosomes, we also centrifuged cell extracts on sucrose gradients to generate polysome profiles. This enabled us to analyze levels of PKR mRNA associated with actively-translating ribosomes during infection. C57BL/6 MEFs were mock infected or infected at an MOI of 2, and lysates were collected at 24 hpi in the presence of cycloheximide, as above. RNA content for mock and infected lysates was estimated by NanoDrop spectrophotometry, and equivalent OD amounts of RNA were centrifuged on 10-50% sucrose gradients to sediment 40S and 60S ribosomal subunits, 80S ribosomes (monosomes), and polyribosomes (polysomes). A typical polysome profile was obtained (Fig. 2.7C). RNA was purified from fractions containing monosomes and polysomes and then used to generate cDNA, which we assayed for PKR mRNA by qPCR (Fig. 2.7D). As a control, GAPDH mRNA was measured by qPCR, and PKR mRNA levels in each fraction were normalized to the GAPDH mRNA content. When the data for percentage of PKR mRNA bound to ribosomes was pooled into monosome and polysome fractions and analyzed (Fig. 2.7E), 90.1% and 91.8% were bound to polysomes (fractions 7-19) for mock and infected samples, respectively, compared to 9.9% and 8.2% bound to monosomes (fractions 1-6). We performed two additional polysome gradient analyses. The pooled data from all three (Fig. 2.7F) were similar to the data for Fig.

2.7E, i.e., 82.7% and 92.7% of PKR mRNA was bound to mock and infected polysomes, respectively, compared to 17.3% and 7.3% bound to monosomes. Thus, PKR protein depletion during MAV-1 infection does not appear to stem from a decrease in PKR mRNA translation.

We also assayed whether PKR mRNA might have a signal that would reduce its translation during MAV-1 infection. We constructed a plasmid that positioned sequence corresponding to the 5' UTR of PKR mRNA upstream of a reporter nanoluciferase gene (58), transfected it into C57BL/6 MEFs or CMT93 cells, then infected with MAV-1 at MOI of 10. Compared to cells transfected with a control plasmid with the human β-globin 5' UTR upstream of the reporter nanoluciferase, there was no significant difference in luciferase activity between mock infected and infected samples (Fig. 2.8). These data suggest that MAV-1 is not affecting PKR translation through interaction with the 5' UTR of PKR. The data are consistent with the ribosome pellet and polysome data that MAV-1 infection does not reduce PKR mRNA translation.

PKR is depleted by proteasomal degradation during MAV-1 infection

There are two main proteolysis pathways in cells, proteasomal degradation and lysosomal degradation (59). To determine whether MAV-1 depletes PKR by either protein degradation pathway, we first assayed whether PKR is lysosomally degraded as follows. CMT93 cells were mock infected or infected with MAV-1 and treated at the time of infection with the lysosome inhibitors ammonium chloride or chloroquine, or water (as a control). At 24 hpi, we collected lysates and analyzed them by immunoblot with antibodies to PKR. In the presence of the lysosomal degradation inhibitors, PKR was depleted by 24 hpi (Fig. 2.9A), indicating that lysosomal degradation was not the cause of PKR depletion during MAV-1 infection.

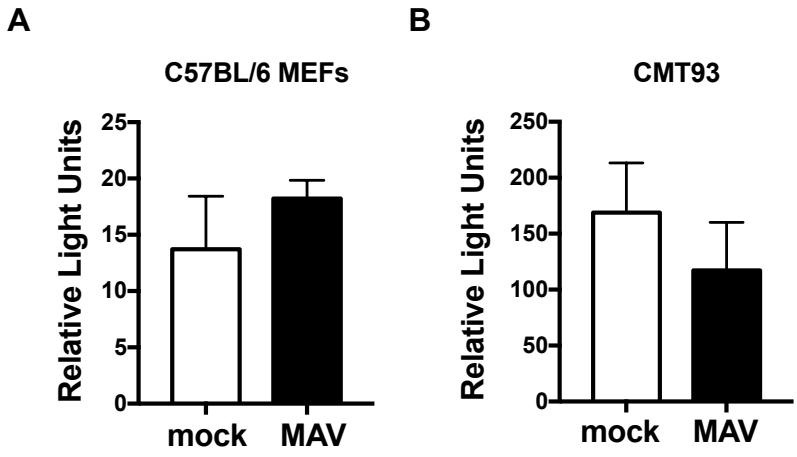

Figure 2.8 PKR mRNA 5' UTR does not result in altered reporter protein levels upon MAV-1 infection. (A) C57BL/6 MEFs or (B) CMT93 cells were co-transfected with pmPKR5UTRfullNL or AUG-NL-3xFLAG and pGL4.13 using jetPRIME reagents (Polyplus #114-01) using the standard Polyplus protocol, with 200 ng total of plasmid and 300 µL of jetPRIME reagent per 35 mm well. At 24 hours after transfection, the cells were infected with MAV-1 at an MOI of 10. At 24 hpi, cells were lysed in 70 µL/well Glo Lysis Buffer (Promega Corp.). After lysing, 25 µL of each lysed sample and 25 µL of OneGlo or NanoGlo (Promega Corp.) was added to two wells in a black 96-well plate. After 5 minutes, the plate was read on a luminometer. Relative light units from the pmPKR5UTRfullNL plasmid were normalized to the firefly luciferase and positive control plasmids. Graphs are representative of 7-9 biological replicates per treatment group. Error bars are SEM.

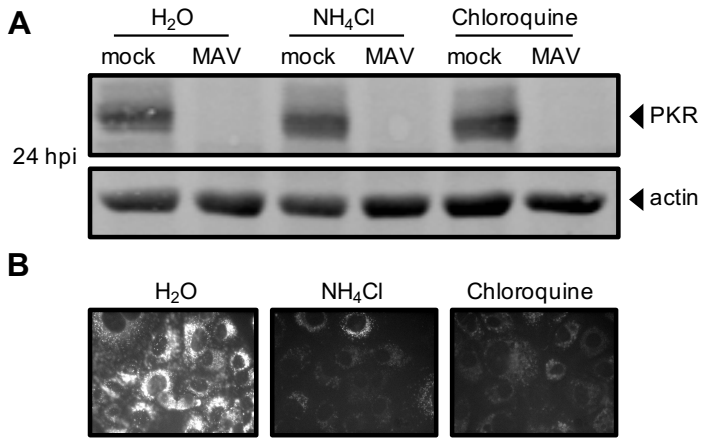

Figure 2.9 PKR is not depleted by lysosomal degradation during MAV-1 infection. (A) CMT93 cells were infected with MAV-1 (MAV) at an MOI of 10 or mock infected (mock) and treated with 10 mM ammonium chloride or 60 µM chloroquine to inhibit lysosomal degradation, or water, as a control. Cell lysates were analyzed by immunoblot with antibodies for PKR (D-20) and actin. Blots are representative of three independent experiments. (B) Inhibitors were tested for activity using a DQ BSA assay; the DQ BSA molecule will only fluoresce if lysosomal degradation is functional. Uninfected cells were treated as indicated and imaged by fluorescence microscopy.

We confirmed that the inhibitor treatment did block lysosomal degradation by incubating cells with dye-quenched bovine serum albumin (DQ BSA) in addition to the lysosomal inhibitors. DQ BSA is self-quenched until it is digested in the lysosome (60, 61), and imaging confirmed that cells treated with lysosome inhibitors did not fluoresce, but cells treated with the vehicle control (H_2O) did, as expected (Fig. 2.9B).

Next, we examined whether proteasomal degradation is responsible for the degradation of PKR by using proteasome inhibitors MG132 and bortezomib. These inhibit proteasome activity by binding to the active sites in the 20S subunit and blocking the proteolytic activity (62-64). We mock infected or infected C57BL/6 MEFs with MAV-1 and treated with MG132 or bortezomib in DMSO at the time of infection. At 24 hpi, we collected lysates and analyzed them by immunoblot for PKR protein levels. While PKR was depleted in the control DMSO-treated MAV-1-infected cells as expected, PKR protein was present in the MG132- and bortezomib-treated cells at levels comparable to mock infected cells (Fig. 2.10A and B). To rule out the possibility that PKR was present (not depleted) because the virus infection itself was inhibited by MG132 or bortezomib, we assayed viral replication of MAV-1 with MG132 and bortezomib treatment by qPCR of viral DNA. Viral replication was equivalent in all three treatment groups (Fig. 2.10C), indicating that the treatments did not affect the ability of the virus to productively infect the cells. Taken together, these data indicate that MAV-1 infection results in PKR depletion by causing PKR to be degraded by the proteasome during infection. This protection of PKR protein levels by proteasome inhibitors was only effective if the proteasome inhibitors were added at an early time point of infection, prior to 24 hpi. When proteasome inhibitors were added at times when PKR protein levels were already significantly reduced (e.g., 24 hpi, lanes 6, 8, 12,

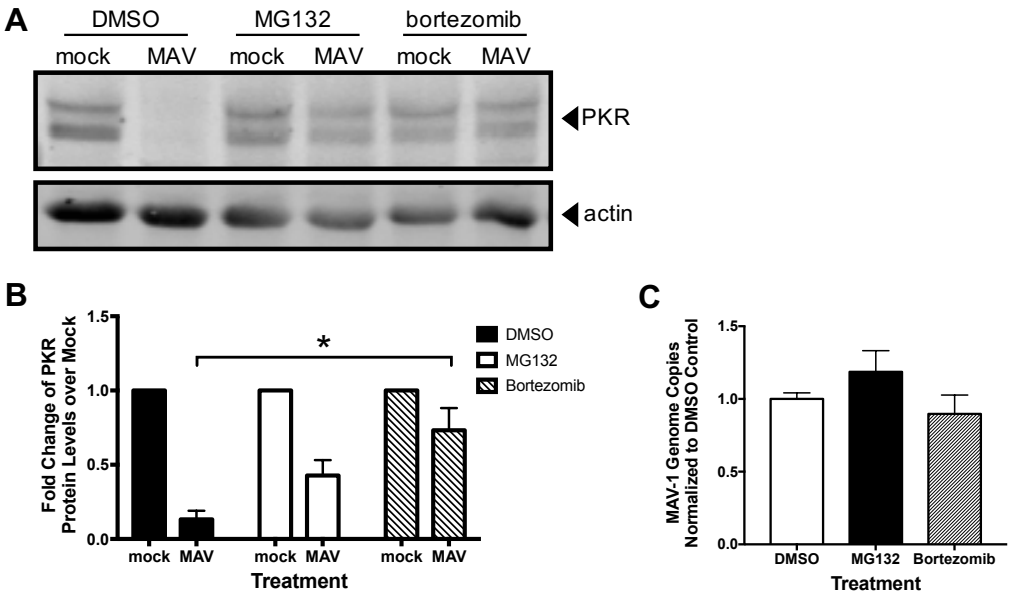

Figure 2.10 PKR is depleted by proteasomal degradation during MAV-1 infection. (A) C57BL/6 MEFs were infected with MAV-1 (MAV) at an MOI of 10 or mock infected (mock) and treated with DMSO (vehicle for inhibitors), 1 μM MG132, or 1 μM bortezomib. Cell lysates were analyzed by immunoblot with antibodies for PKR (D-20) and actin. Blots are representative of four independent experiments. (B) Densitometry quantitation of four independent experiments. Treatment with bortezomib significantly inhibited PKR depletion in MAV-1 infected cells, $*P \leq 0.05$. (C) MG132 and bortezomib treatments do not affect MAV-1 replication at 24 hpi. C57BL/6 MEFs were infected with MAV-1 at an MOI of 10 and treated with DMSO (vehicle for inhibitors), 1 μM MG132 or bortezomib, and collected at 24 hpi. DNA was purified from cell pellets and analyzed for MAV-1 genome copies by qPCR. Graph is representative of five biological replicates per treatment group. Error bars are SEM. $*P \leq 0.05$

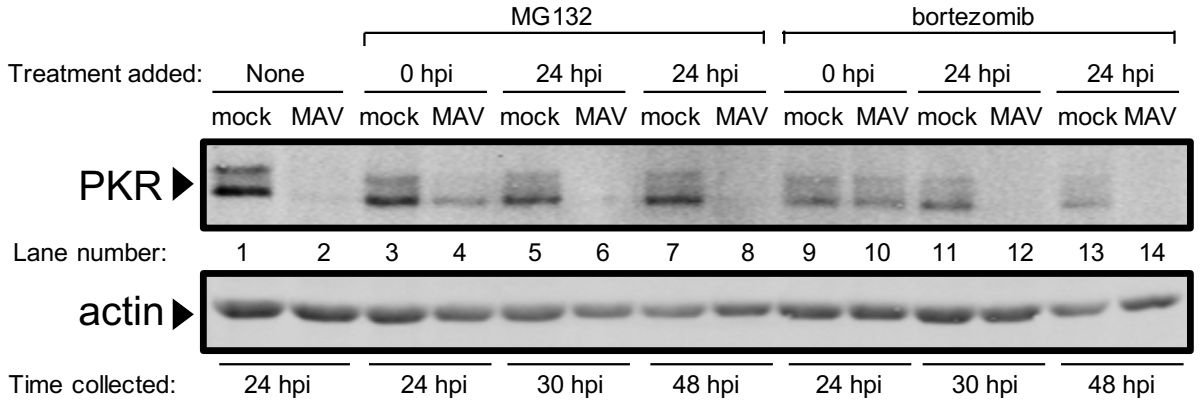

Figure 2.11 Delayed proteasome inhibition does not prevent PKR depletion during MAV-1 infection. C57BL/6 MEFs were infected with MAV-1 (MAV) at an MOI of 10 or mock infected (mock) and treated with DMSO (vehicle for inhibitors), 1 μM MG132, or 1 μM bortezomib at 0 or 24 hpi. Cell lysates were were analyzed by immunoblot with antibodies for PKR (D-20) and actin. Blots are representative of four independent experiments.

14), there was no protective effect from the proteasome inhibitors, even when cells were subsequently treated for a full 24 hours (lanes 8, 14) (Fig. 2.11).

PKR is not detectably ubiquitinated during MAV-1 infection

A signal for proteasomal degradation is the conjugation of ubiquitin to a protein (65, 66). We examined whether PKR is ubiquitinated, assaying by immunoprecipitation and immunoblot. We also assayed the ubiquitination of a positive control, mouse p53, which is degraded in the presence of MAV-1 proteins (67). We transfected CMT93 cells with a GFP-tagged ubiquitin (68), and at 24 hours post transfection (hpt), we infected them with MAV-1 at an MOI of 5 or mock infected. Cells were treated with MG132 at 6 hours prior to harvest to prevent complete PKR degradation. Lysates were immunoprecipitated with PKR (D-20), p53 (DO-1), or corresponding isotype antibodies. The immunoprecipitated samples were analyzed by immunoblot with antibodies to GFP, ubiquitin, PKR (B-10), p53 (1801), or corresponding isotype antibodies (Fig. 2.12A and B). Ubiquitination of p53 was readily evident (Fig. 2.12B). However, even with the use of epitope-tagged ubiquitin, we were unable to detect PKR ubiquitination during infection (Fig. 2.12A). This is consistent with an inability to detect PKR ubiquitination when it is degraded during RVFV infection (32). Although RVFV NSs is known to recruit an E3 ligase to PKR, the authors reported that ubiquitinated PKR is undetectable. Therefore, the cellular degradation signal for PKR remains unclear.

PKR is actively depleted early in infection

We investigated when proteasomal degradation of PKR occurs. Early viral proteins are expressed prior to viral DNA replication, which is then followed by late viral protein expression.

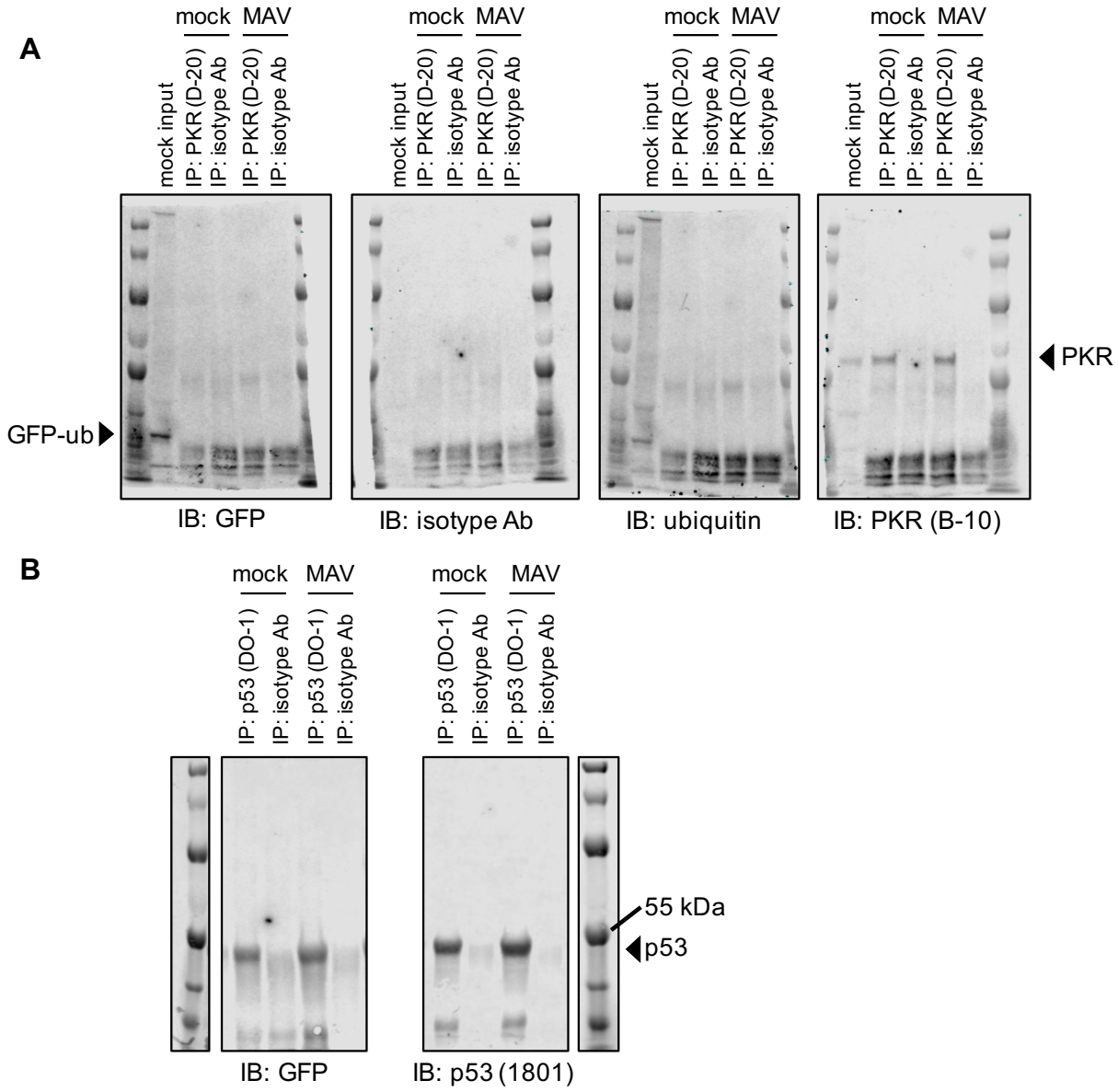

Figure 2.12 PKR is not detectably ubiquitinated during MAV-1 infection. CMT93 cells were transfected with a GFP-ubiquitin plasmid using standard Polyplus transfection protocols. At 24 hpt, the cells were infected with MAV-1 (MAV) at an MOI of 5 or mock infected (mock) and treated with 10 µM MG132 at 6 hpi. Cell lysates were collected at 12 hpi and immunoprecipitated with (A) PKR (D-20) or an isotype control antibody or (B) p53 (DO-1) or an isotype control antibody. Immunoprecipitated samples were analyzed by immunoblot with GFP, ubiquitin, isotype, PKR (B-10), or p53 (1801) antibodies. Input lane (mock input) contains 0.008 volume of mock infected lysate (relative to volume in immunoprecipitations). For (B) GFP and p53 were probed on separate duplicate blots.

First, we examined the kinetics of PKR degradation to determine whether an early or late viral protein was likely responsible. We mock infected and infected CMT93 cells with MAV-1 at an MOI of 10 and collected lysates every six hours for 24 hours and analyzed them by immunoblot with antibodies to PKR or MAV-1 early region 1A (E1A) protein, the first viral protein made during infection (69). In infected cells, PKR degradation was first detected at 12 hpi (Fig. 2.13A), and quantitation of five independent experiments showed that ~20% of the starting levels of PKR protein remained at 24 hpi (Fig 2.13B).

In parallel, to determine the half-life of PKR in uninfected CMT93 cells, we treated CMT93 cells with cycloheximide to halt protein translation and thus production of new PKR. We collected lysates every six hours for 24 hours and analyzed by immunoblot with antibodies to PKR. After 24 hours of cycloheximide treatment, approximately 90% of the starting levels of PKR protein remained (Fig. 2.13A bottom, and B). Comparing the results from MAV-1 infection (Fig. 2.13A top, and 2.13B) and cycloheximide treatment of uninfected cells (Fig. 2.13A bottom, and 2.13B), we conclude that MAV-1 was actively depleting PKR protein early in infection. E1A was detected by immunoblot at 18 hpi (Fig. 2.13C), whereas viral DNA replication was first detected at 24 hpi in CMT93 cells (Fig. 2.14). Thus the 18 hpi timepoint is considered an early time point during MAV-1 infection of CMT93 cells, prior to DNA replication, suggesting the involvement of an early viral protein in PKR depletion.

An early viral function is required for PKR depletion by MAV-1

To determine whether viral gene expression or DNA replication are required for PKR degradation during infection, we infected C57BL/6 MEFs and CMT93 cells with UV-inactivated MAV-1 (which does not replicate, Fig. 2.15C and D). We infected cells at an MOI of 10 with

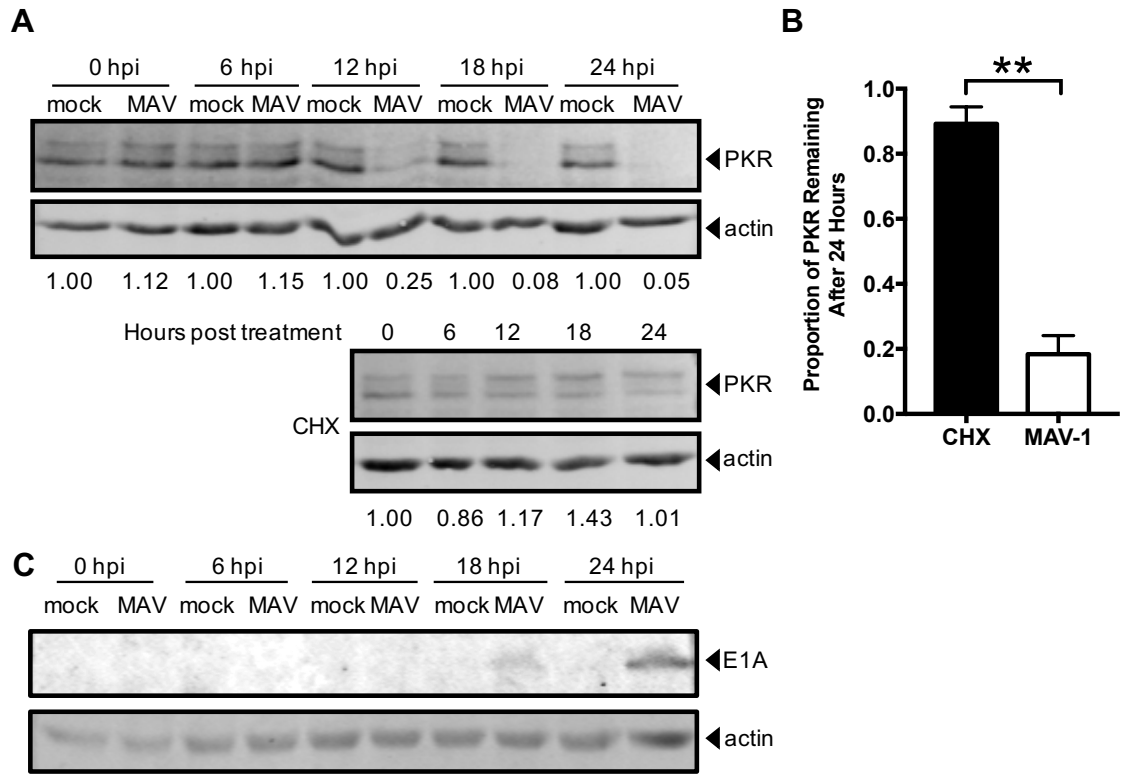

Figure 2.13 PKR is actively depleted early in infection. (A) CMT93 cells were infected with MAV-1 (MAV) at an MOI of 10 or mock infected (mock) (top), or uninfected cells were treated with 50 µg/mL cycloheximide (CHX, bottom) to inhibit elongation of protein synthesis. Cell lysates were analyzed by immunoblot with antibodies for PKR (D-20) and actin. Blots are representative of five independent experiments. (B) Densitometry quantitation of five independent experiments. Error bars are SEM. $^{**}P \leq 0.01$. (C) CMT93 cell lysates from A were analyzed with a second immunoblot with antibodies for E1A and actin. Blots are representative of four replicates from two independent experiments.

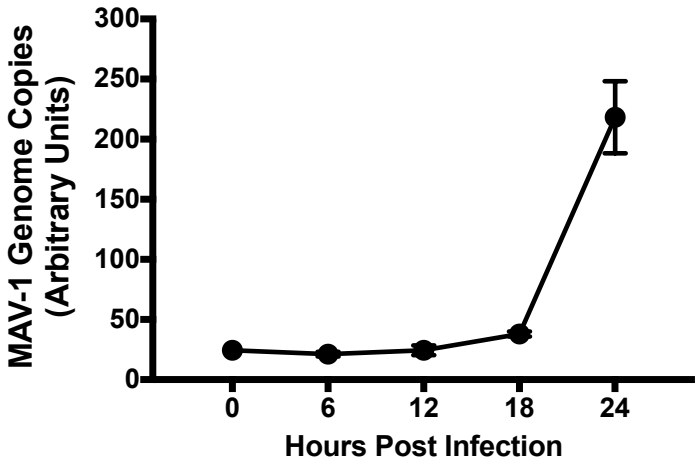

Figure 2.14 Viral replication can be detected at 24 hpi by qPCR. CMT93 cells were infected with MAV-1 (MAV) at an MOI of 10 and collected every 6 hours for 24 hours. DNA was purified from cell pellets and analyzed for MAV-1 genome copies by qPCR. Graph is representative of four to five biological replicates per treatment group. Error bars are SEM.

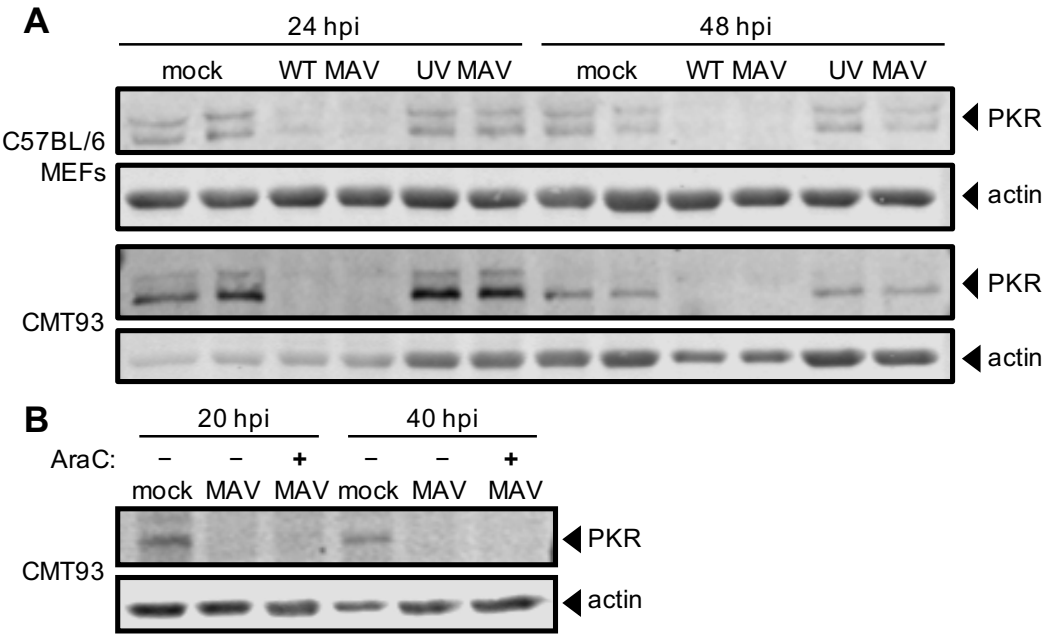
A
24 hpi
48 hpi
mock
WT MAV
UV MAV
mock
WT MAV
UV MAV
C57BL/6 MEFs
PKR
actin
CMT93
PKR
actin

B
20 hpi
40 hpi
AraC: – – + – – +
mock MAV MAV mock MAV MAV
CMT93
PKR
actin

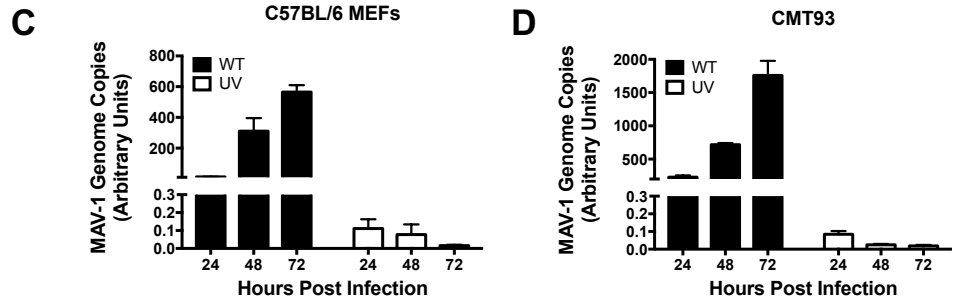
C
C57BL/6 MEFs
MAV-1 Genome Copies (Arbitrary Units)
WT
UV
800
600
400
200
0.3
0.2
0.1
0.0
24 48 72 24 48 72
Hours Post Infection
D
CMT93
MAV-1 Genome Copies (Arbitrary Units)
WT
UV
2000
1500
1000
500
0.3
0.2
0.1
0.0
24 48 72 24 48 72
Hours Post Infection

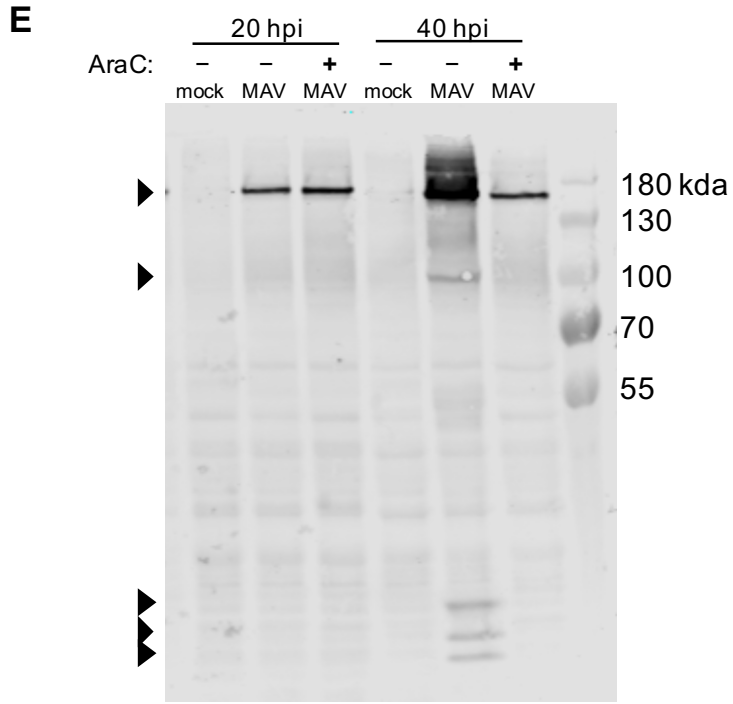
E
20 hpi
40 hpi
AraC: – – + – – +
mock MAV MAV mock MAV MAV
180 kda
130
100
70
55

Figure 2.15 Early gene expression is required for PKR depletion by MAV-1. (A) Cells (as indicated at left) were infected with WT MAV-1 (WT MAV) or UV-inactivated MAV-1 (UV MAV) at an MOI of 10, or mock infected (mock). Cell lysates were analyzed by immunoblot with antibodies for PKR (D-20) and actin. Two independent wells were infected for each condition at both time points. (B) CMT93 cells were infected with WT MAV-1 (MAV) at an MOI of 10 or mock infected (mock). Infected cells were also treated (+) or not (-) with 20 µg/mL cytosine arabinasine (AraC), an inhibitor of DNA synthesis. Cell lysates were analyzed with antibodies for PKR and actin. (C) UV-inactivated virus does not replicate. C57BL/6 MEFs or (D) CMT93 cells were infected with WT MAV-1 (WT) or UV-inactivated MAV-1 (UV) at an MOI of 10 and collected at indicated times. DNA was purified from cell pellets and analyzed for MAV-1 genome copies by qPCR. Graphs are representative of three to four biological replicates per treatment group. Error bars are SEM. (E) AraC treatment inhibited late protein expression. CMT93 cells were infected with WT MAV-1 (MAV) at an MOI of 10 or mock infected (mock). Infected cells were also treated (+) or not (-) with 20 µg/mL cytosine arabinasine (araC), an inhibitor of DNA synthesis. Cell lysates were analyzed with antibodies for late virion proteins (AKO1-103, 1:1000). Arrowheads indicate late viral proteins.

WT MAV-1 or UV-inactivated MAV-1 and analyzed lysates from 24 and 48 hpi by immunoblot for PKR protein levels. In both cell types, while PKR was degraded by 24 hpi in the cells infected with WT MAV-1, PKR protein levels were unaffected at both time points in cells infected with UV-inactivated MAV-1 (Fig. 2.15A). This suggested that either gene expression or DNA replication was required for PKR degradation during MAV-1 infection.

We addressed whether viral DNA replication is needed for PKR degradation. We mock infected or infected CMT93 cells with MAV-1 at an MOI of 10 and treated them with cytosine arabinoside (araC) at the time of infection to inhibit DNA synthesis (70, 71). This would allow the virus to infect the cell and produce early viral proteins, but would inhibit viral DNA replication and prevent late protein synthesis. We collected lysates at 20 and 40 hpi and analyzed them by immunoblot. We confirmed that araC treatment resulted in no late protein synthesis by performing an immunoblot for late virion proteins (Fig. 2.15E). In samples treated with araC, PKR degradation was seen at 20 and 40 hpi (Fig. 2.15B), indicating that DNA replication was not required for PKR degradation. Taken together, the results of Fig. 2.15 are consistent with early viral gene expression prior to DNA replication being involved in induction of PKR degradation by MAV-1.

E1A and E3 are not required for PKR degradation during MAV-1 infection

To investigate the early gene responsible for PKR degradation during MAV-1 infection, we used two mutant viruses, $E1A^-$ and $E3^-$, which replicate successfully but do not express the specified early gene products (69, 72). We infected C57BL/6 primary peritoneal macrophages and C57BL/6 MEFs with wild type MAV-1, $E1A^-$ MAV-1, or $E3^-$ MAV-1 at an MOI of 5 and analyzed lysates from 24, 72, and 96 hpi by immunoblot for PKR protein levels. In the

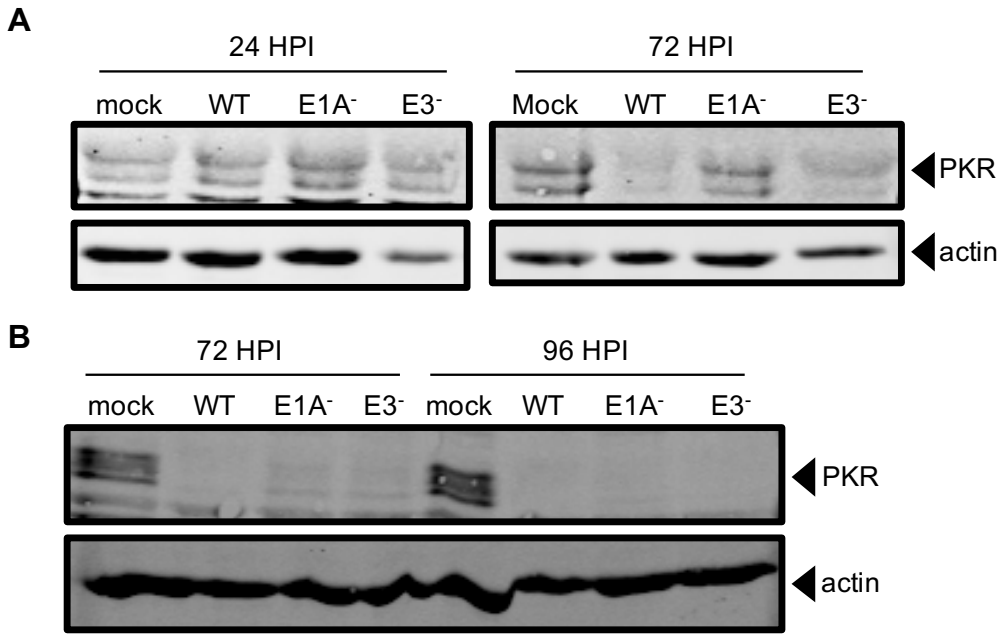

Figure 2.16 E1A and E3 are not required for PKR degradation during MAV-1 infection. (A) C57BL/6 primary peritoneal macrophages or (B) C57BL/6 MEFs were infected with WT MAV-1 (WT), E1A$^-$ mutant MAV-1 (E1A$^-$), or E3$^-$ mutant MAV-1 (E3$^-$) at an MOI of 10, or mock infected (mock). Cell lysates were analyzed by immunoblot with antibodies for PKR (D-20) and actin.

macrophages, PKR protein was still present at 72 hpi in the cells infected with the E1A$^-$ virus, though at levels lower than in mock infected macrophages (Fig. 2.16A). This could mean that E1A is required for PKR degradation, but it could also just be a result of slower infection, because the E1A mutant virus demonstrates slower growth kinetics compared to wild type MAV-1 (73). We examined PKR protein levels in C57BL/6 MEFs after 96 hpi with wild type, E1A$^-$, and E3$^-$ MAV-1. In C57BL/6 MEFs, PKR was completely degraded by all three viruses by 96 hpi, suggesting that neither E1A nor E3 is required for PKR degradation during MAV-1 infection (Fig. 2.16B).

Discussion

We have demonstrated here that PKR is antiviral in MAV-1 infections of cultured cells. Surprisingly, MAV-1 infection of primary and established cultured cells depleted PKR. The depletion was not due to reduced steady-state levels or reduced translation of PKR mRNA. Instead, we showed that PKR depletion is inhibited by proteasome inhibitors, implicating proteasomal degradation of PKR. Several lines of evidence suggest that the degradation is due to a viral early function.

PKR is an IFN-inducible gene product that is an important component of the innate immune response (1, 49). However, not all viruses have increased virulence in PKR$^{-/-}$ MEFs, including EMCV and vaccinia virus (51, 74). While hAds produce VA RNAs that inhibit PKR antiviral activity during infection (10, 75), MAV-1 does not produce such VA RNAs, and how MAV-1 infection is affected by PKR is first described in this report. When we infected PKR$^{-/-}$ MEFs with MAV-1, viral yields were 5 to 6 times higher than viral yields from wild type MEFs (Fig. 2.2A), indicating that PKR plays an antiviral role during MAV-1 infection. At 48 hpi, the

viral yield from the N-MEFs (cells lacking the N terminal region dsRNA binding domain of PKR) was nearly 4 times higher than the C-MEFs (cells lacking the C terminal region kinase domain of PKR), but by 72 hpi the viral yields from both types of $PKR^{-/-}$ MEFs were similar to each other and significantly increased compared to wild type MEFs (Fig. 2.2A). This difference in viral replication kinetics between the two types of $PKR^{-/-}$ MEFs may be due to differences in expression level and activity of the PKR fragments reportedly produced by them; we have not assayed PKR fragment production in our cells.

N-$PKR^{-/-}$ peritoneal macrophages were also more susceptible to MAV-1 infection at 72 hpi than wild type peritoneal macrophages. The viral yield in N-$PKR^{-/-}$ peritoneal macrophages was nearly twice that in wild type peritoneal macrophages. Taken together, these data suggest that PKR activation is an important antiviral response to MAV-1 in multiple cell types. However, *in vivo*, N-$PKR^{-/-}$ mice did not have reduced survival compared to wild type mice when infected with MAV-1 (Fig. 2.3). Thus, while PKR likely plays a significant antiviral role is specific tissues, there may be redundancies in the PKR signaling pathway that compensate when PKR is not present or is inactivated. Alternatively, since N-$PKR^{-/-}$ mice may express a PKR fragment with kinase activity (52), it is possible that this fragment provides enough PKR activity to protect the mice from MAV-1 infection. However, we have not examined *in vivo* expression of this fragment.

We examined PKR protein levels during MAV-1 infection and found that PKR was depleted from the cells as early as 12 hpi (Fig. 2.13A). Depletion was seen in a wide variety of cell types, including immortalized C57BL/6 MEFs, primary C57BL/6 peritoneal macrophages, and CMT93 mouse colon carcinoma cells (Fig. 2.4A). Once depleted, PKR protein levels never returned to mock infected PKR protein levels during infection. Activation (phosphorylation) of

PKR (6-9) was not required for this depletion, because kinase-dead mouse PKR was also depleted from K271R SV40-MEFs during infection (Fig. 2.4C). Both PKR and phospho-PKR were depleted in all cell types examined. huPKR was not depleted by MAV-1 (Fig. 2.5A). This suggests that MAV-1 degrades PKR by recognizing PKR protein sequence in a region that is dissimilar between mouse PKR and human PKR, because the two proteins share only 58% amino acid identity overall. This could help in identifying the region of mouse PKR that is responsible for its degradation by MAV-1.

We examined several possibilities that could explain depletion of PKR protein, including PKR mRNA levels and alterations in translation. PKR mRNA levels remained unchanged during MAV-1 infection in C57BL/6 MEFs at 24 hpi and were increased in primary C57BL/6 peritoneal macrophages during MAV-1 infection (Fig. 2.6), times when the PKR protein levels were depleted (Fig. 2.4A). While PKR mRNAs in C57BL/6 MEFs were depleted 33% at 48 hpi and 40% at 72 hpi compared to mock lysates, this is not sufficient to explain the 84% and 94% reduction, respectively, in PKR protein levels at those time points (Fig. 2.4B). More likely, the reduction in PKR steady-state mRNA levels at the late infection time points can be attributed to other effects from viral infection, including the degradation or inhibition of proteins that induce PKR expression. For example, p53 is capable of binding to the PKR promoter and inducing its expression (76), but MAV-1 proteins cause p53 proteolysis (67). Together our results in C57BL/6 MEFs and macrophages suggest the virus does not cause PKR protein depletion by reducing PKR steady-state mRNA levels.

The differences in total PKR mRNA levels during infection between C57BL/6 MEFs and primary peritoneal macrophages (Fig. 2.6) is possibly due to the fact that macrophages are an immune cell, while MEFs are not. PKR protein took almost 3 times as long to be completely

degraded during infection in macrophages compared to MEFs (72 hours versus 24 hours) (Fig. 2.4A). Total PKR mRNA levels were 2 to 3 times higher in MAV-1-infected macrophages compared to mock infected macrophages, unlike the MEFs where total PKR mRNA levels were unchanged or reduced 33-40% during MAV-1-infection compared to mock infected MEFs. Since PKR is an IFN-stimulated gene (1, 2), higher levels of total PKR mRNA seen during infection in the macrophages suggests IFN induction. This suggests that the immune response mounted by the macrophages was greater than the immune response in the MEFs, and could help explain why PKR took longer to degrade in macrophages compared to MEFs.

We considered whether reduced PKR levels were due to reduced PKR protein translation. There was no change in the total amount of PKR mRNA bound to ribosomes during infection compared to uninfected cells, nor was there a significant change in the amount of actively translating PKR mRNA during infection (Fig. 2.7). We also found that the 5' UTR of mouse PKR placed upstream of a reporter gene produced the same amount of reporter with and without MAV-1 infection (Fig. 2.8). These data indicate that there are not translational effects of MAV-1 infection on PKR protein levels that could explain the depleted PKR levels we observed.

Inhibiting lysosomal degradation resulted in no change in PKR depletion in infected cells (Fig. 2.9A), but adding proteasome inhibitors preserved PKR protein within cells (Fig. 2.10A and B). This indicates that PKR is not degraded by lysosomal degradation during viral infection, but by proteasomal degradation. However, adding proteasome inhibitors later in infection did not have the same protective effect on PKR protein levels as adding them at the start of infection (Fig. 2.11). This is consistent with delayed proteasome inhibition experiments with RVFV. There, the addition of MG132 prevented p62 degradation by RVFV, but only if MG132 was present at the start of infection (77). This is likely due to the fact that MG132 can trigger a

reduction in global translation (78, 79). The authors propose that if i) MG132 is added to an infection at a time where a specific protein has already been degraded by the proteasome to levels unable to detect by immunoblotting, ii) MG132 also reduces protein translation overall, and iii) MG132 treatment is not 100% effective at shutting down proteasomal degradation, then it is likely that if MG132 is added "too late", newly synthesized protein could not be stabilized by proteasomal inhibition to levels high enough to be detectable by immunoblot. Not only would the translation of the protein be reduced, but the proteasome may be functioning just enough to continue degrading any small amounts of nascent proteins that are produced.

Though PKR degradation was due to proteasome activity during MAV-1 infection, we were unable to demonstrate PKR ubiquitination (Fig. 2.12A), although we did detect ubiquitination of mouse p53 (Fig. 2.12B). This inability to demonstrate PKR ubiquitination could be explained if at any given moment there were only low levels of ubiquitinated PKR present in the cell. Perhaps, increasing the time under MG132 treatment could increase the amounts of ubiquitinated proteins enough so that PKR ubiquitination could be seen. However, our inability to detect ubiquitinated PKR is consistent with a similar inability to identify PKR ubiquitination by RVFV NSs, even though NSs is known to recruit an E3 ligase to PKR (32). Alternatively, it is possible that in MAV-1 infection, PKR is degraded in a ubiquitin-independent manner, possibly because of intrinsic disordered regions of PKR or binding of regulating proteins to PKR that target proteins to the proteasome (80, 81).

Our experiments indicate that MAV-1 actively depletes PKR early in infection. Our data using mutant MAV-1 viruses suggest that E1A and E3 are not required for PKR degradation (Fig. 2.16). Ongoing experiments are focused on determining the MAV-1 early protein(s) responsible for PKR degradation. Two possibilities are E4 proteins, the homologs of hAd E4orf6

and E4orf3, which we originally termed E4orfa/b and E4orfa/c, respectively (82). In hAd, E4orf6 interacts with another early hAd protein, E1B 55K, to participate in an E3 ligase complex that ubiquitinates and degrades p53 via proteasomal degradation (83, 84). When MAV-1 E4orf6, E1B 55K, and mouse p53 are introduced by transfection into human cells, all three proteins interact and mouse p53 is degraded (67). If MAV-1 E4orf6 and E1B 55K form a similar complex in mouse cells, it may also degrade PKR. We have preliminary evidence that mouse p53 is ubiquitinated in C57BL/6 MEFs during MAV-1 infection, which suggests that the mouse p53 degradation seen in human cells could be paralleled by degradation of endogenous mouse p53 and mouse PKR in mouse cells, mediated by MAV-1 E4orf6 and E1B 55K during infection. Another hAd E4 protein, E4orf3, causes proteasomal degradation of transcriptional intermediary factor 1γ (85) and general transcription factor II-I (86) in a manner independent of hAd E4orf6 and E1B 55K. E4orf3 has SUMO E3 ligase and E4 elongase activity and induces sumoylation of general transcription factor II-I, leading to its proteasome-dependent degradation (86). MAV-1 E4orf3 may similarly have sumoylation activity that results ultimately in proteasome-dependent PKR degradation. Another possibility of a viral protein involved in PKR degradation is the protease encoded by MAV-1. The hAd protease is encapsidated in virions and proteolytically processes viral proteins IIIa, VI, VII, VIII, mu, and TP (87-90). However, we think it is unlikely that the MAV-1 protease degrades PKR, because we showed that UV-inactivated virus was unable to degrade PKR. We assume that UV treatment would not destroy the MAV-1 protease activity, just as HSV-1 VP16 activity is not altered by UV-inactivation of HSV-1 (91), but we have not tested this directly.

In summary, we demonstrated that PKR has an antiviral role during MAV-1 infection *in vitro*, because when PKR is mutated, viral replication in MEFs is significantly higher compared

to wild type MEFs. Analysis of global PKR steady-state protein levels during infection showed complete PKR depletion by 72 hpi in multiple cell types, including immortalized and primary cells, with even faster kinetics in some. PKR transcription and translation were not decreased by MAV-1 infection, whereas proteasomal inhibition prevented PKR degradation. Taken together, these data suggest that MAV-1 causes PKR to be proteasomally degraded at a post-translational level. This work provides new insight into possible mechanisms of adenovirus inhibition of PKR by DNA viruses. PKR degradation may be induced by other adenoviruses that do not produce VA RNA, which includes all animal adenoviruses except primate adenoviruses and one type of fowl adenovirus (92).

Materials and Methods

Cells, mice, virus, and infections

CMT93 cells (CCL-223) and C57BL/6 MEFs (SCRC-1008) were obtained from the American Type Culture Collection and passaged in Dulbecco's modified eagle media (DMEM) containing 5% or 10% heat-inactivated fetal bovine serum (FBS), respectively, before use. Primary peritoneal macrophages were obtained from 6-10 week old C57BL/6J mice purchased from Jackson Laboratory (#000664) as described (93). Briefly, 6-10 week old C57BL/6J mice were injected intraperitoneally with 1.2 mL 3% thioglycolate and euthanized 3-5 days later. The abdominal skin was carefully removed, exposing the peritoneum, which was then injected with 5 mL of sterile phosphate-buffered saline (PBS). The abdomen was massaged gently, then the PBS containing the peritoneal macrophages was carefully withdrawn. The macrophages were centrifuged at 100 x g for 4 minutes, red blood cells lysed in lysis buffer (0.15 M ammonium chloride, 1 mM potassium bicarbonate, and 0.1 mM EDTA disodium salt) for 2 minutes at room

temperature, centrifuged at 100 x g for 4 minutes, washed twice in PBS, resuspended in DMEM + 5% heat-inactivated FBS, and plated in 6 well plates. WT and PKR$^{-/-}$ MEFs (termed PKR WT MEFs and N-PKR$^{-/-}$ MEFs, respectively, throughout this paper) were obtained from Robert Silverman, Cleveland Clinic (94) and were passaged in DMEM containing 10% heat-inactivated FBS before use. PKR$^{-/-}$ MEFs stably transfected with empty vector (termed C-PKR$^{-/-}$ MEFs throughout this paper), full length human PKR (full length huPKR), kinase dead human PKR (kinase-dead huPKR), or RNA binding-deficient human PKR (huPKR) were obtained from Dr. Gokhan Hotamisligil, Harvard University (56) and were passaged in DMEM containing 10% heat-inactivated FBS before use. WT (SV40-MEFs) and K271R PKR mutant (K271R SV40-MEFs) MEFs were obtained from Anthony Sadler, Hudson Institute of Medical Research (55) and were passaged in DMEM containing 10% heat-inactivated FBS before use.

N-PKR$^{-/-}$ mice on the C57BL/6J background were obtained from Robert Silverman (Cleveland Clinic) (53). The N-PKR$^{-/-}$ mice were bred in-house and both sexes were used in experiments. No differences based on sex was noted. All animal work complied with relevant federal and University of Michigan policies. Mice were housed in microisolator cages and provided with food and water ad libitum. C57BL/6J mice were purchased from Jackson Laboratory (#000664).

Wild type MAV-1 stock was prepared and titrated on mouse NIH 3T6 fibroblasts as described previously (95). WT MAV-1 was UV-inactivated by UV-treating 200 µL of virus for 10 min at 800 mJ/cm^2. UV inactivation was confirmed by qPCR and plaque assay. E1A$^-$ and E3$^-$ mutant viruses, *pm*E109 (69) and *pm*E314 (72), respectively, have been described previously.

For infections, media was removed from cells and adsorption was performed in 0.4 mL of inocula for 6-well plate 35-mm wells (unless otherwise noted) for 1 hour at 37˚C. After 60

minutes, 2 mL of DMEM+5% FBS was added without removing inocula; this time was designated as 0 hpi. For araC experiments, 20 μg/mL araC (Sigma C1768) was added at 0 hpi and replenished every 12-16 hours.

Plasmids

We purchased GFP-epitope tagged ubiquitin plasmids from Addgene (Addgene #11928). pmPKR5UTRfullNL contains the 189 nucleotide 5' UTR of mouse PKR (96) (inserted between AflII and HindIII restriction sites) upstream of a nanoluciferase gene. The vector containing the nanoluciferase gene, AUG-NL-3xFLAG pcDNA3.1, was a gift from the lab of Peter Todd (58). pGL4.13 is a standard firefly luciferase plasmid from Promega (Promega E6681).

Immunoblots

At room temperature, cells were washed once with PBS and Pierce™ RIPA lysis buffer (Thermo Scientific #89900) with 1x protease inhibitors (Protease Inhibitor Cocktail Kit, Thermo Scientific #78410) was added to the plate. The cells were allowed to lyse at room temperature for 10 minutes before being harvested and centrifuged at 4˚C at 14,000 x g for 10 minutes to remove debris. Equivalent amounts of protein, determined by a BCA assay (Pierce BCA Protein Assay Kit, Thermo Scientific #23227), were acetone precipitated by incubating with 4x volume ice cold acetone overnight at -20˚C. Precipitated proteins were pelleted at 4˚C at 13,000 x g for 10 minutes and the pellets were dried for 30 minutes at room temperature. Pellets were resuspended in 10 μL Pierce™ RIPA lysis buffer (Thermo Scientific #89900), 3.25 μL NuPAGE 4x LDS Sample Buffer (Invitrogen Cat #NP0007), and 1.25 μL 1M DTT. Samples were incubated at 37˚C for 10 minutes and then loaded into a well of an 8% acrylamide gel (8.3 cm wide x 7.3 cm

high x 0.1 cm thick) with a 2.5% stacking gel, electrophoresed for 30 minutes at 50 V and 85 minutes at 150 V, and then transferred to a PVDF membrane (BioRad #1620177) for 1 hour at 100V at 4˚C. Blots were blocked in 5% bovine serum albumin (BSA, Sigma A7906) in tris-buffered saline (BioRad #1706435) and 0.1% Tween 20 (Sigma P1379). Blots were probed with primary antibodies to detect mouse PKR (Santa Cruz D-20 sc-708, 1:2000, or B-10 sc-6282, 1:200), mouse actin (Santa Cruz sc-1616-R, 1:1000), MAV-1 E1A (AKO-7-147, 1:1000, described previously (69)), or MAV-1 late viral proteins (AKO 1-103, 1:1000, described previously (97, 98)). Secondary antibodies used were IRDye 800CW anti-rabbit (Li-Cor 925-32213, 1:15,000) or IgG peroxidase-conjugated anti-mouse (Jackson Immuno 515-035-062, 1:20,000). Blots were visualized by LI-COR Odyssey imaging (LI-COR Biosciences) or enhanced chemiluminescent substrates (Pierce ECL Western Blotting Substrate #32106) and X-ray film (Dot Scientific #BDB810). Densitometric quantification was performed on .tif files using ImageJ software from NIH (99).

Ubiquitination immunoprecipitations

To examine PKR ubiquitination status during MAV-1 infection, C57BL/6 MEFs were transfected with GFP-epitope tagged ubiquitin plasmids (Addgene #11928) 24 hours before infection. We used Polyplus jetPRIME transfection reagent (Polyplus #114-01) with 10 µg plasmid DNA and 30 µL jetPRIME reagent per 10 cm plate. At 6 hpi (30 hpt), we treated mock and infected C57BL/6 MEFs with 10 µM MG132 (Sigma M7449) for 6 hours before collecting lysates at 12 hpi in 300 µL/plate of HCN buffer (50 mM HEPES, 150 mM NaCl, 2 mM $CaCl_2$, 1% Triton X-100 (Sigma T9284), 1x protease inhibitors (Protease Inhibitor Cocktail Kit, Thermo Scientific #78410), and 5 mM N-ethylmalemide). The lysates were split into two aliquots, and 3

µg PKR (D-20 sc-708, discontinued) or 3 µg isotype rabbit polyclonal antibody (Jackson Immuno #011-000-002) was added to lysates. After rocking samples overnight at 4˚C, 20 µL protein A agarose suspension (Calbiochem/Millipore #IP02-1.5ML) was added to each and samples were rocked at 4˚C for 2 hours. After incubation, agarose was washed 3 times with 1 mL HCN buffer, resuspended in 40 µL 2x Laemmli buffer (BioRad #161-0737) with 5% 2-mercaptoethanol (Sigma M6250), and boiled for 10 minutes. Lysate supernatants remaining after the initial PKR immunoprecipitation were then immunoprecipitated again using the same procedure but with 4 µg anti-p53 (DO-1, Santa Cruz sc-126) or 4 µg isotype mouse monoclonal antibodies (ThermoFisher Scientific #02-6200). Immunoprecipitated proteins were immunoblotted for GFP-epitope tagged ubiquitin with antibodies for GFP (1:3,000, Roche #11814460001). Blots were also probed for PKR (1:200, PKR B-10 sc-6282), p53 (1:200, anti-p53 1801 sc-98), ubiquitin (1:1000, ThermoFisher #13-1600), isotype (1:1000, mouse IgG1 eBioscience 14-4714-82), and IRDye 800CW anti-mouse (Li-Cor 925-32212, 1:15,000) to confirm the immunoprecipitations were successful.

Viral yield analysis by qPCR

Cells were washed twice with room temperature PBS and harvested by scraping into PBS, centrifuging at 100 x g for 4 minutes at 4˚C, and resuspending in PBS. Total cellular DNA was purified using the Invitrogen PureLink DNA Purification Kit (Thermo Scientific #K1820-02) and quantitated by a NanoDrop Spectrophotometer. 10 ng of total cellular DNA was analyzed by qPCR using custom primers specific to MAV-1 E1A (mE1Agenomic Fwd: 5' GCA CTC CAT GGC AGG ATT CT 3' and mE1Agenomic Rev 5' GGT CGA AGC AGA CGG TTC

TTC 3') and the results were normalized to GAPDH, which was analyzed using a GAPDH-specific primer/probe set (ThermoFisher Scientific, Mm99999915_g1, #4331182).

mRNA analysis by qPCR

Cells were harvested by scraping into media, centrifuging at 100 x g for 4 min at 4˚C, and washing the cell pellet three times with ice-cold PBS. RNA was purified using the Qiagen RNeasy Mini Kit (Qiagen #74134) and stored at -80˚C. 125 ng of RNA per sample was used to make cDNA using the High Capacity cDNA Reverse Transcription Kit (Applied Biosystems #4368814), and 2 µL of the cDNA was analyzed by qPCR using a primer/probe set specific to mouse PKR sequence (Thermo Fisher, Mm01235643_m1, #4331182). The results were normalized to GAPDH, which was analyzed using a GAPDH-specific primer/probe set (ThermoFisher Scientific, Mm99999915_g1, #4331182). Arbitrary units were calculated as follows: Mean C_T PKR – mean C_T GAPDH = ΔC_T for sample. Arbitrary unit = 2^-ΔC_T.

Proteasome inhibition

C57BL/6 MEFs were infected at an MOI of 10, and DMSO, 1 µM MG132 (Sigma M7449), or 1 µM bortezomib (Selleckchem #S1013) were added to the media after a 1 hour adsorption. At 24 hpi, cells were washed once with room temperature PBS, and Pierce™ RIPA lysis buffer (Thermo Scientific #89900) with 1x protease inhibitors (Protease Inhibitor Cocktail Kit, Thermo Scientific #78410) was added to the plate. The cells were allowed to lyse at room temperature for 10 minutes before being harvested and centrifuged at 4˚C at 14,000 x g for 10 minutes to remove debris.

Lysosome inhibition and DQ BSA assay

CMT93 cells were infected at an MOI of 10. After a 1 hour adsorption, 10 μL water, 10 mM NH_4Cl (final concentration, Baker Chemical Company #0660-1), or 60 μM chloroquine (final concentration, Sigma C6628) was added to the media. At 24 hpi, at room temperature, cells were washed once with PBS and Pierce™ RIPA lysis buffer (Thermo Scientific #89900) with 1x protease inhibitors (Protease Inhibitor Cocktail Kit, Thermo Scientific #78410) was added to the plate. The cells were allowed to lyse at room temperature for 10 minutes before being harvested and centrifuged at 4˚C at 14,000 x g for 10 minutes to remove debris.

The DQ BSA assay was performed as described (61). Briefly, C57BL/6 MEFs and CMT93 cells were plated at 1.5 x 10^5 cells/plate or 3 x 10^5 cells/plate, respectively, in MatTek Glass Bottom Microwell Dishes (Part No: P35G-1.5-14C) with 2 mL of DMEM + 10% or 5% FBS, respectively. The next day, the cell media was treated with 10 μL water, 10 mM NH_4Cl (final concentration), or 60 μM chloroquine (final concentration, Sigma C6628). Four hours after adding inhibitors, DQ Red BSA (Invitrogen Cat #D12051) was added to the media to a final concentration of 5 μg/mL in 2 mL DMEM + 10% or 5% FBS, respectively. At 24 hours post treatment, the cells were imaged on a Nikon TE300 inverted microscope equipped with a mercury arc lamp, Plan-Apochromat 60x, 1.4 NA objective, cooled digital CCD camera (Quantix Photometrics, Tucson, AZ), and a temperature-controlled stage, set at 37˚C. To image the DQ-BSA, we used an excitation filter centered at 572 nm and an emission filter centered at 635 nm. The exposure time was the same for all images.

Ribosome pelleting

Ribosomes were pelleted as described (100). Briefly, C57BL/6 MEFs were plated on 10 cm plates, $3x10^5$ cells per plate. The next day, the cells (~90% confluent) were infected with MAV-1 at an MOI of 5. C57BL/6 MEF lysates were collected at 48 hpi by scraping the cells in ice-cold PBS containing 100 µg/mL cycloheximide (Sigma C7698), pelleting, and resuspending in lysis buffer, which was 10 mM HEPES pH 7.5, 100 mM KCl, 5 mM $MgCl_2$, 4 mM DTT, 0.5% NP-40, 100 µg/mL cycloheximide, 20 U/mL RNasin (Promega # N2511), 10% sucrose, and 1x protease inhibitors (Protease Inhibitor Cocktail Kit, Thermo Scientific #78410). Cells were lysed by passage through a chilled 26G needle five times and cleared by centrifugation for 10 min at 21,000 x g at 4˚C. 400 µL of cleared lysate (10 OD_{260nm} units) was layered onto 25% sucrose and centrifuged 29,500 rpm in an SW41 rotor (107,458 rcf average) for 4 hours at 4˚C. After pelleting, the supernatant was removed with a micropipet and 350 µL of 4˚C Buffer RLT Plus (from Qiagen RNeasy Mini Kit) was added to the pellet to collect the RNA. RNA was purified immediately using the Qiagen RNeasy Mini Kit (Qiagen #74134) and stored at -80˚C until analysis.

Polyribosome gradients

C57BL/6 MEFs were plated on 10 cm plates, 2 x 10^6 cells per plate. The next day, the cells were infected with MAV-1 at an MOI of 2. Following a standard protocol (101), 5 minutes prior to collection, cycloheximide was added at a final concentration of 100 µg/mL and incubated at 37˚C. Cells were collected at 24 hpi by scraping in ice-cold PBS containing 100 µg/mL cycloheximide, pelleting, and resuspending in 500 µL lysis buffer (20 mM Tris-Cl, 150 mM NaCl, 15 mM $MgCl_2$, 8% glycerol, 20 IU/mL SUPERase•In (ThermoFisher Scientific Cat#

AM2696), 80 IU/mL Murine RNAse Inhibitor (New England BioLabs Cat# M0314S), 0.1 mg/mL heparin (Sigma H3393-50), 0.1mg/mL cycloheximide, 1 mM DTT, 1x protease inhibitor (Protease Inhibitor Cocktail Kit, Thermo Scientific #78410), 20 IU/mL Turbo DNAse (ThermoFisher Scientific Cat# AM2238), and 1% Triton X-100 (Sigma T9284). Cells were lysed by passaging through a chilled 26G needle ten times, vortexing for 30 seconds, and then incubating on ice for 5 min. Lysates were cleared by centrifugation for 5 min at 14,000 x g at 4˚C. 500 µL of cleared lysate (10 OD_{260nm}) was layered onto a 10-50% sucrose gradient and centrifuged at 35,000 rpm in an SW41 rotor (151,000 rcf) for 3 hours at 4˚C. After centrifugation, gradients were pumped out of the top with a Brandel BR-188 Density Gradient Fractionation System with a continuous reading of the $OD_{254\ nm}$. From 24-34 fractions (350-500 µL) were collected. RNA was purified from selected fractions immediately using the Qiagen RNeasy Mini Kit (Qiagen #74134) and stored at -80˚C until analysis by RT-qPCR.

Nanoluciferase assays

For both CMT93 cells and C57BL/6 MEFs, approximately 7500 cells were seeded into each well of a 96-well plate. The following day, the cells were co-transfected with pmPKR5UTRfullNL and pGL4.13 using jetPRIME reagent (Polyplus 114-01) using the standard Polyplus protocol, with 200 ng total of plasmid and 0.6 µL of jetPRIME reagent per well. 24 hours after transfection, the cells were infected with MAV-1 at an MOI of 10. 24 hours after infection (48 hpt), cells were lysed in 70 µL/well Glo Lysis buffer (Promega E2661). 25 µL of each lysed sample was added to each of two wells of a black 96-well plate (Greiner Microlon black microplate, Fisher Scientific #07-000-634). To each sample, we added either 25 µL of OneGlo (Promega E6110) or 25 µL NanoGlo (Promega N1110). After 5 minutes, the plate was

read on a Promega Glomax luminometer. Each NanoGlo reading (from pmPKR5UTRfullNL) was normalized to its corresponding OneGlo reading (from pGL4.13).

Statistical analyses

Data were analyzed with GraphPad Prism 7.0 software. For qPCR and densitometry analyses, the data were analyzed by individual Mann-Whitney tests. A value of $P < 0.5$ was considered significant.

Acknowledgments

We thank Robert Silverman, Gokhan Hotamisligil, and Anthony Sadler for PKR mutant and wild type cells. We thank Katelyn Green, Becky Billmire, and Peter Todd for the use of and assistance with the Brandel BR-188 Density Gradient Fractionation System and for providing the nanoluciferase and firefly luciferase plasmids. We thank Zachary Mendel and Joel Swanson for assistance with imaging the DQ BSA assay. We thank Jason Weinberg, Michael Imperiale, Christiane Wobus, Billy Tsai, Andrew Mehle, Mitch Ledwith, Mike Mathews, Chuck Samuel, and Britt Glaunsinger for helpful discussions. We thank Carla Pretto, Michael Imperiale, and Christiane Wobus for comments on the manuscript.

This work was supported by HHS/NIH/National Institute of Allergy and Infectious Diseases (NIAID), 5 R01AI091721 and 1 R01AI133935 (Katherine R. Spindler); and NIH Cellular and Molecular Biology Training Grant T32 GM007315, and Rackham Pre-Candidate and Candidate Student Research Grants (Danielle E. Goodman).

Bibliography

1. Meurs E, Chong K, Galabru J, Thomas NS, Kerr IM, Williams BR, Hovanessian AG. 1990. Molecular cloning and characterization of the human double-stranded RNA-activated protein kinase induced by interferon. Cell 62:379-90.

2. McCormack SJ, Thomis DC, Samuel CE. 1992. Mechanism of interferon action: identification of a RNA binding domain within the N-terminal region of the human RNA-dependent P1/eIF-2 alpha protein kinase. Virology 188:47-56.

3. Feng GS, Chong K, Kumar A, Williams BR. 1992. Identification of double-stranded RNA-binding domains in the interferon-induced double-stranded RNA-activated p68 kinase. Proc Natl Acad Sci USA 89:5447-51.

4. Kuhen KL, Samuel CE. 1997. Isolation of the interferon-inducible RNA-dependent protein kinase Pkr promoter and identification of a novel DNA element within the 5'-flanking region of human and mouse Pkr genes. Virology 227:119-30.

5. Patel RC, Sen GC. 1992. Identification of the double-stranded RNA-binding domain of the human interferon-inducible protein kinase. J Biol Chem 267:7671-6.

6. Dabo S, Meurs EF. 2012. dsRNA-dependent protein kinase PKR and its role in stress, signaling and HCV infection. Viruses 4:2598-635.

7. Mundschau LJ, Faller DV. 1994. Endogenous inhibitors of the dsRNA-dependent eIF-2 alpha protein kinase PKR in normal and ras-transformed cells. Biochimie 76:792-800.

8. Hovanessian AG, Galabru J. 1987. The double-stranded RNA-dependent protein kinase is also activated by heparin. Eur J Biochem 167:467-73.

9. Galabru J, Hovanessian A. 1987. Autophosphorylation of the protein kinase dependent on double-stranded RNA. J Biol Chem 262:15538-44.

10. Berk AJ. 2013. Adenoviridae: The viruses and their replication. *In* Knipe DM, Howley P (ed), Fields Virology, 6th ed, vol 2. Lippincott Williams & Wilkins, Philadelphia.

11. Wek RC. 2018. Role of eIF2alpha kinases in translational control and adaptation to cellular stress. Cold Spring Harb Perspect Biol 10.

12. Farrell PJ, Balkow K, Hunt T, Jackson RJ, Trachsel H. 1977. Phosphorylation of initiation factor elF-2 and the control of reticulocyte protein synthesis. Cell 11:187-200.

13. Tahara SM, Traugh JA, Sharp SB, Lundak TS, Safer B, Merrick WC. 1978. Effect of hemin on site-specific phosphorylation of eukaryotic initiation factor 2. Proc Natl Acad Sci USA 75:789-93.

14. Dzananovic E, McKenna SA, Patel TR. 2018. Viral proteins targeting host protein kinase R to evade an innate immune response: A mini review. Biotechnol Genet Eng Rev 34:33-59.

15. Chang HW, Jacobs BL. 1993. Identification of a conserved motif that is necessary for binding of the vaccinia virus E3L gene products to double-stranded RNA. Virology 194:537-47.

16. Rice AD, Turner PC, Embury JE, Moldawer LL, Baker HV, Moyer RW. 2011. Roles of vaccinia virus genes E3L and K3L and host genes PKR and RNase L during intratracheal infection of C57BL/6 mice. J Virol 85:550-67.

17. Carroll K, Elroy-Stein O, Moss B, Jagus R. 1993. Recombinant vaccinia virus K3L gene product prevents activation of double-stranded RNA-dependent, initiation factor 2 alpha-specific protein kinase. J Biol Chem 268:12837-42.

18. Lu Y, Wambach M, Katze MG, Krug RM. 1995. Binding of the influenza virus NS1 protein to double-stranded RNA inhibits the activation of the protein kinase that phosphorylates the elF-2 translation initiation factor. Virology 214:222-8.

19. Tan SL, Katze MG. 1998. Biochemical and genetic evidence for complex formation between the influenza A virus NS1 protein and the interferon-induced PKR protein kinase. J Interferon Cytokine Res 18:757-66.

20. Cardenas WB, Loo YM, Gale M, Jr., Hartman AL, Kimberlin CR, Martinez-Sobrido L, Saphire EO, Basler CF. 2006. Ebola virus VP35 protein binds double-stranded RNA and inhibits alpha/beta interferon production induced by RIG-I signaling. J Virol 80:5168-78.

21. Poppers J, Mulvey M, Khoo D, Mohr I. 2000. Inhibition of PKR activation by the proline-rich RNA binding domain of the herpes simplex virus type 1 Us11 protein. J Virol 74:11215-21.

22. Cassady KA, Gross M, Roizman B. 1998. The herpes simplex virus US11 protein effectively compensates for the gamma1(34.5) gene if present before activation of protein kinase R by precluding its phosphorylation and that of the alpha subunit of eukaryotic translation initiation factor 2. J Virol 72:8620-6.

23. Cai R, Carpick B, Chun RF, Jeang KT, Williams BR. 2000. HIV-I TAT inhibits PKR activity by both RNA-dependent and RNA-independent mechanisms. Arch Biochem Biophys 373:361-7.

24. McMillan NA, Chun RF, Siderovski DP, Galabru J, Toone WM, Samuel CE, Mak TW, Hovanessian AG, Jeang KT, Williams BR. 1995. HIV-1 Tat directly interacts with the interferon-induced, double-stranded RNA-dependent kinase, PKR. Virology 213:413-24.

25. Park H, Davies MV, Langland JO, Chang HW, Nam YS, Tartaglia J, Paoletti E, Jacobs BL, Kaufman RJ, Venkatesan S. 1994. TAR RNA-binding protein is an inhibitor of the interferon-induced protein kinase PKR. Proc Natl Acad Sci USA 91:4713-7.

26. Thimmappaya B, Weinberger C, Schneider RJ, Shenk T. 1982. Adenovirus VAI RNA is required for efficient translation of viral mRNAs at late times after infection. Cell 31:543-51.

27. Mathews MB, Grodzicker T. 1981. Virus-associated RNAs of naturally occurring strains and variants of group C adenoviruses. J Virol 38:849-62.

28. Reich PR, Forget BG, Weissman SM. 1966. RNA of low molecular weight in KB cells infected with adenovirus type 2. J Mol Biol 17:428-39.

29. Kalveram B, Ikegami T. 2013. Toscana virus NSs protein promotes degradation of double-stranded RNA-dependent protein kinase. J Virol 87:3710-8.

30. Habjan M, Pichlmair A, Elliott RM, Overby AK, Glatter T, Gstaiger M, Superti-Furga G, Unger H, Weber F. 2009. NSs protein of Rift Valley fever virus induces the specific degradation of the double-stranded RNA-dependent protein kinase. J Virol 83:4365-75.

31. Ikegami T, Narayanan K, Won S, Kamitani W, Peters CJ, Makino S. 2009. Rift Valley fever virus NSs protein promotes post-transcriptional downregulation of protein kinase PKR and inhibits eIF2alpha phosphorylation. PLoS Pathog 5:e1000287.

32. Mudhasani R, Tran JP, Retterer C, Kota KP, Whitehouse CA, Bavari S. 2016. Protein kinase R degradation Is essential for Rift Valley fever virus infection and is regulated by SKP1-CUL1-F-box (SCF)FBXW11-NSs E3 ligase. PLoS Pathog 12:e1005437.

33. Black TL, Barber GN, Katze MG. 1993. Degradation of the interferon-induced 68,000-M(r) protein kinase by poliovirus requires RNA. J Virol 67:791-800.

34. Black TL, Safer B, Hovanessian A, Katze MG. 1989. The cellular 68,000-Mr protein kinase is highly autophosphorylated and activated yet significantly degraded during poliovirus infection: Implications for translational regulation. J Virol 63:2244-51.

35. Li W, Zhu Z, Cao W, Yang F, Zhang X, Li D, Zhang K, Li P, Mao R, Liu X, Zheng H. 2016. Esterase D enhances type I interferon signal transduction to suppress foot-and-mouth disease virus replication. Mol Immunol 75:112-21.

36. Li C, Zhu Z, Du X, Cao W, Yang F, Zhang X, Feng H, Li D, Zhang K, Liu X, Zheng H. 2017. Foot-and-mouth disease virus induces lysosomal degradation of host protein kinase PKR by 3C proteinase to facilitate virus replication. Virology 509:222-231.

37. Rabouw HH, Langereis MA, Knaap RC, Dalebout TJ, Canton J, Sola I, Enjuanes L, Bredenbeek PJ, Kikkert M, de Groot RJ, van Kuppeveld FJ. 2016. Middle East respiratory coronavirus accessory protein 4a inhibits PKR-mediated antiviral stress responses. PLoS Pathog 12:e1005982.

38. Hovanessian AG, Galabru J, Meurs E, Buffet-Janvresse C, Svab J, Robert N. 1987. Rapid decrease in the levels of the double-stranded RNA-dependent protein kinase during virus infections. Virology 159:126-36.

39. Chang YH, Lau KS, Kuo RL, Horng JT. 2017. dsRNA binding domain of PKR is proteolytically released by enterovirus A71 to facilitate viral replication. Front Cell Infect Microbiol 7:284.

40. Kalveram B, Ikegami T. 2013. Toscana virus NSs protein promotes degradation of double-stranded RNA-dependent protein kinase. J Virol 87:3710-8.

41. Kainulainen M, Lau S, Samuel CE, Hornung V, Weber F. 2016. NSs virulence factor of Rift Valley fever virus engages the F-box proteins FBXW11 and beta-TRCP1 to degrade the antiviral protein kinase PKR. J Virol 90:6140-7.

42. Kring SC, King CS, Spindler KR. 1995. Susceptibility and signs associated with mouse adenovirus type 1 infection of adult outbred Swiss mice. J Virol 69:8084-8.

43. Spindler KR, Moore ML, Cauthen AN. 2007. Mouse adenoviruses, p 49-65, The mouse in biomedical research, 2nd ed, vol 2. Academic Press, New York, NY.

44. Blailock ZR, Rabin ER, Melnick JL. 1968. Adenovirus myocarditis in mice. An electron microscopic study. Exp Mol Pathol 9:84-96.

45. McCarthy MK, Procario MC, Twisselmann N, Wilkinson JE, Archambeau AJ, Michele DE, Day SM, Weinberg JB. 2015. Proinflammatory effects of interferon gamma in mouse adenovirus 1 myocarditis. J Virol 89:468-79.

46. Guida JD, Fejer G, Pirofski LA, Brosnan CF, Horwitz MS. 1995. Mouse adenovirus type 1 causes a fatal hemorrhagic encephalomyelitis in adult C57BL/6 but not BALB/c mice. J Virol 69:7674-81.

47. Mathews MB, Shenk T. 1991. Adenovirus virus-associated RNA and translation control. J Virol 65:5657-62.

48. Meissner JD, Hirsch GN, LaRue EA, Fulcher RA, Spindler KR. 1997. Completion of the DNA sequence of mouse adenovirus type 1: Sequence of E2B, L1, and L2 (18-51 map units). Virus Res 51:53-64.

49. Balachandran S, Roberts PC, Brown LE, Truong H, Pattnaik AK, Archer DR, Barber GN. 2000. Essential role for the dsRNA-dependent protein kinase PKR in innate immunity to viral infection. Immunity 13:129-41.

50. Stojdl DF, Abraham N, Knowles S, Marius R, Brasey A, Lichty BD, Brown EG, Sonenberg N, Bell JC. 2000. The murine double-stranded RNA-dependent protein kinase PKR is required for resistance to vesicular stomatitis virus. J Virol 74:9580-5.

51. Xiang Y, Condit RC, Vijaysri S, Jacobs B, Williams BR, Silverman RH. 2002. Blockade of interferon induction and action by the E3L double-stranded RNA binding proteins of vaccinia virus. J Virol 76:5251-9.

52. Baltzis D, Li S, Koromilas AE. 2002. Functional characterization of pkr gene products expressed in cells from mice with a targeted deletion of the N terminus or C terminus domain of PKR. J Biol Chem 277:38364-72.

53. Yang YL, Reis LF, Pavlovic J, Aguzzi A, Schafer R, Kumar A, Williams BR, Aguet M, Weissmann C. 1995. Deficient signaling in mice devoid of double-stranded RNA-dependent protein kinase. EMBO J 14:6095-106.

54. Abraham N, Stojdl DF, Duncan PI, Methot N, Ishii T, Dube M, Vanderhyden BC, Atkins HL, Gray DA, McBurney MW, Koromilas AE, Brown EG, Sonenberg N, Bell JC. 1999. Characterization of transgenic mice with targeted disruption of the catalytic domain of the double-stranded RNA-dependent protein kinase, PKR. J Biol Chem 274:5953-62.

55. Yim HC, Wang D, Yu L, White CL, Faber PW, Williams BR, Sadler AJ. 2016. The kinase activity of PKR represses inflammasome activity. Cell Res 26:367-79.

56. Nakamura T, Kunz RC, Zhang C, Kimura T, Yuan CL, Baccaro B, Namiki Y, Gygi SP, Hotamisligil GS. 2015. A critical role for PKR complexes with TRBP in Immunometabolic regulation and eIF2alpha phosphorylation in obesity. Cell Rep 11:295-307.

57. Felicetti L, Colombo B, Baglioni C. 1966. Inhibition of protein synthesis in reticulocytes by antibiotics. II. The site of action of cycloheximide, streptovitacin A and pactamycin. Biochim Biophys Acta 119:120-9.

58. Kearse MG, Green KM, Krans A, Rodriguez CM, Linsalata AE, Goldstrohm AC, Todd PK. 2016. CGG repeat-associated non-AUG translation utilizes a cap-dependent scanning mechanism of initiation to produce toxic proteins. Mol Cell 62:314-322.

59. Cooper GM. 2000. Protein Degradation, The Cell: A Molecular Approach, 2nd ed. Sinauer Associates, Sunderland, MA.

60. Marwaha R, Sharma M. 2017. DQ-Red BSA Trafficking Assay in Cultured Cells to Assess Cargo Delivery to Lysosomes. Bio Protoc 7.

61. Palm W, Park Y, Wright K, Pavlova NN, Tuveson DA, Thompson CB. 2015. The utilization of extracellular proteins as nutrients is suppressed by mTORC1. Cell 162:259-270.

62. Guo N, Peng Z. 2013. MG132, a proteasome inhibitor, induces apoptosis in tumor cells. Asia Pac J Clin Oncol 9:6-11.

63. Chen D, Frezza M, Schmitt S, Kanwar J, Dou QP. 2011. Bortezomib as the first proteasome inhibitor anticancer drug: current status and future perspectives. Curr Cancer Drug Targets 11:239-53.

64. Berkers CR, Verdoes M, Lichtman E, Fiebiger E, Kessler BM, Anderson KC, Ploegh HL, Ovaa H, Galardy PJ. 2005. Activity probe for in vivo profiling of the specificity of proteasome inhibitor bortezomib. Nat Methods 2:357-62.

65. Ciechanover A, Heller H, Elias S, Haas AL, Hershko A. 1980. ATP-dependent conjugation of reticulocyte proteins with the polypeptide required for protein degradation. Proc Natl Acad Sci USA 77:1365-8.

66. Hershko A, Ciechanover A, Heller H, Haas AL, Rose IA. 1980. Proposed role of ATP in protein breakdown: conjugation of protein with multiple chains of the polypeptide of ATP-dependent proteolysis. Proc Natl Acad Sci USA 77:1783-6.

67. Gilson T, Blanchette P, Ballmann MZ, Papp T, Penzes JJ, Benko M, Harrach B, Branton PE. 2016. Using the E4orf6-Based E3 ubiquitin ligase as a tool to analyze the evolution of adenoviruses. J Virol 90:7350-7367.

68. Bernardi KM, Williams JM, Inoue T, Schultz A, Tsai B. 2013. A deubiquitinase negatively regulates retro-translocation of nonubiquitinated substrates. Mol Biol Cell 24:3545-56.

69. Smith K, Ying B, Ball AO, Beard CW, Spindler KR. 1996. Interaction of mouse adenovirus type 1 early region 1A protein with cellular proteins pRb and p107. Virology 224:184-97.

70. Mayne LV. 1984. Inhibitors of DNA synthesis (aphidicolin and araC/HU) prevent the recovery of RNA synthesis after UV-irradiation. Mutat Res 131:187-91.

71. Zittoun J, Marquet J, David JC, Maniey D, Zittoun R. 1989. A study of the mechanisms of cytotoxicity of Ara-C on three human leukemic cell lines. Cancer Chemother Pharmacol 24:251-5.

72. Beard CW, Spindler KR. 1996. Analysis of early region 3 mutants of mouse adenovirus type 1. J Virol 70:5867-74.

73. Smith K, Brown CC, Spindler KR. 1998. The role of mouse adenovirus type 1 early region 1A in acute and persistent infections in mice. J Virol 72:5699-706.

74. Zhou A, Paranjape JM, Der SD, Williams BR, Silverman RH. 1999. Interferon action in triply deficient mice reveals the existence of alternative antiviral pathways. Virology 258:435-40.

75. Ma Y, Mathews MB. 1996. Structure, function, and evolution of adenovirus-associated RNA: a phylogenetic approach. J Virol 70:5083-99.

76. Yoon CH, Lee ES, Lim DS, Bae YS. 2009. PKR, a p53 target gene, plays a crucial role in the tumor-suppressor function of p53. Proc Natl Acad Sci USA 106:7852-7.

77. Kainulainen M, Habjan M, Hubel P, Busch L, Lau S, Colinge J, Superti-Furga G, Pichlmair A, Weber F. 2014. Virulence factor NSs of rift valley fever virus recruits the F-box protein FBXO3 to degrade subunit p62 of general transcription factor TFIIH. J Virol 88:3464-73.

78. Kalveram B, Lihoradova O, Ikegami T. 2011. NSs protein of rift valley fever virus promotes posttranslational downregulation of the TFIIH subunit p62. J Virol 85:6234-43.

79. Neznanov N, Dragunsky EM, Chumakov KM, Neznanova L, Wek RC, Gudkov AV, Banerjee AK. 2008. Different effect of proteasome inhibition on vesicular stomatitis virus and poliovirus replication. PLoS One 3:e1887.

80. Baugh JM, Viktorova EG, Pilipenko EV. 2009. Proteasomes can degrade a significant proportion of cellular proteins independent of ubiquitination. J Mol Biol 386:814-27.

81. Maupin-Furlow J. 2011. Proteasomes and protein conjugation across domains of life. Nat Rev Microbiol 10:100-11.

82. Kring SC, Ball AO, Spindler KR. 1992. Transcription mapping of mouse adenovirus type 1 early region 4. Virology 190:248-55.

83. Querido E, Blanchette P, Yan Q, Kamura T, Morrison M, Boivin D, Kaelin WG, Conaway RC, Conaway JW, Branton PE. 2001. Degradation of p53 by adenovirus E4orf6 and E1B55K proteins occurs via a novel mechanism involving a Cullin-containing complex. Genes Dev 15:3104-17.

84. Harada JN, Shevchenko A, Shevchenko A, Pallas DC, Berk AJ. 2002. Analysis of the adenovirus E1B-55K-anchored proteome reveals its link to ubiquitination machinery. J Virol 76:9194-206.

85. Forrester NA, Patel RN, Speiseder T, Groitl P, Sedgwick GG, Shimwell NJ, Seed RI, Catnaigh PO, McCabe CJ, Stewart GS, Dobner T, Grand RJ, Martin A, Turnell AS. 2012. Adenovirus E4orf3 targets transcriptional intermediary factor 1gamma for proteasome-dependent degradation during infection. J Virol 86:3167-79.

86. Sohn SY, Hearing P. 2016. The adenovirus E4-ORF3 protein functions as a SUMO E3 ligase for TIF-1gamma sumoylation and poly-SUMO chain elongation. Proc Natl Acad Sci USA 113:6725-30.

87. Weber J. 1976. Genetic analysis of adenovirus type 2 III. Temperature sensitivity of processing viral proteins. J Virol 17:462-71.

88. Anderson CW, Baum PR, Gesteland RF. 1973. Processing of adenovirus 2-induced proteins. J Virol 12:241-52.

89. Weber JM, Anderson CW. 1988. Identification of the gene coding for the precursor of adenovirus core protein X. J Virol 62:1741-5.

90. Anderson CW. 1990. The proteinase polypeptide of adenovirus serotype 2 virions. Virology 177:259-72.

91. Sanfilippo CM, Chirimuuta FN, Blaho JA. 2004. Herpes simplex virus type 1 immediate-early gene expression is required for the induction of apoptosis in human epithelial HEP-2 cells. J Virol 78:224-39.

92. Harrach B, Benko M, Both GW, Brown M, Davison AJ, Echavarria M, Hess M, Jones MS, Kajon A, Lehmkuhl HD, Mautner V, Mittal SK, Wadell G. 2011. Virus Taxonomy: Ninth report of the international committee on taxonomy of viruses, p 128. *In* King AMQ, Adams MJ, Carstens EB, Lefkowitz EJ (ed). Elsevier.

93. Ashley SL, Welton AR, Harwood KM, Van Rooijen N, Spindler KR. 2009. Mouse adenovirus type 1 infection of macrophages. Virology 390:307-14.

94. Sawicki DL, Silverman RH, Williams BR, Sawicki SG. 2003. Alphavirus minus-strand synthesis and persistence in mouse embryo fibroblasts derived from mice lacking RNase L and protein kinase R. J Virol 77:1801-11.

95. Cauthen AN, Welton AR, Spindler KR. 2007. Construction of mouse adenovirus type 1 mutants. Methods Mol Med 130:41-59.

96. Tanaka H, Samuel CE. 1994. Mechanism of interferon action: structure of the mouse PKR gene encoding the interferon-inducible RNA-dependent protein kinase. Proc Natl Acad Sci USA 91:7995-9.

97. Kajon AE, Brown CC, Spindler KR. 1998. Distribution of mouse adenovirus type 1 in intraperitoneally and intranasally infected adult outbred mice. J Virol 72:1219-23.

98. Cauthen AN, Spindler KR. 1999. Novel expression of mouse adenovirus type 1 early region 3 gp11K at late times after infection. Virology 259:119-28.

99. Schindelin J, Rueden CT, Hiner MC, Eliceiri KW. 2015. The ImageJ ecosystem: An open platform for biomedical image analysis. Mol Reprod Dev 82:518-29.

100. Sheets MD, Fritz B, Hartley RS, Zhang Y. 2010. Polyribosome analysis for investigating mRNA translation in Xenopus oocytes, eggs and embryos. Methods 51:152-6.

101. Morita M, Alain T, Topisirovic I, Sonenberg N. 2013. Polysome profiling analysis. Bio-protocol 3:e833.

Chapter III

Changes in immune response in GCN2$^{-/-}$ mice and macrophages during mouse adenovirus type 1 infection

Abstract

During viral infection, the production of double-stranded (ds) RNA by viruses triggers protein kinase R (PKR) activation and subsequent eukaryotic translation initiation factor 2α (eIF2α) phosphorylation, reducing cellular translation, and viral translation and replication. This antiviral host response, resulting in eIF2α kinase phosphorylation, may also occur with the other three eIF2α-phosphorylating kinases (general control nonderepressible 2 [GCN2], PKR-like endoplasmic reticulum kinase, and heme-regulated inhibitor kinase), resulting in protein synthesis inhibition in response to viral infection. GCN2 phosphorylates eIF2α in response to amino acid starvation, UV irradiation, and oxidative stress. Several viruses indirectly or directly cause GCN2 activation during infection. Here we describe that GCN2$^{-/-}$ deficient (*atchoum or atc*) mice and peritoneal macrophages are significantly more susceptible to infection by mouse adenovirus type 1 (MAV-1). Viral yield assays of infected organs showed that only the cecum of *atc* mice at 8 days post infection (dpi) had significantly higher viral yields than infected organs from wild type mice, indicating that the difference in survival between *atc* and wild type mice is not likely a result of increased viremia in *atc* mice. There was also no significant difference in histology of organs from MAV-1-infected *atc* and wild type mice. However, cytokine analysis

showed that MAV-1-infected wild type mice had significantly higher levels of interleukin 1α (IL-1α), interleukin 1β (IL-1β), tumor necrosis factor α (TNFα), interleukin 6 (IL-6), and interferon γ (IFNγ) in the brain compared to infected *atc* mouse brains at 8 dpi, suggesting that a difference in inflammatory response could be responsible for the decreased survival of *atc* mice in response to MAV-1 infection.

Introduction

One host response to viral infection is to reduce global cellular translation through eIF2α phosphorylation, reducing viral translation and viral replication (1-4). As discussed in the introduction to Chapter II, PKR is the canonical eIF2α kinase that is activated during viral infection by dsRNA (5-7). However, many viruses encode proteins that inhibit PKR activation or block its activity (8). In response to this viral circumvention of the host PKR response, it is possible that the host cell also recruits one of the other three eIF2α-phosphorylating kinases (GCN2, PKR-like endoplasmic reticulum kinase, and heme-regulated inhibitor kinase) to inhibit protein synthesis in response to viral infection (9-11).

GCN2 is comprised of four main domains: an eIF2α kinase domain, a histidyl-tRNA synthetase (HisRS)-like domain, a general control of amino-acid synthesis 1 (GCN1) binding domain, and a ribosomal binding domain (Fig. 3.1) (11-15). GCN2 first binds to ribosomes, and then uncharged tRNAs bind to the HisRS-like domain and cause a conformational change that causes GCN2 activation (16-21). GCN1 is an activator of GCN2; it binds to ribosomes, and assists in the transfer of uncharged tRNA to GCN2 (16). GCN2 phosphorylates eIF2α in response to amino acid starvation, UV irradiation, and oxidative stress; in yeast, GCN1 is required for GCN2 activation in each of these responses (16).

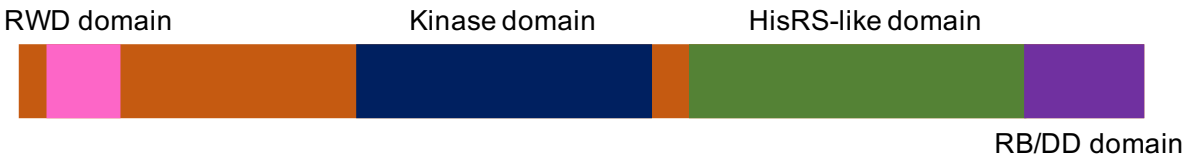

Figure 3.1 GCN2 (*Eif2ak4*) domains, adapted from Figure 1B from Jaspart et al. GCN2 contains four major domains: RING finger-containing proteins, WD-repeat-containing proteins, and yeast DEAD (DEXD)-like helicases (RWD) binding domain; kinase domain; histidyl-tRNA synthetase (HisRS)-like domain; and the ribosome binding/homodimerization domain (RB/DD). GCN2 binds to GCN1 using the GCN2 RWD domain; uncharged tRNA binds using the HisRS-like domain; and the ribosome binds to the RB domain. GCN2 homodimerizes using the RB/DD domain.

GCN2$^{-/-}$ (*atchoum or atc*) mice were created using N-ethyl-N-nitrosourea-mutagenesis of mice on a C57BL/6 background (22). When infected with mouse cytomegalovirus (MCMV) or a human adenovirus reporter construct, peritoneal macrophages from the *atc* mice have increased susceptibility to both viruses compared to wild type mouse peritoneal macrophages. Additionally, *atc* mice infected with MCMV have a significantly lower survival rate than wild type mice. Genome sequencing showed that the *atc* mice have a missense mutation (T to C transition) in exon 2 of the *Eif2ak4* gene, which causes exon skipping. *Eif2ak4* encodes GCN2. In *atc* macrophages, GCN2 is not detectable by immunoblotting, and in *atc* mouse embryonic fibroblasts (MEFs), phosphorylation of eIF2α does not occur in response to UVB treatment or MCMV infection. Thus *atc* is a loss-of-function mutation with respect to eIF2α phosphorylation.

While there is much research implicating PKR in the innate immune response to a wide range of viruses, the fact that *atc* mice are more susceptible to MCMV infection supports findings that GCN2 may play a role in the innate immune response to viruses (22). Two viruses, MCMV (23) and yellow fever virus vaccine (YF-17D) (24), indirectly activate GCN2 by triggering changes in amino acid metabolism. MCMV infection leads to the production of 25-hydroxycholesterol, which activates GCN2 by reducing the levels of intracellular cysteine and/or by generating oxidative stress (23). YF-17D has much the same effect. After incubation with YF-17D, dendritic cells have a significant reduction in levels of free arginine and a subsequent increase in phosphorylated GCN2 and eIF2α (24).

Other viruses, however, trigger GCN2 activation directly through the production of RNA, such as Sindbis virus (25) and HIV-1 (26). Both viruses produce RNA that binds to the HisRS-like domain of GCN2, leading to activation. The prunnus necrotic ringspot virus, a plant

virus, causes GCN2 activation through the production of a viral movement protein, though the mechanism of activation is not known (27).

To oppose the effect of GCN2 activation on cellular translation, several viruses also have mechanisms for inhibiting GCN2 activation or activity. Herpes simplex virus 1 indirectly inhibits GCN2 by targeting GCN1 (28, 29). Herpes simplex virus 1 glycoprotein H directly interacts with GCN1, changing its localization from the cytoplasm to the nuclear rim, effectively sequestering GCN1 and inhibiting its ability to activate GCN2 during infection. Severe acute respiratory syndrome-related coronavirus also indirectly inhibits GCN2. It does so by causing a depletion of GCN2 protein from the cell late in infection, likely by decreasing host gene transcription overall (30). Vaccinia virus and HIV-1 have more direct mechanisms of GCN2 inhibition. The vaccinia virus K3L protein inactivates GCN2 by binding to the kinase domain and preventing GCN2 activation (31). HIV-1^{pro}, a protease produced by HIV-1, cleaves GCN2, and once GCN2 is cleaved, it loses nearly all of its capability to phosphorylate eIF2α (26).

To determine whether GCN2 plays an antiviral role during MAV-1 infection, we infected *atc* and wild type mice for survival studies. At three different doses, *atc* mice had a significantly lower survival rate compared to wild type mice. Peritoneal macrophages from *atc* mice infected with MAV-1 also had increased viral yields compared to peritoneal macrophages from wild type mice. However, there was no difference in viral yields between MAV-1-infected *atc* MEFs compared to wild type MEFs. Viral yield determinations from infected mouse organs showed that only the cecum of *atc* mice at 8 dpi had higher viral yields than cecum from wild type mice. This result suggests that the difference in survival between *atc* and wild type mice was not a result of increased viremia in *atc* mice. There was also no significant difference in the histology of organs from MAV-1-infected *atc* and wild type mice. However, cytokine analysis showed a

difference in IL-1α, IL-1β, TNFα, IL-6, and IFNγ levels in the brains of *atc* and wild type mice at 7 and 8 dpi, suggesting that a difference in inflammatory response could be responsible for the decreased survival of *atc* mice in response to MAV-1 infection.

Results

Atc mice are more susceptible to infection by MAV-1 than wild type mice

To determine whether GCN2-deficient mice are more susceptible to MAV-1 infection, we infected *atc* and C57BL/6 (wild type) mice intraperitoneally (i.p.) with 10^2, 10^3, or 10^4 PFU MAV-1 and recorded survival for 21 dpi. At all three doses, *atc* mice had a significantly lower survival than wild type mice, with their survival being 24%, 41%, and 40% lower than the survival of the wild type mice, respectively (Fig. 3.2). These results indicate that GCN2 plays a role in the survival of mice infected with MAV-1.

Viral yield is increased in *atc* peritoneal macrophages

To further characterize the role GCN2 plays during MAV-1 infection, peritoneal macrophages or immortalized MEFs isolated from *atc* and wild type mice were plated and infected with MAV-1 at MOI of 1, and cells were collected at 24, 48, and 72 hpi. DNA was purified from the cell pellets and analyzed for MAV-1 genome copies by qPCR. At 72 hpi, the *atc* macrophages had a more than three-fold increase in viral yield compared to the wild type macrophages (Fig. 3.3A). These results correlate with the results of the survival studies and suggest that GCN2 is antiviral in MAV-1-infected peritoneal macrophages. However, in *atc* and wild type MEFs infected with MAV-1 at MOI of 1, the *atc* MEFs had lower viral yields

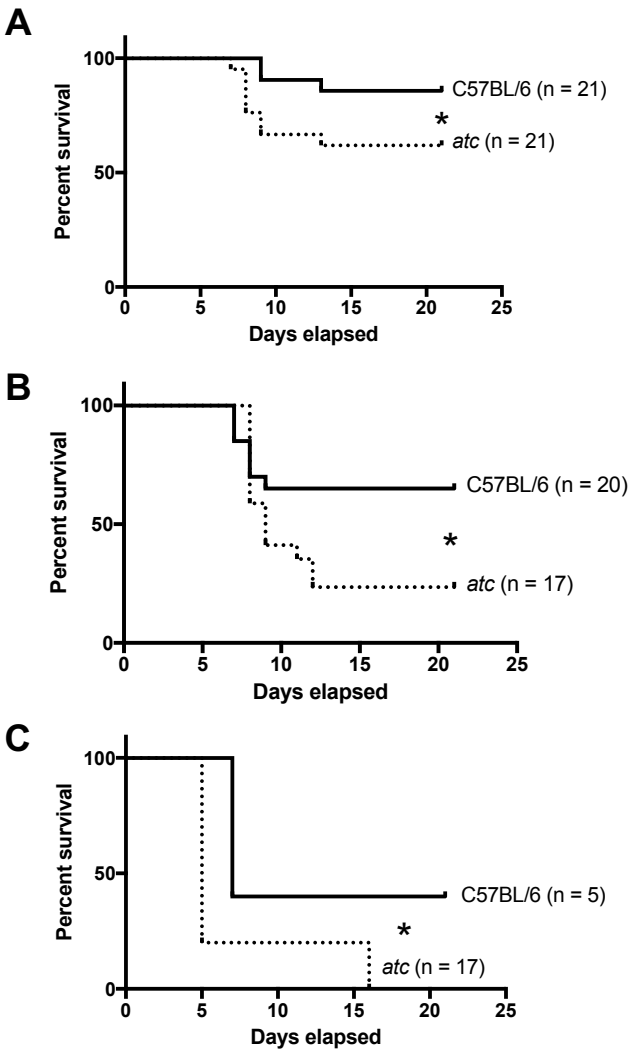

Figure 3.2 *Atc* mutation reduces survival of MAV-1-infected mice. Wild type mice (C57BL/6) and GCN2$^{-/-}$ mice (*atc*) were infected intraperitoneally with (A) 10^2, (B) 10^3, or (C) 10^4 pfu MAV-1, and survival was recorded for 21 days. *$P \leq 0.05$. The data shown are pooled from independent experiments. The number of mice in each group is listed next to the line label.

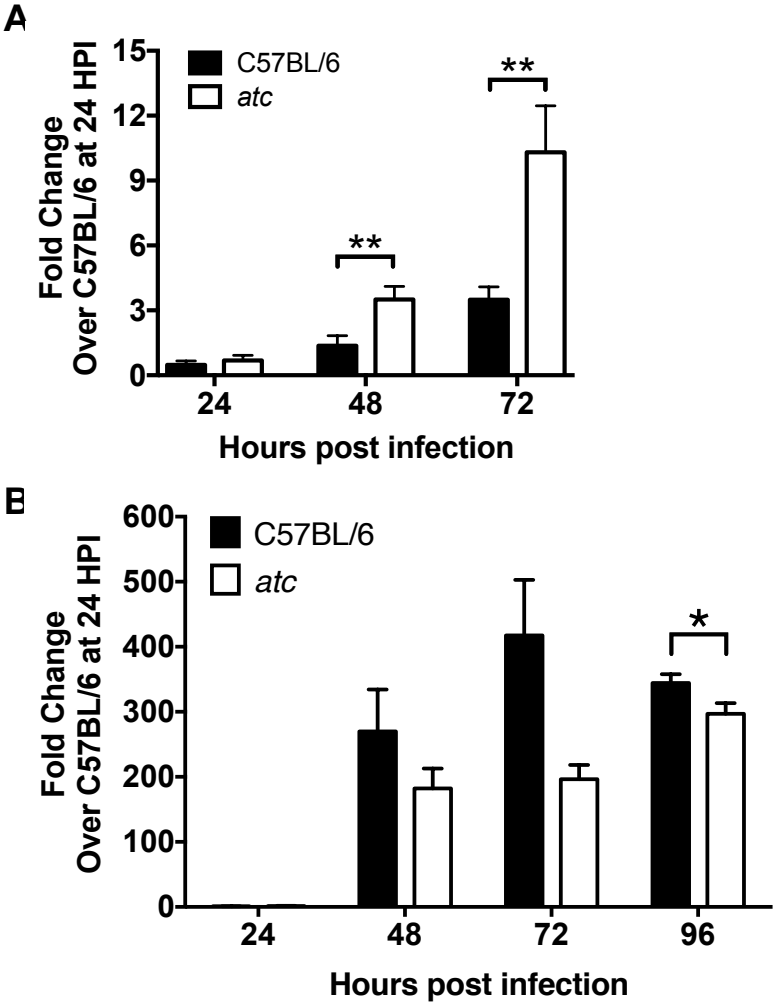

Figure 3.3 Viral yield in wild type and GCN2$^{-/-}$ primary macrophages and MEFs. (A) Wild type (C57BL/6) and GCN2$^{-/-}$ (*atc*) macrophages or (B) MEFs were infected with MAV-1 at an MOI of 1 and collected at 24, 48, and 72 hours post infection (hpi), as well as 96 hpi for MEFs. DNA was purified from cell pellets and analyzed for MAV-1 genome copies by qPCR. Graphs are representative of multiple experiments, 6-18 biological replicates per cell line per time point. Error bars are standard error of the mean (SEM). *$P \leq 0.05$, **$P \leq 0.01$

compared to wild type MEFs (Fig. 3.3B). This is consistent with the results of MCMV infection in *atc* mice, peritoneal macrophages, and MEFs, where *atc* mice and macrophages are more susceptible to MCMV infection, but *atc* MEFs are not (22). Taken together, these data suggest that the antiviral role of GCN2 may vary based on cell type for both MAV-1 and MCMV.

Atchoum mice only have significantly higher viral titers in the cecum during infection

MAV-1 is an encephalitic virus, so we quantitated viral loads in the brains of MAV-1-infected *atc* and wild type mice. Mice were infected i.p. with 10^3 PFU MAV-1 and brains were harvested at 3, 5, and 7 dpi. DNA was purified from homogenized tissue samples and analyzed for MAV-1 genome copies by qPCR. There was no significant difference between the viral loads in the brains of *atc* mice compared to wild type mice at any of the analyzed time points (Fig. 3.4A). To determine if any other organ in the *atc* mice was more susceptible to MAV-1 than wild type mice, we quantitated the viral loads at 5 and 7 dpi in the liver, lung, heart, spleen, kidney, and cecum of *atc* and wild type mice infected i.p. with 10^3 PFU MAV-1. There was no significant difference in the viral load in any organ between the *atc* and wild type mice at either time point except for the cecum at 7 dpi (Fig. 3.4B and C). Higher viral yields in the cecum could indicate a gastrointestinal component to the increased mortality of *atc* mice during MAV-1 infection. However, histology analysis of the cecum and all other organs showed no significant differences in inflammation or damage between *atc* organs and wild type organs. We also analyzed a portion of the brains and livers for infectious virus by plaque assay, and there were no differences in infectious titers from the brains or livers of MAV-1-infected wild type or *atc* mice (Fig. 3.5). Taken together, these results suggest that the increased mortality seen in *atc*

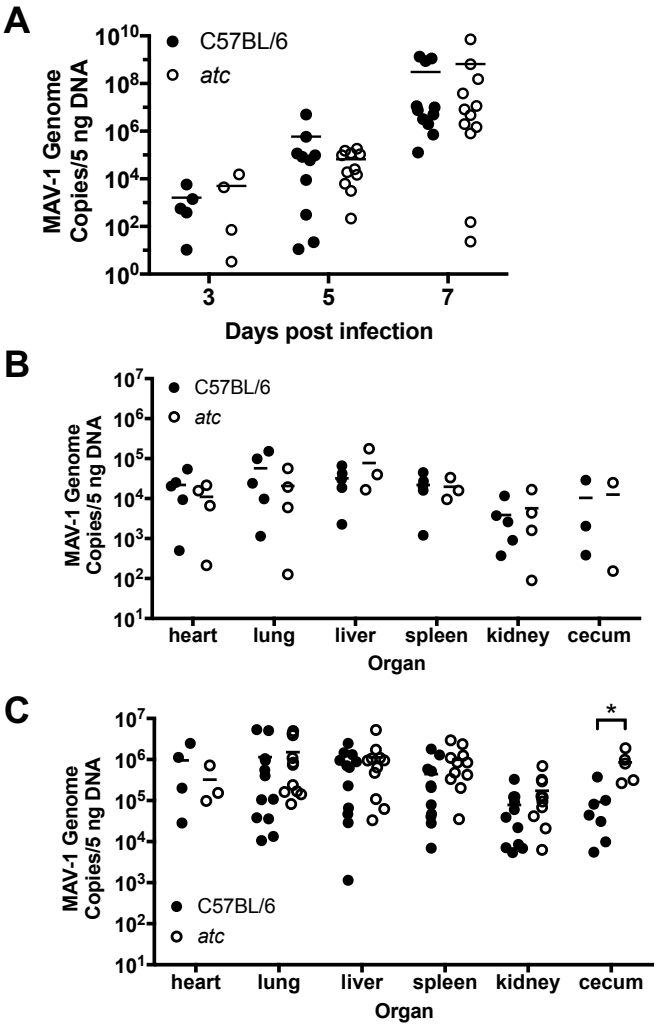

Figure 3.4 Viral load is increased in the cecum of GCN2$^{-/-}$ (*atc*) mice. (A) Wild type (C57BL/6) and GCN2$^{-/-}$ (*atc*) mice were infected with MAV-1 at 10^3 pfu. After 3, 5, or 7 days post infection, mice were euthanized with CO_2, perfused with phosphate-buffered saline, and organs were collected. DNA was purified from (A) brain tissue at 3, 5, and 7 days post infection or heart, lung, liver, spleen, kidney, and cecum at (B) 5 days post infection or (C) 7 days post infection. DNA was analyzed for MAV-1 genome copies by qPCR. Graph is representative of multiple experiments; each dot represents a different mouse. Error bars are standard error of the mean (SEM). *$P \leq 0.05$.

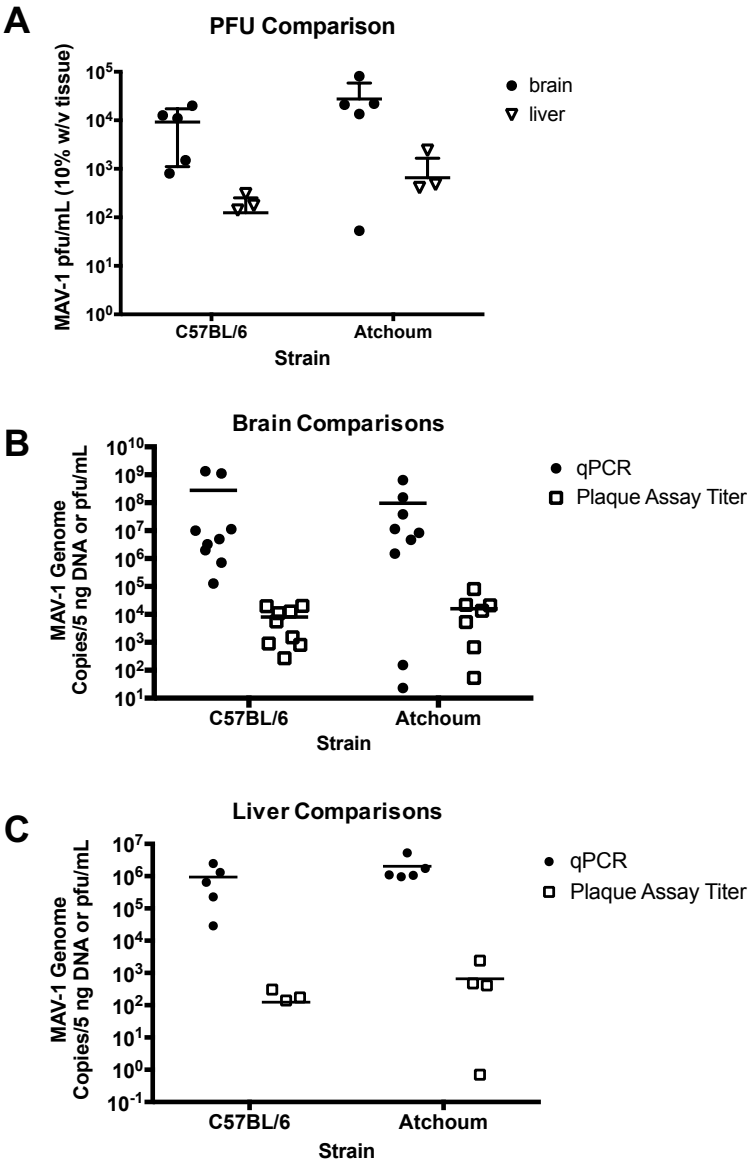

Figure 3.5 Comparison of infectious virus and viral DNA yields in brains and livers of MAV-1-infected wild type and GCN2$^{-/-}$ mice. Wild type (C57BL/6) and GCN2$^{-/-}$ (Atchoum) mice were infected with MAV-1 at 10^3 pfu. After 7 days, mice were euthanized with CO_2, perfused with phosphate-buffered saline, and organs were collected. (A) Brains and livers were homogenized and infectious virus was titrated by plaque assay on 3T6 cells. DNAs purified from (B) brains and (C) livers were analyzed for MAV-1 genome copies by qPCR and compared to the infectious viral titers. Each symbol represents an individual mouse. There were no statistical differences between mouse strains for titers or viral DNA yield.

mice compared to wild type mice was not due to increased viral replication or inflammatory damage.

MAV-1-infected *atc* mice have a different inflammatory cytokine response than wild type mice in the brain

During infection, cytokines and chemokines can be secreted in the brain by resident cells or by infiltrating inflammatory cells (32). IL-1α, IL-1β, IL-6, and TNFα are proinflammatory cytokines that are secreted by resident CNS cells and macrophages found in the brain (33), while monocyte chemoattractant protein-1 (MCP-1) and KC are secreted in response to the proinflammatory cytokines (34, 35). IL-1β and TNFα specifically enhance encephalitis during rabies infections in rats (36). However, mice deficient in IL-1 signaling have reduced survival during MAV-1 infection compared to wild type mice, suggesting that the IL-1 signaling pathway has a protective role during MAV-1 infection specifically (37). We analyzed cytokine levels in the brains of MAV-1-infected or mock infected *atc* and wild type mice. Mice were infected i.p. with 10^3 PFU MAV-1, and brains were harvested at 7 and 8 dpi. Brain extracts were analyzed by ELISA for IL-1α, IL-1β, IL-6, IL-10, interferon γ-induced protein 10 (IP-10), TNFα, IFNγ, KC, MCP-1, and RANTES (cytokines that were previously shown to be elevated in wild type mouse brains during MAV-1 infection (37)).

At 7 dpi, IL-1α, IL-1β, and IFNγ levels (normalized to the corresponding mock levels) were significantly higher in MAV-1-infected *atc* brains compared to wild type brains. In contrast, at 8 dpi, IL-1α, IL-6, TNFα, KC, and MCP-1 levels (normalized to the corresponding mock levels) were significantly lower in MAV-1-infected *atc* brains compared to wild type (Fig. 3.6). These results suggest that *atc* mice may have an earlier inflammatory response in the brain

Table 3.1 Reduced cytokine levels in MAV-1-infected *atc* mouse brains compared to C57BL/6 mouse brains.

Cytokine	dpi	Mean cytokine levels in infected C57BL/6 brains (pg/mL)	Mean cytokine levels in infected *atc* brains (pg/mL)
IL-1α	7	43.1	44.8
	8	39.0[a]	29.0
IL-1β	7	62.5	62.5
	8	90.4[a]	75.8
IL-6	7	33.3	32.3
	8	26.1[b]	16.2
IL-10	7	24.3	21.1
	8	56.5	50.4
IP-10	7	2474.8	2835.4
	8	3873.6	2634.5
TNFα	7	12.9	10.9
	8	30.5[b]	21.5
IFNγ	7	18.9	17.6
	8	23.6	21.9
KC	7	170.5	182.8
	8	138.5[a]	77.4
MCP-1	7	488.0	384.5
	8	601.5[a]	152.0
RANTES	7	207.1	235.9
	8	248.1	186.3

[a] $P \leq 0.05$
[b] $P \leq 0.01$

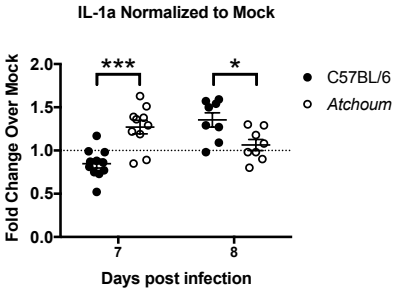
IL-1a Normalized to Mock
Fold Change Over Mock
2.0
1.5
1.0
0.5
0.0
***
*
C57BL/6
Atchoum
7
8
Days post infection

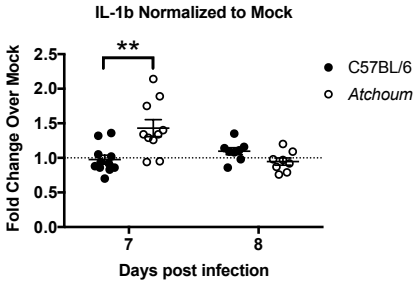
IL-1b Normalized to Mock
Fold Change Over Mock
2.5
2.0
1.5
1.0
0.5
0.0
**
C57BL/6
Atchoum
7
8
Days post infection

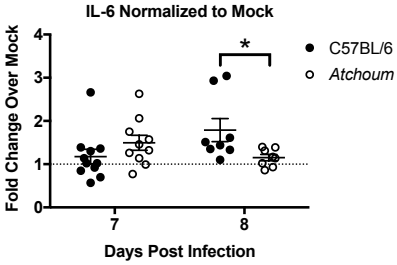
IL-6 Normalized to Mock
Fold Change Over Mock
4
3
2
1
0
*
C57BL/6
Atchoum
7
8
Days Post Infection

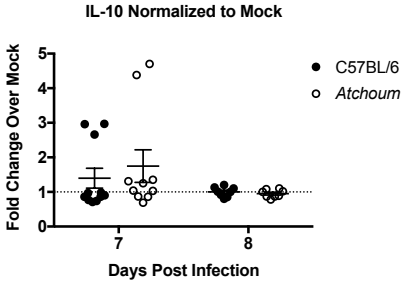
IL-10 Normalized to Mock
Fold Change Over Mock
5
4
3
2
1
0
C57BL/6
Atchoum
7
8
Days Post Infection

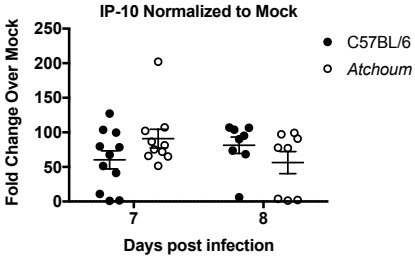
IP-10 Normalized to Mock
Fold Change Over Mock
250
200
150
100
50
0
C57BL/6
Atchoum
7
8
Days post infection

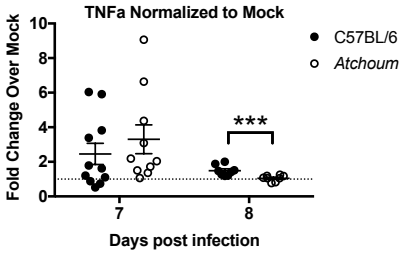
TNFa Normalized to Mock
Fold Change Over Mock
10
8
6
4
2
0
***
C57BL/6
Atchoum
7
8
Days post infection

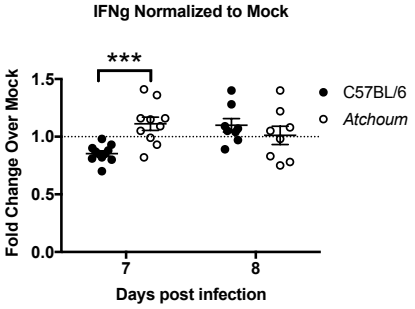
IFNg Normalized to Mock
Fold Change Over Mock
1.5
1.0
0.5
0.0
***
C57BL/6
Atchoum
7
8
Days post infection

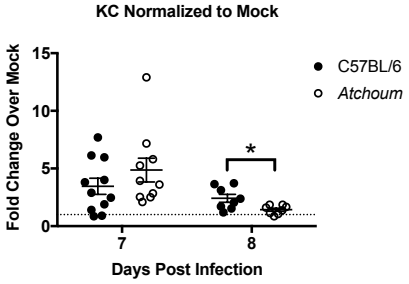
KC Normalized to Mock
Fold Change Over Mock
15
10
5
0
*
C57BL/6
Atchoum
7
8
Days Post Infection

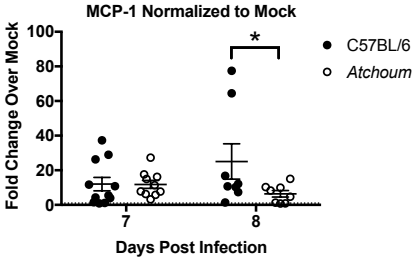
MCP-1 Normalized to Mock
Fold Change Over Mock
100
80
60
40
20
0
*
C57BL/6
Atchoum
7
8
Days Post Infection

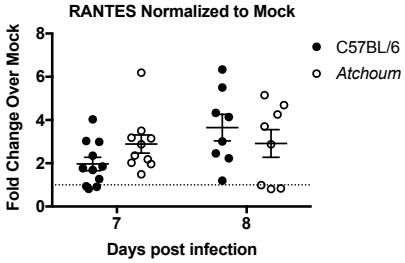
RANTES Normalized to Mock
Fold Change Over Mock
8
6
4
2
0
C57BL/6
Atchoum
7
8
Days post infection

Figure 3.6 Changes in cytokine levels between MAV-1-infected *atchoum* and wild type mouse brains. GCN2$^{-/-}$ (*Atchoum*) and wild type (C57BL/6) mice were infected i.p. with 10^3 PFU MAV-1 or mock infected and brains were harvested at 7 and 8 dpi. Brain extracts were prepared in a 10% weight/volume PBS and analyzed by ELISA for IL-1α, IL-1β, IFN-γ, MCP-1, KC, and TNFα. Each dot represents a different mouse. Horizontal bar represents the mean. *$P \leq 0.05$, **$P \leq 0.01$, **$P \leq 0.001$.

than wild type mice. At 8 dpi, wild type mice also had higher absolute levels of IL-1α, IL-1β, IL-6, TNFα, KC, and MCP-1 than *atc* mice (Table 3.1). The differences in cytokine and chemokine responses to MAV-1 infection between *atc* and wild type mouse brains suggest that the immune cells that produce these cytokine and chemokines may have different levels of activity or localization in the presence of GCN2.

Discussion

We have characterized the *atc* phenotype during MAV-1 infection. $GCN2^{-/-}$ mice and primary peritoneal macrophages were more susceptible to MAV-1 infection compared to wild type mice and macrophages, but $GCN2^{-/-}$ MEFs were not (Fig. 3.2 and 3.3). The lower survival of $GCN2^{-/-}$ mice compared to wild type mice was not explained by increased viremia or tissue damage, because there was no difference in viral yields or histology between any organs assayed from MAV-1-infected $GCN2^{-/-}$ or wild type mice except for the cecum (Fig. 3.4). However, there were differences in pro-inflammatory cytokine and chemokine responses to MAV-1 infection in the brains of $GCN2^{-/-}$ and wild type mice. Normalized levels of IL-1α, IL-1β, and IFNγ were significantly higher in MAV-1-infected *atc* brains compared to wild type brains at 7 dpi, while normalized levels of IL-1α, IL-6, TNFα, KC, and MCP-1 levels were significantly lower in MAV-1-infected *atc* brains compared to wild type at 8 dpi (Fig. 3.6). This suggests that the cytokine response in the *atc* brains peaks earlier during infection than the cytokine response in wild type mice. This early peak at 7 dpi and drop in cytokines at 8 dpi may explain why the *atc* mouse survival decreases significantly after 7 dpi compared to the survival of the wild type mice (Fig. 3.2).

Compared to wild type cells, the higher viral yield in GCN2$^{-/-}$ macrophages, similar viral yields in GCN2$^{-/-}$ MEFs, and the differences in brain cytokine levels during infection between mice of each strain suggest that the GCN2$^{-/-}$ mice may mount a different immune response to MAV-1 infection than wild type mice, specifically in immune cells. Other viruses serve as precedents for this. YF-17D infection of GCN2$^{-/-}$ mice and dendritic cells results in decreased immune response (24). In GCN2$^{-/-}$ dendritic cells incubated with YF-17D, autophagy is reduced compared to wild type dendritic cells. Autophagy in dendritic cells is critical for proper antigen cross-presentation during infection, and consequently GCN2$^{-/-}$ mice immunized with YF-17D also have reduced proliferation of CD8^{+} and CD4^{+} YF-17D-specific T-cells compared to control mice. This suggests that GCN2 plays a role in promoting antigen cross-presentation and priming secondary immunity during YF-17D immunization. Assaying MAV-1-infected GCN2$^{-/-}$ dendritic cells for levels of autophagy markers would show whether autophagy is similarly impaired, and measuring CD8^{+} and CD4^{+} specific T-cells in the organs of GCN2$^{-/-}$ mice infected with MAV-1 would give additional insight into the immune response mounted by GCN2$^{-/-}$ mice during MAV-1 infection.

In summary, we have shown that GCN2$^{-/-}$ mice and primary peritoneal macrophages were more susceptible to MAV-1 infection than wild type mice, indicating that GCN2 is antiviral during MAV-1 infection. However, we have been unable to demonstrate GCN2 activation (phosphorylation) during MAV-1 infection due to the unavailability of good antibodies to mouse GCN2 (Goodman and Spindler, unpublished). The reduced survival of GCN2$^{-/-}$ mice is not likely to be due to increased viremia or extensive inflammatory damage in any organs, because the viral loads and histology in GCN2$^{-/-}$ mouse organs were similar those in wild type mouse organs except for the cecum. This difference seen in the cecum could be investigated more thoroughly

to determine if GCN2 plays an antiviral role in the gut. However, there was a difference in inflammatory cytokine response in MAV-1-infected GCN2$^{-/-}$ mouse brains compared to wild type mouse brains, suggesting that the differences in survival could stem from a difference in the immune response in the brain. GCN2$^{-/-}$ primary macrophages produced more MAV-1 genome replication compared to wild type primary macrophages. However, this was not seen in MEFs, where higher yields occurred for wild type cells than GCN2$^{-/-}$ cells (Fig. 3.3B). Similar results were seen in GCN2$^{-/-}$ macrophages and MEFs when compared to wild type MEFs when infected with MCMV (22). This suggests that the effects of GCN2 are cell-type specific. Assaying the responses from specific immune cells, including GCN2$^{-/-}$ dendritic cells, macrophages, and T-cells, could help to further characterize the differences in immune response between GCN2$^{-/-}$ and wild type animals.

Materials and methods

Virus, mice, and cells

Wild type MAV-1 stock was prepared and titrated on mouse NIH 3T6 fibroblasts as described previously (38).

Atc mice on the C57BL/6J background were obtained from Bruce Beutler (UT Southwestern Medical Center) (22). The *atc* mice were bred in-house and both sexes were used in experiments. *Atc* mutation was confirmed by genotyping mice as described below. No differences based on sex was noted. All animal work complied with relevant federal and University of Michigan policies. Mice were housed in microisolator cages and provided food and water ad libitum. C57BL/6J mice were purchased from Jackson Laboratory (#000664).

C57BL/6 MEFs (SCRC-1008) were obtained from the American Type Culture Collection and passaged in Dulbecco's modified eagle media (DMEM) containing 10% heat-inactivated fetal bovine serum (FBS) before use. *Atc* MEFs were obtained from 13-16 day old embryos (estimated) using previously described methods (39). Briefly, a pregnant *atc* mouse was euthanized by CO_2 asphyxiation and the embryos were removed from the uterus and placed in a sterile petri dish. The heads and viscera were removed from the embryos and the remaining tissue was minced up and trypsinized with 0.25% trypsin/EDTA for 15 minutes. Cells were seeded at a density of one embryo/175 cm^2 tissue culture treated flask in DMEM + 10% FBS and incubated at 37˚C with 5% CO_2 for three to four days. When the flasks became confluent, the cells were split into 10 cm plates.

Atc MEFs were immortalized using a modified 3T3 immortalization protocol (40). Briefly, a frozen aliquot of non-immortalized *atc* MEFs at passage 2 was thawed and plated on a 100 mm plate (day 1) in DMEM containing 10% heat-inactivated FBS. On day 4, the MEFs were trypsinized, counted on a hemocytometer, and 3.5×10^5 cells were plated on 60 mm plates; all cells were plated. This step was repeated every 3 days. Cell numbers decreased between passage 6-10, and cells started to show signs of immortalization around passage 15-20. After consistent cell number increases for several passages, cells were transitioned to 100 mm plates and genotyped as described below to confirm that the *atc* mutation was maintained.

Primary peritoneal macrophages were obtained from 6-10 week old *atc* mice, or C57BL/6J mice purchased from Jackson Laboratory (#000664) as described (41). Briefly, 6-10 week old C57BL/6 mice were injected intraperitoneally with 1.2 mL 3% aged thioglycollate and euthanized 3-5 days later. The abdominal skin was carefully removed, exposing the peritoneum, which was then injected with 5 mL of sterile phosphate-buffered saline (PBS). The abdomen was

massaged gently, then the PBS containing the peritoneal cells was carefully withdrawn. The cells were centrifuged at 100 x g for 4 minutes, red blood cells lysed in lysis buffer (0.15 M ammonium chloride, 1 mM potassium bicarbonate, and 0.1 mM EDTA disodium salt) for 2 minutes at room temperature. The macrophage cells were centrifuged at 100 x g for 4 minutes, washed twice in PBS, resuspended in DMEM + 5% heat-inactivated FBS, and plated in 6 well plates.

Genotyping for GCN2 mutation

DNA from mouse tails was obtained as described (42). DNA from immortalized MEFs was purified using Invitrogen PureLink DNA Purification Kit (Thermo Scientific #K1820-02) and PCR amplified the mutation region using primers Eif2ak4atc F: 5'-AAT TGG CTG GGA CGG TGT CAA G-3' and Eif2ak4atc R – 5'-GGA AGC ACT TTA AAT GCT CGC CAC-3' (22). The PCR was cleaned up with the Qiagen PCR Clean up kit and submitted for sequencing using the Eif2ak4atc F primer to the University of Michigan DNA Sequencing Core.

Immunoblots (Information for Fig. 4.2)

At room temperature, cells were washed once with PBS and Pierce^{TM} RIPA lysis buffer (Thermo Scientific #89900) with 1x protease inhibitors (Protease Inhibitor Cocktail Kit, Thermo Scientific #78410) was added to the plate. The cells were allowed to lyse at room temperature for 10 minutes before being harvested and centrifuged at 4˚C at 14,000 x g for 10 minutes to remove debris. Equivalent amounts of protein, determined by a BCA assay (Pierce BCA Protein Assay Kit, Thermo Scientific #23227), were acetone precipitated by incubating with 4x volume ice cold acetone overnight at -20˚C. Precipitated proteins were pelleted at 4˚C at 13,000 x g for 10

minutes and the pellets were dried for 30 minutes at room temperature. Pellets were resuspended in 10 µL Pierce™ RIPA lysis buffer (Thermo Scientific #89900), 3.25 µL NuPAGE 4x LDS Sample Buffer (Invitrogen Cat #NP0007), and 1.25 µL 1M DTT. Samples were incubated at 37˚C for 10 minutes and then loaded into a well of an 8% acrylamide gel (8.3 cm wide x 7.3 cm high x 0.1 cm thick) with a 2.5% stacking gel, electrophoresed for 30 minutes at 50 V and 85 minutes at 150 V, and then transferred to a PVDF membrane (BioRad #1620177) for 1 hour at 100V at 4˚C. Blots were blocked in 5% bovine serum albumin (BSA, Sigma A7906) in tris-buffered saline (BioRad #1706435) and 0.1% Tween 20 (Sigma P1379). Blots were probed with primary antibodies to detect mouse p-eIF2α (Invitrogen #44728G, 1:2000), eIF2α (Invitrogen #AHO1182, 1:500), and actin (Santa Cruz sc-1616-R, 1:1000). The secondary antibody used was IgG peroxidase-conjugated anti-rabbit (Thermo Scientific #31462, 1:30,000). Blots were visualized by enhanced chemiluminescent substrates (Pierce ECL Western Blotting Substrate #32106) and X-ray film (Dot Scientific #BDB810). Densitometric quantification was performed on .tif files using ImageJ software from NIH (43).

Mouse infections

Mice 4-5 weeks old were infected via i.p. injection with 10^2, 10^3, or 10^4 PFU in a volume of 100 µL. Virus was diluted in 10-fold serial dilutions in endotoxin-free Dulbecco's phosphate-buffered saline (DPBS; Gibco 14190-144). Mock infected mice were injected with conditioned media diluted similarly in DPBS. Mice were monitored twice daily for signs of disease (e.g., ruffled fur, hunched posture, seizures, inability to feed) and were euthanized by CO_2 asphyxiation if moribund or at the indicated time points. Organs were harvested, snap frozen on dry ice, and stored at -20˚C or -70˚C until processed.

Quantitating viral yield by qPCR from cells and tissue

DNA for measurement of viral load was extracted from 20 mg of organ tissue or cells using the Invitrogen PureLink DNA Purification Kit (Thermo Scientific #K1820-02) and quantitated by a NanoDrop Spectrophotometer. 5 ng of total DNA for organ tissue or 2 µL of purified cellular DNA was analyzed by qPCR using custom primers specific to MAV-1 E1A (mE1Agenomic Fwd: 5' GCA CTC CAT GGC AGG ATT CT 3' and mE1Agenomic Rev 5' GGT CGA AGC AGA CGG TTC TTC 3'), and the results were either normalized to GAPDH (Fig. 3.3), which was analyzed using a GAPDH-specific primer/probe set (ThermoFisher Scientific, Mm99999915_g1, #4331182) or compared to a standard curve of mE1A (Fig. 3.4). Results normalized to GAPDH ($\Delta\Delta C_T$) were also normalized to mock at 24 hpi (Fig. 3.3). Each sample was assayed in triplicate.

Mouse brain and liver plaque assays

90-110 mg of brain or liver tissue were prepared in a 10% weight/volume solution with PBS by adding the tissue and corresponding amount of PBS to bead beater tubes. They were then homogenized with sterile glass beads in a mini Beadbeater (Biospec Products) three times for 1 minute, with a 1 minute rest on ice between each homogenization. The tubes were put through 3 freeze/thaw cycles and then centrifuged at 2000 x g for 5 minutes at 4˚C to remove the remaining tissue debris. The supernatant was transferred to a new tube. The supernatants were then analyzed for infectious virus by plaque assay on 3T6 cells.

Histology

C57BL/6 and *atc* mice were infected via i.p. injection with 10^3 PFU MAV-1 in a volume of 100 μL. At 5 or 7 dpi, mice were euthanized CO_2 asphyxiation and perfused with 10% formalin (3.7% formaldehyde in PBS), and organs were collected for histopathology. Organs (thymus, lung, heart, brain, liver, kidney, spleen, stomach, small intestine, colon/cecum) were immersion-fixed in 10% neutral buffered formalin for 24 hours, embedded in paraffin, and sectioned at 5 μm. Sections were stained with hematoxylin and eosin. The University of Michigan Comprehensive Cancer Center Research Histology and Immunoperoxidase Laboratory performed sectioning and staining. Slides were randomized and blinded for evaluation by a board-certified pathologist.

Analysis of cytokine and chemokine levels

50-100 mg of brain tissue were prepared in a 10% weight/volume solution with extraction buffer (50 mM Tris-HCl, 150 mM NaCl, 1% IGEPAL [Sigma I8896]) by adding the tissue and corresponding amount of buffer to bead beater tubes. They were then homogenized with sterile glass beads in a mini Beadbeater (Biospec Products) three times for 30 seconds, with a 10 second rest on ice between each homogenization. The tubes were then incubated on ice for 30 minutes and then centrifuged at 2000 x g for 10 minutes at 4˚C to remove the remaining tissue debris. The supernatant was transferred to a new microcentrifuge tube and centrifuged again at 20,000 x g for 20 minutes at 4˚C. The supernatant was transferred to a new tube. Protein concentrations were determined by a BCA assay (Pierce BCA Protein Assay Kit, Thermo Scientific #23227). The levels of cytokines and chemokines were measured in mouse brain lysates by ELISA by the University of Michigan Cancer Center Immunology Core. In each brain

lysate sample we measured IL-1α, IL-1β, IL-10, IP-10, IFNγ, MCP-1, RANTES, KC, and TNFα. Plates were read using a MAGPIX plate reader and analyzed using xPONENT Software (Merck Millipore).

Statistical analyses

Data were analyzed with GraphPad Prism 7.0 software. For comparisons of qPCR analyses, the data were analyzed by individual Mann-Whitney tests. A value of $P < 0.05$ was considered significant.

Acknowledgments

We thank Oded Foreman for evaluating the histology. We also thank the University of Michigan DNA Sequencing Core, ELISA Core, and the Cancer Center Histology Core. Research reported in this thesis was supported by the National Cancer Institute of the National Institutes of Health under award number P30CA046592.

Bibliography

1. Berk AJ. 2013. Adenoviridae: The viruses and their replication. *In* Knipe DM, Howley P (ed), Fields Virology, 6th ed, vol 2. Lippincott Williams & Wilkins, Philadelphia.

2. Wek RC. 2018. Role of eIF2alpha kinases in translational control and adaptation to cellular stress. Cold Spring Harb Perspect Biol 10.

3. Farrell PJ, Balkow K, Hunt T, Jackson RJ, Trachsel H. 1977. Phosphorylation of initiation factor elF-2 and the control of reticulocyte protein synthesis. Cell 11:187-200.

4. Tahara SM, Traugh JA, Sharp SB, Lundak TS, Safer B, Merrick WC. 1978. Effect of hemin on site-specific phosphorylation of eukaryotic initiation factor 2. Proc Natl Acad Sci USA 75:789-93.

5. Feng GS, Chong K, Kumar A, Williams BR. 1992. Identification of double-stranded RNA-binding domains in the interferon-induced double-stranded RNA-activated p68 kinase. Proc Natl Acad Sci USA 89:5447-51.

6. Kuhen KL, Samuel CE. 1997. Isolation of the interferon-inducible RNA-dependent protein kinase Pkr promoter and identification of a novel DNA element within the 5'-flanking region of human and mouse Pkr genes. Virology 227:119-30.

7. Patel RC, Sen GC. 1992. Identification of the double-stranded RNA-binding domain of the human interferon-inducible protein kinase. J Biol Chem 267:7671-6.

8. Dzananovic E, McKenna SA, Patel TR. 2018. Viral proteins targeting host protein kinase R to evade an innate immune response: A mini review. Biotechnol Genet Eng Rev 34:33-59.

9. Ranu RS. 1979. Regulation of protein synthesis in rabbit reticulocyte lysates: the hemeregulated protein kinase (HRI) and double stranded RNA induced protein kinase (dRI) phosphorylate the same site(s) on initiation factor eIF-2. Biochem Biophys Res Commun 91:1437-44.

10. Harding HP, Zhang Y, Ron D. 1999. Protein translation and folding are coupled by an endoplasmic-reticulum-resident kinase. Nature 397:271-4.

11. Wek RC, Ramirez M, Jackson BM, Hinnebusch AG. 1990. Identification of positive-acting domains in GCN2 protein kinase required for translational activation of GCN4 expression. Mol Cell Biol 10:2820-31.

12. Wek RC, Jackson BM, Hinnebusch AG. 1989. Juxtaposition of domains homologous to protein kinases and histidyl-tRNA synthetases in GCN2 protein suggests a mechanism for coupling GCN4 expression to amino acid availability. Proc Natl Acad Sci U S A 86:4579-83.

13. Ramirez M, Wek RC, Hinnebusch AG. 1991. Ribosome association of GCN2 protein kinase, a translational activator of the GCN4 gene of Saccharomyces cerevisiae. Mol Cell Biol 11:3027-36.

14. Garcia-Barrio M, Dong J, Ufano S, Hinnebusch AG. 2000. Association of GCN1-GCN20 regulatory complex with the N-terminus of eIF2alpha kinase GCN2 is required for GCN2 activation. EMBO J 19:1887-99.

15. Marton MJ, Crouch D, Hinnebusch AG. 1993. GCN1, a translational activator of GCN4 in Saccharomyces cerevisiae, is required for phosphorylation of eukaryotic translation initiation factor 2 by protein kinase GCN2. Mol Cell Biol 13:3541-56.

16. Anda S, Zach R, Grallert B. 2017. Activation of Gcn2 in response to different stresses. PLoS One 12:e0182143.

17. Qiu H, Dong J, Hu C, Francklyn CS, Hinnebusch AG. 2001. The tRNA-binding moiety in GCN2 contains a dimerization domain that interacts with the kinase domain and is required for tRNA binding and kinase activation. EMBO J 20:1425-38.

18. Dong J, Qiu H, Garcia-Barrio M, Anderson J, Hinnebusch AG. 2000. Uncharged tRNA activates GCN2 by displacing the protein kinase moiety from a bipartite tRNA-binding domain. Mol Cell 6:269-79.

19. Lageix S, Zhang J, Rothenburg S, Hinnebusch AG. 2015. Interaction between the tRNA-binding and C-terminal domains of Yeast Gcn2 regulates kinase activity in vivo. PLoS Genet 11:e1004991.

20. Qiu H, Hu C, Dong J, Hinnebusch AG. 2002. Mutations that bypass tRNA binding activate the intrinsically defective kinase domain in GCN2. Genes Dev 16:1271-80.

21. Zhu S, Wek RC. 1998. Ribosome-binding domain of eukaryotic initiation factor-2 kinase GCN2 facilitates translation control. J Biol Chem 273:1808-14.

22. Won S, Eidenschenk C, Arnold CN, Siggs OM, Sun L, Brandl K, Mullen TM, Nemerow GR, Moresco EM, Beutler B. 2012. Increased susceptibility to DNA virus infection in mice with a GCN2 mutation. J Virol 86:1802-1808.

23. Shibata N, Carlin AF, Spann NJ, Saijo K, Morello CS, McDonald JG, Romanoski CE, Maurya MR, Kaikkonen MU, Lam MT, Crotti A, Reichart D, Fox JN, Quehenberger O, Raetz CR, Sullards MC, Murphy RC, Merrill AH, Jr., Brown HA, Dennis EA, Fahy E, Subramaniam S, Cavener DR, Spector DH, Russell DW, Glass CK. 2013. 25-Hydroxycholesterol activates the integrated stress response to reprogram transcription and translation in macrophages. J Biol Chem 288:35812-23.

24. Ravindran R, Khan N, Nakaya HI, Li S, Loebbermann J, Maddur MS, Park Y, Jones DP, Chappert P, Davoust J, Weiss DS, Virgin HW, Ron D, Pulendran B. 2014. Vaccine activation of the nutrient sensor GCN2 in dendritic cells enhances antigen presentation. Science 343:313-317.

25. Berlanga JJ, Ventoso I, Harding HP, Deng J, Ron D, Sonenberg N, Carrasco L, de Haro C. 2006. Antiviral effect of the mammalian translation initiation factor 2alpha kinase GCN2 against RNA viruses. EMBO J 25:1730-1740.

26. del Pino J, Jimenez JL, Ventoso I, Castello A, Munoz-Fernandez MA, de Haro C, Berlanga JJ. 2012. GCN2 has inhibitory effect on human immunodeficiency virus-1 protein synthesis and is cleaved upon viral infection. PLoS One 7:e47272.

27. Aparicio F, Aparicio-Sanchis R, Gadea J, Sanchez-Navarro JA, Pallas V, Murguia JR. 2011. A plant virus movement protein regulates the Gcn2p kinase in budding yeast. PLoS One 6:e27409.

28. Hirohata Y, Kato A, Oyama M, Kozuka-Hata H, Koyanagi N, Arii J, Kawaguchi Y. 2015. Interactome analysis of herpes simplex virus 1 envelope glycoprotein H. Microbiol Immunol 59:331-7.

29. Vazquez de Aldana CR, Marton MJ, Hinnebusch AG. 1995. GCN20, a novel ATP binding cassette protein, and GCN1 reside in a complex that mediates activation of the eIF-2 alpha kinase GCN2 in amino acid-starved cells. EMBO J 14:3184-99.

30. Krahling V, Stein DA, Spiegel M, Weber F, Muhlberger E. 2009. Severe acute respiratory syndrome coronavirus triggers apoptosis via protein kinase R but is resistant to its antiviral activity. J Virol 83:2298-309.

31. Qian W, Zhu S, Sobolev AY, Wek RC. 1996. Expression of vaccinia virus K3L protein in yeast inhibits eukaryotic initiation factor-2 kinase GCN2 and the general amino acid control pathway. J Biol Chem 271:13202-7.

32. Griffin DE. 1997. Cytokines in the brain during viral infection: clues to HIV-associated dementia. J Clin Invest 100:2948-51.

33. Schobitz B, De Kloet ER, Holsboer F. 1994. Gene expression and function of interleukin 1, interleukin 6 and tumor necrosis factor in the brain. Prog Neurobiol 44:397-432.

34. Gu L, Rutledge B, Fiorillo J, Ernst C, Grewal I, Flavell R, Gladue R, Rollins B. 1997. In vivo properties of monocyte chemoattractant protein-1. J Leukoc Biol 62:577-80.

35. Roy M, Richard JF, Dumas A, Vallieres L. 2012. CXCL1 can be regulated by IL-6 and promotes granulocyte adhesion to brain capillaries during bacterial toxin exposure and encephalomyelitis. J Neuroinflammation 9:18.

36. Marquette C, Van Dam AM, Ceccaldi PE, Weber P, Haour F, Tsiang H. 1996. Induction of immunoreactive interleukin-1 beta and tumor necrosis factor-alpha in the brains of rabies virus infected rats. J Neuroimmunol 68:45-51.

37. Castro-Jorge LA, Pretto CD, Smith AB, Foreman O, Carnahan KE, Spindler KR. 2017. A Protective Role for Interleukin-1 Signaling during Mouse Adenovirus Type 1-Induced Encephalitis. J Virol 91.

38. Cauthen AN, Welton AR, Spindler KR. 2007. Construction of mouse adenovirus type 1 mutants. Methods Mol Med 130:41-59.

39. Arat S, Rzucidlo SJ, Stice SL. 2003. Gene expression and in vitro development of inter-species nuclear transfer embryos. Mol Reprod Dev 66:334-42.

40. Aaronson SA, Todaro GJ. 1968. Development of 3T3-like lines from Balb-c mouse embryo cultures: transformation susceptibility to SV40. J Cell Physiol 72:141-8.

41. Ashley SL, Welton AR, Harwood KM, Van Rooijen N, Spindler KR. 2009. Mouse adenovirus type 1 infection of macrophages. Virology 390:307-14.

42. Schauwecker PE, Williams RW, Santos JB. 2004. Genetic control of sensitivity to hippocampal cell death induced by kainic acid: a quantitative trait loci analysis. J Comp Neurol 477:96-107.

43. Schindelin J, Rueden CT, Hiner MC, Eliceiri KW. 2015. The ImageJ ecosystem: An open platform for biomedical image analysis. Mol Reprod Dev 82:518-29.

Chapter IV

Conclusions and Future Directions

Protein kinase R (PKR) Chapter Review

In Chapter II, we demonstrated that PKR has an antiviral role during mouse adenovirus type 1 (MAV-1) infection, because when PKR is mutated, viral replication in mouse embryonic fibroblasts (MEFs) is significantly higher compared to wild type MEFs. Analysis of global PKR steady-state protein levels during infection showed complete PKR depletion by 72 hours post infection (hpi) in multiple cell types, including immortalized and primary cells, with even faster kinetics in some. PKR steady-state mRNA levels and translation were not decreased by MAV-1 infection, whereas proteasomal inhibition prevented PKR degradation. These data suggest that MAV-1 causes PKR to be proteasomally degraded at a post-translational level by an early viral protein, and we ruled out E1A and E3 as being required for this degradation (Fig. 4.1).

Determining which early protein is responsible for PKR degradation during MAV-1 infection

The next obvious step is to determine which MAV-1 protein functioning early in infection is responsible for PKR degradation. Using mutant viruses, we have ruled out E1A and E3 as being required for PKR degradation. As described in the discussion of Chapter II, two

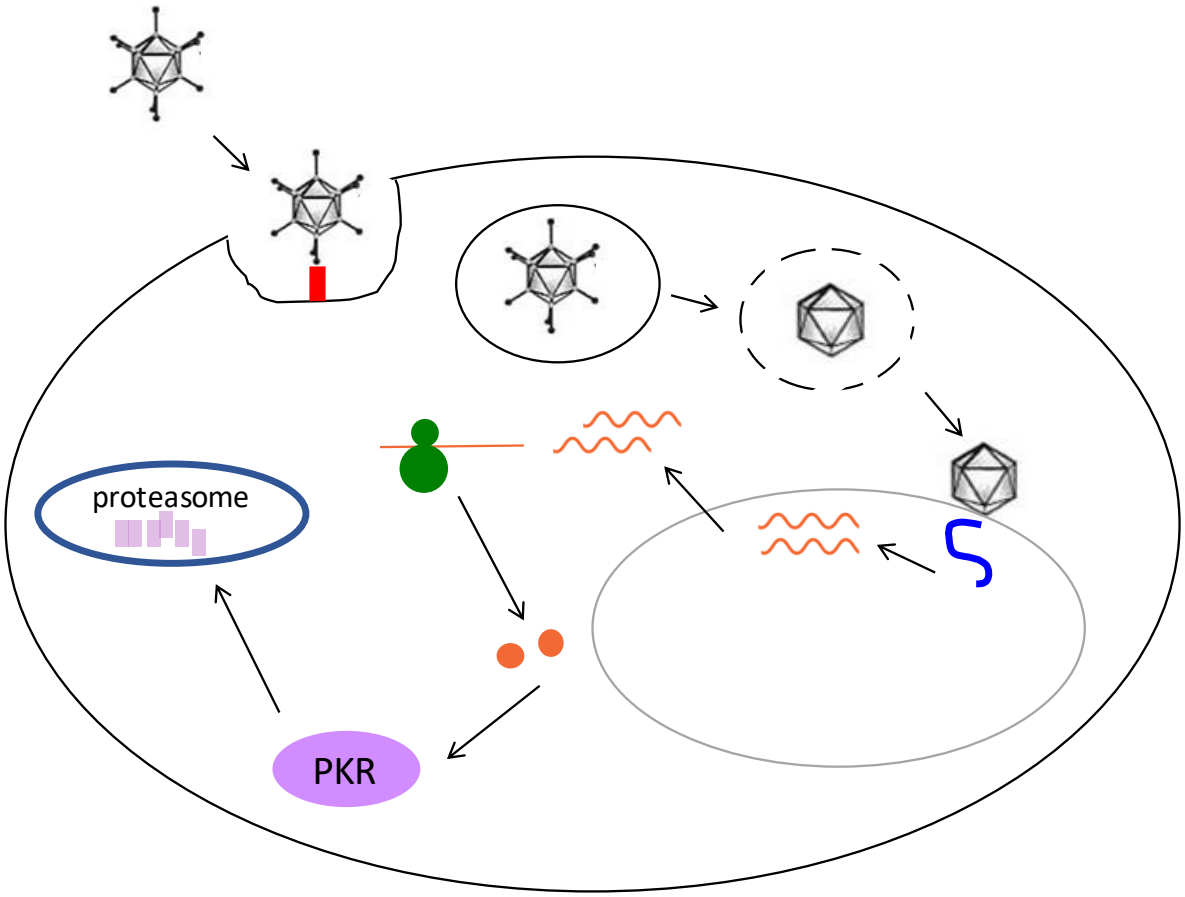

Figure 4.1 PKR degradation during MAV-1 infection. During MAV-1 infection, an as yet unidentified viral protein is produced by the virus and causes PKR to be degraded by the proteasome early in infection.

possibilities are E4 proteins, the homologs of human adenovirus (hAd) E4orf6 and E4orf3 (1). In hAd, E4orf6 interacts with another early hAd protein, E1B 55K, to participate in an E3 ligase complex that ubiquitinates and degrades p53 via proteasomal degradation (2, 3). When mouse p53 and MAV-1 E4orf6 and E1B 55K are introduced by transfection into human cells, all three proteins interact and mouse p53 is degraded (4). If MAV-1 E4orf6 and E1B 55K form a similar complex in mouse cells, it may also degrade PKR. We have preliminary evidence that mouse p53 is ubiquitinated in C57BL/6 MEFs during MAV-1 infection, which suggests that the mouse p53 degradation seen in human cells could be paralleled by degradation of endogenous mouse p53 and mouse PKR (mPKR) in mouse cells, mediated by MAV-1 E4orf6 and E1B 55K during infection.

Another hAd E4 protein, E4orf3, causes proteasomal degradation of transcriptional intermediary factor 1γ (5) and general transcription factor II-I (6) in a manner independent of hAd E4orf6 and E1B 55K. E4orf3 has SUMO E3 ligase and E4 elongase activity and induces sumoylation of general transcription factor II-I, leading to its proteasome-dependent degradation (6). MAV-1 E4orf3 may similarly have sumoylation activity that results ultimately in proteasome-dependent PKR degradation. All of the known targets of E4 degradation play a role in DNA damage response. Because PKR also affects the DNA damage response (7), it is possible that E4 proteins are responsible for PKR degradation.

Another possibility of a viral protein involved in PKR degradation is the protease encoded by MAV-1. The hAd protease is encapsidated in virions and proteolytically processes viral proteins IIIa, VI, VII, VIII, mu, and TP (8-11). However, we think it is unlikely that the MAV-1 protease degrades PKR, because we showed that UV-inactivated virus was unable to degrade PKR (Chapter II). We assume that UV treatment would not destroy the MAV-1 protease

activity, just as herpes simplex virus 1 (HSV-1) VP16 activity is not altered by UV-inactivation of HSV-1 (12), but we have not tested this directly.

A way to screen these early viral proteins and others would be to transfect these proteins directly into mouse cells and assay for PKR protein levels in the absence of viral infection by immunoblot 24 to 48 hpi. We have constructs of FLAG-tagged E1A, E1B 19K, E1B 55K, E2 DBP, E2 pTP, E3 class 1, E3 class 2, E3 class 3, E4orfa/b (E4orf6), E4orfa/c (E4orf3), E4orfd, and the proteinase. The proteins could be transfected individually or in combination, followed by immunoblot assay to obtain evidence of PKR degradation. If transfection into mouse cells proves to be difficult, the transfections could first be done in an easily transfectable human cell line as long as mPKR is also transfected in (we have a FLAG-tagged mPKR construct that can be used for this).

If we see degradation with any of the constructs, then we will be able to determine the exact mechanism of PKR degradation by MAV-1. Once we know which early viral protein(s) are required for mPKR degradation, cells transfected with these viral proteins can be immunoprecipitated for the viral protein to identify any other host proteins that immunoprecipitate, suggesting they are recruited to degrade PKR. We can also mutate different regions of the viral protein to determine regions necessary for PKR binding or recruiting other proteins to degrade PKR. For example, we already have mutated versions of E4orf6 that prevent E4orf6 from recruiting Cul2 to the ligase complex normally formed by E4orf6 to degrade mouse p53 during infection (4).

If we do not see degradation of PKR with any of the aforementioned constructs alone, we would test combinations of viral proteins, like E4orf6 and E1B 55K, to determine if multiple viral proteins are required for PKR degradation. We would also validate the transfection assay

system by transfecting the full MAV-1 genome into cells to determine whether PKR is degraded like it is during normal infection. Alternatively, we would immunoprecipitate PKR from MAV-1-infected cells that had been treated with MG132 to prevent PKR degradation, and use mass spectrometry to determine if any viral or host proteins are associating with PKR differentially during MAV-1 infection. This could point to proteins responsible for PKR degradation during MAV-1 infection.

Effects of PKR phosphorylation on PKR degradation rate during MAV-1 infection

While we never immunoblotted for phospho-PKR during MAV-1 infection, all of my immunoblotting of mPKR showed up as doublet bands (Fig. 2.4A), except for the immunoblotting of the K271R SV40-MEFs, which expressed a kinase-dead PKR. The PKR signal produced in the K271R SV40-MEFs, when compared to the wild type SV40-MEFs, only showed a single band, at the position of the lower band of the doublet seen in the SV40-MEFs (Fig. 2.4C). This suggests that the upper band of the doublet is the phosphorylated form of PKR. In all cell types examined, this upper band was degraded at the same rate as the lower band. This is consistent with the degradation of PKR by Rift Valley Fever virus (RVFV) and foot-and-mouth disease virus, where phospho-PKR is degraded in addition to PKR during infection (13-16). However, in contrast, enterovirus A71 does not appear to cleave phospho-PKR during infection (17).

While phospho-PKR levels decrease during MAV-1, RVFV, and foot-and-mouth disease virus infection, this does not prove that phospho-PKR itself is being degraded by the viruses. That is, perhaps phospho-PKR is first dephosphorylated to PKR and then PKR is degraded. When PKR becomes transautophosphorylated, many sites can be phosphorylated, but the main

sites that affect activity are S242, T255, T258, and T446 (18, 19). Modifying these residues to become chemically similar to a phosphorylated amino acid would create a phosphomimetic version of PKR. For example, replacing a serine or threonine with aspartic acid or glutamic acid, respectively, will chemically mimic phosphoserine or phosphothreonine (20). To determine whether phosphorylation protects PKR from being degraded, $PKR^{-/-}$ MEFs could be transfected with a wild type mPKR construct or a phosphomimetic mPKR construct, and degradation of each construct could be evaluated during MAV-1 infection by immunoblot. If the phosphomimetic PKR is degraded similarly to the wild type PKR, it would suggest that mPKR is degraded during MAV-1 infection regardless of its phosphorylation status.

In vivo degradation of mPKR during MAV-1 infection

In Figure 2.2 of Chapter II, we showed that MAV-1 viral replication is higher in $PKR^{-/-}$ primary peritoneal macrophages and immortalized MEFs compared to wild type macrophages and MEFs. We also showed PKR degradation in a variety of other infected immortalized cell lines and in primary peritoneal macrophages (Fig. 2.4A). However, *in vivo*, $PKR^{-/-}$ mice had the same survival rate during MAV-1 infection as wild type mice (Fig. 2.3). To further characterize the *in vivo* effects of MAV-1 infection on PKR, it would be useful to analyze cells and organs from infected mice and determine whether PKR is degraded *in vivo*. Mock and MAV-1-infected wild type mice could have peritoneal macrophages, bone marrow macrophages, and organs removed and lysates from these cells or tissues could be analyzed by immunoblot for PKR protein levels. Determining if and in what cells PKR is degraded *in vivo* could provide evidence into why there is no difference in survival between $PKR^{-/-}$ and wild type mice during MAV-1

infection. The difference in survival could also be attributed to the incomplete knockout of PKR in these particular $PKR^{-/-}$ mice.

These mice are not complete PKR knockouts; MEFs from these mice produce a C-terminal fragment of PKR (Fig. 2.1) that still has kinase activity (21). However, this partial PKR fragment has not been characterized *in vivo*, so we do not know where or if it is expressed in mice and how much is produced. There currently are no complete PKR knockout mice in existence, so it would be useful to use CRISPR/Cas9 to create a complete or tissue-specific PKR knockout mouse to accurately measure the effect of PKR on survival of mice infected with MAV-1.

MAV-1 replication kinetics in $PKR^{-/-}$ N-MEFs versus C-MEFs

There are two different $PKR^{-/-}$ MEF lines: N-MEFs (pronounced N minus MEFs), which lack the double-stranded (ds) RNA binding domain but retain the kinase domain activity and the C-MEFs (pronounced C minus MEFs), which lack the kinase domain activity but retain the dsRNA binding domain activity (Fig. 2.1) (21). At 48 hpi, with MAV-1, the viral yield from the N-MEFs was nearly 4 times higher than the C-MEFs, but by 72 hpi the viral yields from both types of $PKR^{-/-}$ MEFs were similar to each other and significantly higher compared to wild type MEFs (Fig. 2.2A). This difference in viral replication kinetics between the two types of $PKR^{-/-}$ MEFs may be due to differences in expression level and activity of the PKR fragments reportedly produced by them (21). Although we have not assayed for PKR fragment production in our cells and mice, the fact that MAV-1 replicates to lower levels at intermediate times of infection in C-MEFs compared to N-MEFs suggests that presence of the dsRNA binding domain (present in the C-MEFs but not the N-MEFs) contributes more to PKR's antiviral effects during

MAV-1 infection than the kinase domain. It would be useful to determine the levels of PKR fragment production and their activity levels in our hands in these MEFs to reinforce this conclusion.

As proposed above, having complete $PKR^{-/-}$ MEFs to compare with wild type MEFs for MAV-1 replication would provide clearer information about the contribution of PKR to innate immunity during MAV-1 infection. It would be useful to create these MEFs directly, isolate them from a complete $PKR^{-/-}$ mouse if one is created, or from embryos if a complete PKR knockout mouse is embryonic lethal. If such $PKR^{-/-}$ MEFs are generated, constructs expressing the two main PKR domains (dsRNA binding and kinase domains) could be expressed in these $PKR^{-/-}$ MEFs during MAV-1 infection and the direct effects of each domain on MAV-1 replication kinetics could be observed.

Human PKR and MAV-1

Mouse PKR and human (hu) PKR share 58% amino acid identity and are 71% similar. Specifically, the dsRNA binding domains share 60% identity and are 75% similar, and the kinase domains share 67% identity and are 77% similar. When we infected $PKR^{-/-}$ MEFs reconstituted with FLAG-tagged huPKR variants, they were not degraded by MAV-1 infection, suggesting that MAV-1 does not degrade huPKR like it does mPKR (Fig. 2.5A). However, an important control missing from that experiment was $PKR^{-/-}$ MEFs reconstituted with FLAG-tagged mPKR to show it is degraded and that the FLAG tag is not likely to be inhibiting the degradation of huPKR. If FLAG-tagged mPKR is not degraded by MAV-1, that opens the possibility that MAV-1 actually could degrade huPKR. In that case, the $PKR^{-/-}$ MEFs should be reconstituted

with an untagged huPKR construct to confirm whether or not untagged huPKR can be degraded by MAV-1.

If FLAG-tagged mPKR is degraded by MAV-1, that would confirm the conclusion that huPKR is not degraded by MAV-1. In that case, creating chimeric PKR constructs containing regions from mPKR and huPKR could help identify the region(s) of mPKR necessary for mPKR degradation by MAV-1. Constructs that swap mPKR and huPKR dsRNA binding domains or kinase domains would be obvious places to start.

There were some interesting differences in MAV-1 replication in C-PKR$^{-/-}$ MEFs reconstituted to constitutively express FLAG-tagged full length, kinase-dead, or RNA binding-deficient human PKR. MAV-1 replicated efficiently in the vector, full length, and RNA binding-deficient huPKR lines, but replicated poorly in the kinase-dead huPKR line (Fig. 2.5B). Interestingly, the presence of full length huPKR doubled the amount of MAV-1 replication compared to the vector cell line, which contained no PKR at all, and this higher replication was reproduced in three separate experiments. These data suggest that the kinase domain of huPKR contributes significantly to MAV-1 infection. However, examining the immunoblot of the different huPKR variant expression levels (Fig. 2.5A), the amount of MAV-1 replication does seem to inversely correlate with the amount of huPKR present in each cell line. So while the virus replicated best in the full length huPKR cell line, that cell line also had the least amount of huPKR protein, and while the virus replicated the worst in the kinase-dead huPKR cell line, there was also the highest amount of huPKR protein. Thus, these differences in viral replication could be attributed to varying amounts of huPKR expressed in each cell line.

Ubiquitination of PKR during MAV-1 infection

A signal for proteasomal degradation is the conjugation of ubiquitin to a protein (22, 23). Though we determined that PKR is being degraded by the proteasome during MAV-1 infection (Fig. 2.10), we were unable to show ubiquitination of PKR during MAV-1 infection (Fig. 2.12). This inability to demonstrate PKR ubiquitination could be explained if at any given moment there were only low levels of ubiquitinated PKR present in the cell. Perhaps increasing the time under MG132 treatment could increase the amounts of ubiquitinated proteins enough so that PKR ubiquitination could be. However, our inability to detect ubiquitinated PKR is consistent with a similar inability to identify PKR ubiquitination by RVFV NSs, even though NSs is known to recruit an E3 ligase to PKR (14).

To completely rule out the possibility that PKR is ubiquitinated before being degraded by the proteasome during MAV-1 infection, PKR constructs could be made that mutate the lysine residues to prevent ubiquitination. These constructs could then be expressed in $PKR^{-/-}$ MEFs, infected with MAV-1, then analyzed by immunoblot for PKR. If PKR is still degraded during infection even with the ubiquitination sites mutated, it would suggest that PKR is being degraded by the proteasome independent of ubiquitin. This ubiquitin-independent method could involve intrinsic disordered regions of PKR or binding of regulating proteins to PKR that target proteins to the proteasome (24, 25).

General control derepressible 2 (GCN2) Chapter Overview

We have characterized the *atc* phenotype during MAV-1 infection. $GCN2^{-/-}$ mice and primary peritoneal macrophages have increased susceptibility to MAV-1 infection, but $GCN2^{-/-}$ MEFs do not (Fig. 3.2 and 3.3). The decrease in survival between $GCN2^{-/-}$ mice and wild type

mice is not explained by increased viremia or inflammatory disease, because there was no difference in viral yields or histology between any organs assayed from MAV-1-infected GCN2$^{-/-}$ or wild type mice (Fig. 3.4). There was, however, a difference in the cytokine and chemokine response to MAV-1 infection in the brains of GCN2$^{-/-}$ and wild type mice. At 7 days post infection (dpi), infected GCN2$^{-/-}$ mouse brains had higher levels of interleukin 1α, interleukin 1β, and interferon γ compared to infected wild type mouse brains while at 8 dpi, infected wild type mouse brains had higher levels of interleukin 1α, interleukin 6, tumor necrosis factor α, KC, and monocyte chemoattractant protein-1 compared to GCN2$^{-/-}$ mouse brains (Fig. 3.6). We also have preliminary data that in the serum at 8 dpi, increases in levels of interleukin 6 and tumor necrosis factor α (relative to mock) were higher in MAV-1-infected *atc* mice than in MAV-1-infected wild type mice, whereas interleukin 1β and interferon γ were not (data not shown).

GCN2 activation by general control of amino-acid synthesis 1 (GCN1)

Using immunoblots to detect GCN2 or phospho-GCN2 proteins has proven difficult due to unreliable antibodies and low endogenous levels of GCN2. Our approach (in progress) is to epitope tag GCN2 to determine whether infection induces altered levels of GCN2 and phospho-GCN2. In addition, it may be possible to analyze GCN1 levels by immunoblot as an indirect way of looking at GCN2 activation. GCN1 is an activator of GCN2 and also binds to ribosomes assisting in the transfer of uncharged tRNA to GCN2 (26). In yeast, GCN1 is required for GCN2 activation during amino acid stress and UV irradiation, suggesting that GCN1 may be required for GCN2 activation in all scenarios. HSV-1 indirectly inhibits GCN2 by targeting GCN1 (27, 28). HSV-1 glycoprotein H directly interacts with GCN1, changing its localization from the

cytoplasm to the nuclear rim, effectively sequestering GCN1 and not allowing it to assist in activating GCN2 during infection. We also have preliminary evidence showing that MAV-1 E1A interacts with GCN1 during infection from a GST pulldown screen using GST-tagged E1A (unpublished data, Fang and Spindler) (29). This result should be validated using our FLAG-tagged E1A construct. FLAG-E1A could be transfected into C57BL/6 MEFs and immunoprecipitated after a period of time using the FLAG tag. Then the immunoprecipitates could be probed for GCN1. The reverse could also be done using GCN1 antibodies for the immunoprecipitation and E1A antibodies for E1A detection. If E1A associates with GCN1, it could be sequestering it from GCN2, as HSV glycoprotein H does in infection, or it could be preventing GCN1 from activating GCN2 to reduce GCN2 activity during MAV-1 infection.

To determine whether MAV-1 affects GCN1 protein levels during infection, C57BL/6 peritoneal macrophages and MEFs could be infected with MAV-1 or mock infected, and levels of GCN1 protein examined by immunoblot. If GCN1 levels decrease during infection, it would suggest that MAV-1 modulates GCN2 activation by interacting with GCN1 and reducing the amount of GCN1 present in the cell. If GCN1 levels stay the same or increase during infection, then it would be useful to compare the localization of GCN1 in mock and MAV-1-infected cells to determine whether MAV-1, possibly through E1A, is changing the location of GCN1 during infection.

GCN2 activation by 25-hydroxycholesterol (25OHC)

GCN2 activation by viruses can occur directly or indirectly. For example, mouse cytomegalovirus (MCMV) infection leads to the production of 25OHC, which triggers GCN2 activation by reducing the levels of intracellular cysteine and/or by generating oxidative stress

(30). We showed that MAV-1 and MCMV had similar phenotypes in *atc* mice and cells, i.e., *atc* mice were more susceptible to MAV-1 and MCMV infection than wild type mice, and primary *atc* peritoneal macrophages also had higher viral replication of both viruses in comparison to wild type peritoneal macrophages (Fig. 3.2 and 3.3A) (31). However, *atc* and wild type immortalized MEFs showed no difference in viral replication with MAV-1 or MCMV (Fig. 3.3B) (31). Since these phenotypes are similar for the two viruses, it is possible that MAV-1 also triggers the production of 25OHC, which could lead to GCN2 activation during infection. C57BL/6 peritoneal macrophages, bone marrow macrophages, and MEFs could be infected with MAV-1 or mock infected and 25OHC levels assayed by liquid chromatography/mass spectrophotometry at different times post infection. If 25OHC levels are increased during infection, that could indicate that MAV-1 is indirectly triggering GCN2 during infection.

GCN2 activation through amino acid deprivation

One of the main activators of GCN2 under non-infected conditions is amino acid starvation (26). Some viruses can trigger amino acid depletion during infection, such as yellow fever virus vaccine (YF-17D) (32) and HIV-1 (33). To determine whether MAV-1 activates GCN2 by causing amino acid deficiency during infection, C57BL/6 peritoneal macrophages and MEFs could be infected with MAV-1, and intracellular levels of free amino acids could be measured by liquid chromatography/mass spectrophotometry at different times post infection. If any levels of amino acids drop significantly, that could indicate that MAV-1 is indirectly triggering GCN2 during infection.

Phosphorylation of eukaryotic translation initiation factor 2α (eIF2α)

GCN2 and PKR are both eIF2α kinases, along with heme-regulated inhibitor kinase and PKR-like endoplasmic reticulum kinase. Thus, changes in GCN2 and PKR activation or activity during infection could have effects on eIF2α phosphorylation. Assaying eIF2α and eIF2α phosphorylation over the course of MAV-1 infection in wild type, $PKR^{-/-}$, and $GCN2^{-/-}$ MEFs would enable determination of whether knocking out specific kinases has a significant impact on the amount of phosphorylated eIF2α, or whether the other three eIF2α kinases have redundant activity to reduce global cellular translation during MAV-1 infection. I have preliminary data in $GCN2^{-/-}$ peritoneal macrophages that very early in infection (2 hpi), there is a greater increase in eIF2α phosphorylation compared to MAV-1-infected wild type peritoneal macrophages at the same time point (Fig. 4.2). However, this was only a single experiment at an extremely early time point and only with $GCN2^{-/-}$ peritoneal macrophages. Repeating this experiment with more time points and $PKR^{-/-}$ peritoneal macrophages and both types of $PKR^{-/-}$ MEFs and $GCN2^{-/-}$ MEFs, and possibly creating double knockout $PKR^{-/-}$and $GCN2^{-/-}$ MEFs, would provide more insight into the impact of knocking out these kinases on eIF2α phosphorylation.

Effects of GCN2 deficiency on T-cell proliferation during MAV-1 infection

During viral infections, $CD8^+$ T-cells can be activated by dendritic cells through cross-presentation (34). Dendritic cells are antigen-presenting cells that can take up exogenous viral particles or virally infected cells and cross-present those antigens on their MHC class I molecules, activating $CD8^+$ T-cells. The $CD8^+$ T-cells can then destroy any other infected cells presenting those viral antigens. Autophagy plays a key role in antigen presentation, because dendritic cells and virally infected cells need to digest and present viral protein peptides on their

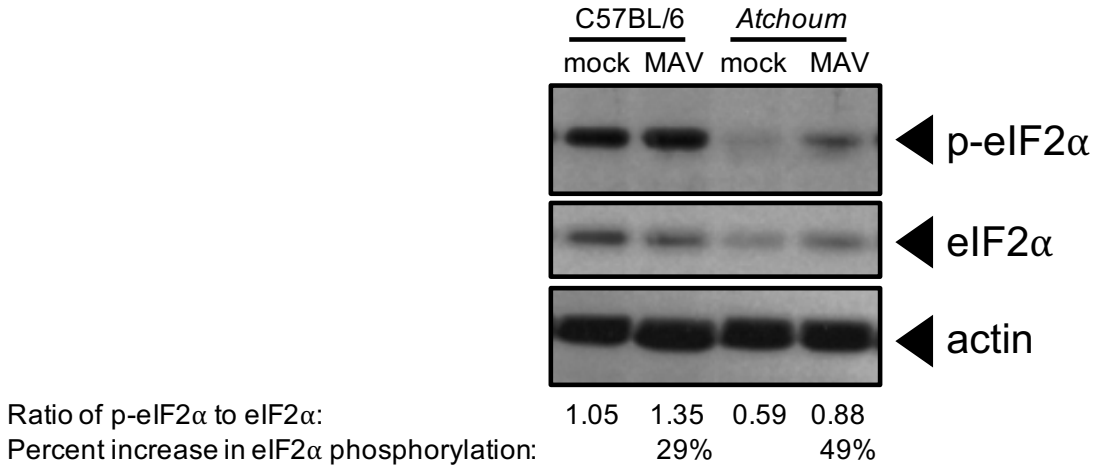

Figure 4.2 *Atc* peritoneal macrophages have a higher increase in phosphorylated eIF2α during MAV-1 infection. Wild-type (C57BL/6) and GCN2$^{-/-}$ (*Atchoum*) peritoneal macrophages were mock-infected (mock) or infected with MAV-1 at a MOI of 10 (MAV). Cell lysates were collected at 2 hours post infection and analyzed by immunoblot with antibodies for p-eIF2α, eIF2α, and actin. The blot was scanned and values were normalized to actin. The ratio of p-eIF2α to eIF2α and percent increase in eIF2α phosphorylation in infected cells is shown below each line. Blot represents a single experiment.

MHC class I or class II molecules in order to signal $CD8^+$ and $CD4^+$ T-cells, respectively, to the presence of virus (35). In $GCN2^{-/-}$ dendritic cells incubated with YF-17D, autophagy was reduced compared to wild type dendritic cells (32). $GCN2^{-/-}$ mice immunized with YF-17D also showed a reduction in the proliferation of $CD8^+$ and $CD4^+$ YF-17D-specific T-cells, suggesting that GCN2 plays a role in promoting antigen cross presentation and priming secondary immunity during YF-17D immunization.

To determine if autophagy is disrupted in MAV-1-infected $GCN2^{-/-}$ dendritic cells, $GCN2^{-/-}$ dendritic cells or macrophages could be infected or mock infected, and levels of autophagy markers, like LC3 and Atg5, could be measured by immunoblot. If autophagy is impaired in infected $GCN2^{-/-}$ cells, this would suggest that antigen presentation may not be happening effectively in $GCN2^{-/-}$ animals during infection. Measuring $CD8^+$- and $CD4^+$-specific T-cells in the organs of $GCN2^{-/-}$ mice infected with MAV-1 by flow cytometry would provide additional insight into the immune response mounted by $GCN2^{-/-}$ mice during MAV-1 infection.

Cell-type specific effects of GCN2

In Chapter III, we showed that $GCN2^{-/-}$ mice and primary peritoneal macrophages have increased susceptibility to MAV-1 infection, but $GCN2^{-/-}$ MEFs do not (Fig. 3.2 and 3.3). This suggests that the antiviral role of GCN2 during MAV-1 infection may be cell-type specific. To further characterize how GCN2 deficiency affects immune and hematopoietic cells, four types of bone marrow chimeric mice (wild type bone marrow transplanted into wild type mice [wt→wt], wt→*atc*, *atc*→wt, and *atc*→*atc*) could be created. After reconstitution, the mice could be infected with MAV-1 and survival, viral load, cytokines and chemokine levels, and inflammatory responses would be measured. If GCN2 plays a critical antiviral role in this

compartment, wild type mice reconstituted with *atc* hematopoietic cells would have a decreased survival compared to mice reconstituted with wild type hematopoietic cells.

Conclusions

PKR and GCN2 are both eIF2α kinases that function to phosphorylate eIF2α in response to specific stressors. This in turn leads to a reduction in global cellular translation, a cellular antiviral response that reduces viral protein synthesis. We know that MAV-1 does not induce host cell translation shutoff, indicating that in MAV-1 infected cells, cellular translation is intact (36). We also now know that MAV-1 degrades PKR during infection, reducing the number of active eIF2α kinases to three. Determining whether GCN2 or even PKR-like endoplasmic reticulum kinase is activated during MAV-1 infection and how MAV-1 interacts with GCN2 during infection would provide information on the potential redundancies to maintain eIF2α phosphorylation during MAV-1 infection in spite of PKR degradation and the interplay between eIF2α kinases and MAV-1. It is possible that there is more crosstalk between the PKR and GCN2 pathways than previously studied, and this could have implications beyond immunity in viral infection.

In this work, we have shown a novel mechanism for PKR inhibition in DNA viruses. PKR is degraded by the proteasome during MAV-1 infection, and the virus mediates this degradation through an early viral protein. Determining which viral protein is responsible for PKR degradation will provide further insight into innate immune evasion by DNA viruses, and may help to identify other DNA viruses that could degrade PKR during infection. We have also shown that $GCN2^{-/-}$ mice and primary peritoneal macrophages are more susceptible to MAV-1 infection compared to wild type mice. Also, brain cytokines and chemokines are altered in

GCN2$^{-/-}$ mice during infection, showing that GCN2 could be an important antiviral response during DNA virus infection. Determining how GCN2 is triggered during MAV-1 infection and whether the virus has any mechanism to inhibit that activation could provide insight into how GCN2 is playing an antiviral role in DNA virus infection.

Bibliography

1. Kring SC, Ball AO, Spindler KR. 1992. Transcription mapping of mouse adenovirus type 1 early region 4. Virology 190:248-55.

2. Querido E, Blanchette P, Yan Q, Kamura T, Morrison M, Boivin D, Kaelin WG, Conaway RC, Conaway JW, Branton PE. 2001. Degradation of p53 by adenovirus E4orf6 and E1B55K proteins occurs via a novel mechanism involving a Cullin-containing complex. Genes Dev 15:3104-17.

3. Harada JN, Shevchenko A, Shevchenko A, Pallas DC, Berk AJ. 2002. Analysis of the adenovirus E1B-55K-anchored proteome reveals its link to ubiquitination machinery. J Virol 76:9194-206.

4. Gilson T, Blanchette P, Ballmann MZ, Papp T, Penzes JJ, Benko M, Harrach B, Branton PE. 2016. Using the E4orf6-Based E3 ubiquitin ligase as a tool to analyze the evolution of adenoviruses. J Virol 90:7350-7367.

5. Forrester NA, Patel RN, Speiseder T, Groitl P, Sedgwick GG, Shimwell NJ, Seed RI, Catnaigh PO, McCabe CJ, Stewart GS, Dobner T, Grand RJ, Martin A, Turnell AS. 2012. Adenovirus E4orf3 targets transcriptional intermediary factor 1gamma for proteasome-dependent degradation during infection. J Virol 86:3167-79.

6. Sohn SY, Hearing P. 2016. The adenovirus E4-ORF3 protein functions as a SUMO E3 ligase for TIF-1gamma sumoylation and poly-SUMO chain elongation. Proc Natl Acad Sci USA 113:6725-30.

7. Cheng X, Byrne M, Brown KD, Konopleva MY, Kornblau SM, Bennett RL, May WS. 2015. PKR inhibits the DNA damage response, and is associated with poor survival in AML and accelerated leukemia in NHD13 mice. Blood 126:1585-94.

8. Weber J. 1976. Genetic analysis of adenovirus type 2 III. Temperature sensitivity of processing viral proteins. J Virol 17:462-71.

9. Anderson CW, Baum PR, Gesteland RF. 1973. Processing of adenovirus 2-induced proteins. J Virol 12:241-52.

10. Weber JM, Anderson CW. 1988. Identification of the gene coding for the precursor of adenovirus core protein X. J Virol 62:1741-5.

11. Anderson CW. 1990. The proteinase polypeptide of adenovirus serotype 2 virions. Virology 177:259-72.

12. Sanfilippo CM, Chirimuuta FN, Blaho JA. 2004. Herpes simplex virus type 1 immediate-early gene expression is required for the induction of apoptosis in human epithelial HEP-2 cells. J Virol 78:224-39.

13. Kainulainen M, Lau S, Samuel CE, Hornung V, Weber F. 2016. NSs virulence factor of Rift Valley fever virus engages the F-box proteins FBXW11 and beta-TRCP1 to degrade the antiviral protein kinase PKR. J Virol 90:6140-7.

14. Mudhasani R, Tran JP, Retterer C, Kota KP, Whitehouse CA, Bavari S. 2016. Protein kinase R degradation Is essential for Rift Valley fever virus infection and is regulated by SKP1-CUL1-F-box (SCF)FBXW11-NSs E3 ligase. PLoS Pathog 12:e1005437.

15. Ikegami T, Narayanan K, Won S, Kamitani W, Peters CJ, Makino S. 2009. Rift Valley fever virus NSs protein promotes post-transcriptional downregulation of protein kinase PKR and inhibits eIF2alpha phosphorylation. PLoS Pathog 5:e1000287.

16. Li C, Zhu Z, Du X, Cao W, Yang F, Zhang X, Feng H, Li D, Zhang K, Liu X, Zheng H. 2017. Foot-and-mouth disease virus induces lysosomal degradation of host protein kinase PKR by 3C proteinase to facilitate virus replication. Virology 509:222-231.

17. Chang YH, Lau KS, Kuo RL, Horng JT. 2017. dsRNA binding domain of PKR is proteolytically released by enterovirus A71 to facilitate viral replication. Front Cell Infect Microbiol 7:284.

18. Dey M, Mann BR, Anshu A, Mannan MA. 2014. Activation of protein kinase PKR requires dimerization-induced cis-phosphorylation within the activation loop. J Biol Chem 289:5747-57.

19. Taylor DR, Lee SB, Romano PR, Marshak DR, Hinnebusch AG, Esteban M, Mathews MB. 1996. Autophosphorylation sites participate in the activation of the double-stranded-RNA-activated protein kinase PKR. Mol Cell Biol 16:6295-302.

20. Gokirmak T, Denison FC, Laughner BJ, Paul AL, Ferl RJ. 2015. Phosphomimetic mutation of a conserved serine residue in Arabidopsis thaliana 14-3-3omega suggests a regulatory role of phosphorylation in dimerization and target interactions. Plant Physiol Biochem 97:296-303.

21. Baltzis D, Li S, Koromilas AE. 2002. Functional characterization of pkr gene products expressed in cells from mice with a targeted deletion of the N terminus or C terminus domain of PKR. J Biol Chem 277:38364-72.

22. Ciechanover A, Heller H, Elias S, Haas AL, Hershko A. 1980. ATP-dependent conjugation of reticulocyte proteins with the polypeptide required for protein degradation. Proc Natl Acad Sci USA 77:1365-8.

23. Hershko A, Ciechanover A, Heller H, Haas AL, Rose IA. 1980. Proposed role of ATP in protein breakdown: conjugation of protein with multiple chains of the polypeptide of ATP-dependent proteolysis. Proc Natl Acad Sci USA 77:1783-6.

24. Baugh JM, Viktorova EG, Pilipenko EV. 2009. Proteasomes can degrade a significant proportion of cellular proteins independent of ubiquitination. J Mol Biol 386:814-27.

25. Maupin-Furlow J. 2011. Proteasomes and protein conjugation across domains of life. Nat Rev Microbiol 10:100-11.

26. Anda S, Zach R, Grallert B. 2017. Activation of Gcn2 in response to different stresses. PLoS One 12:e0182143.

27. Hirohata Y, Kato A, Oyama M, Kozuka-Hata H, Koyanagi N, Arii J, Kawaguchi Y. 2015. Interactome analysis of herpes simplex virus 1 envelope glycoprotein H. Microbiol Immunol 59:331-7.

28. Vazquez de Aldana CR, Marton MJ, Hinnebusch AG. 1995. GCN20, a novel ATP binding cassette protein, and GCN1 reside in a complex that mediates activation of the eIF-2 alpha kinase GCN2 in amino acid-starved cells. EMBO J 14:3184-99.

29. Fang L, Stevens JL, Berk AJ, Spindler KR. 2004. Requirement of Sur2 for efficient replication of mouse adenovirus type 1. J Virol 78:12888-900.

30. Shibata N, Carlin AF, Spann NJ, Saijo K, Morello CS, McDonald JG, Romanoski CE, Maurya MR, Kaikkonen MU, Lam MT, Crotti A, Reichart D, Fox JN, Quehenberger O, Raetz CR, Sullards MC, Murphy RC, Merrill AH, Jr., Brown HA, Dennis EA, Fahy E, Subramaniam S, Cavener DR, Spector DH, Russell DW, Glass CK. 2013. 25-Hydroxycholesterol activates the integrated stress response to reprogram transcription and translation in macrophages. J Biol Chem 288:35812-23.

31. Won S, Eidenschenk C, Arnold CN, Siggs OM, Sun L, Brandl K, Mullen TM, Nemerow GR, Moresco EM, Beutler B. 2012. Increased susceptibility to DNA virus infection in mice with a GCN2 mutation. J Virol 86:1802-1808.

32. Ravindran R, Khan N, Nakaya HI, Li S, Loebbermann J, Maddur MS, Park Y, Jones DP, Chappert P, Davoust J, Weiss DS, Virgin HW, Ron D, Pulendran B. 2014. Vaccine activation of the nutrient sensor GCN2 in dendritic cells enhances antigen presentation. Science 343:313-317.

33. Jiang G, Santos Rocha C, Hirao LA, Mendes EA, Tang Y, Thompson GR, 3rd, Wong JK, Dandekar S. 2017. HIV Exploits antiviral host innate GCN2-ATF4 signaling for establishing viral replication early in infection. MBio 8.

34. Rosendahl Huber S, van Beek J, de Jonge J, Luytjes W, van Baarle D. 2014. T cell responses to viral infections - opportunities for peptide vaccination. Front Immunol 5:171.

35. Crotzer VL, Blum JS. 2009. Autophagy and its role in MHC-mediated antigen presentation. J Immunol 182:3335-41.

36. Ying B, Smith K, Spindler KR. 1998. Mouse adenovirus type 1 early region 1A is dispensable for growth in cultured fibroblasts. J Virol 72:6325-31.